The science and practice of metal-organic vapor phase epitaxy (MOVPE)

1. Introduction

Since the publication of the Handbook of Crystal Growth in 1994 significant changes have taken place in the science and technology of Metal Organic Vapor Phase Epitaxy (MOVPE) [1]. Many of these changes have arisen because of the revolutionary advances enabled by compound semiconductors, especially GaAs-based communication devices and GaN-based Light Emitting Diodes (LEDs). High demand for these consumer devices has driven the development of larger-area, improved-design MOVPE growth systems, along with higher purity sources and diagnostic tools for monitoring growth in real-time. MOVPE has also become the technique of choice for the manufacturing of lasers for telecommunications and DVDs and concentrated photovoltaics. This article emphasizes the general science and practice of MOVPE mainly for the III-V alloys.

This chapter will cover advances in MOVPE since 1994. It will acquaint the reader with a review of the MOVPE technique including comparison to other growth techniques currently used in the semiconductor industry such as MBE and HVPE. The name MOVPE is often used interchangeably with Metal-Organic Chemical Vapor Deposition (MOCVD), Organometallic Vapor Phase Epitaxy (OMVPE) and Organometallic Chemical Vapor Deposition (OMCVD). We choose MOVPE because we feel that this name is the most descriptive in that metal-organic emphasizes the metal which ultimately ends up in the compound semiconductor and vapor phase epitaxy emphasizes the desired single crystal, or epitaxial growth of the reacting, gas-phase molecules on the substrate.

In section 1 of this chapter we will give a brief historical overview of the development of MOVPE, a comparison of this technique to other common techniques, and an overview of the types of materials and devices that have been investigated by MOVPE. In section 2 we will cover the fundamental science aspects of MOVPE, including the chemistry, kinetics, and thermodynamics of MOVPE, as well as the general operation aspects of the growth of different materials. Section 3 will delve into the role of impurities and dopants in controlling the properties of the grown materials. Section 4 will describe the types of sources and equipment that are used by this technique and the recent advances in the design of systems for the implementation of MOVPE. Finally we will conclude in Section 5 with a summation of the versatile technique of MOVPE. Since the MOVPE technique is far too great to comprehensively cover in the limited space of this chapter the reader is referred to other chapters in this volume, 3a, as well as the companion volume, 3b, of this Handbook, and several excellent reviews and voluminous manuscripts published on the details of the MOVPE technique only some of which are referenced here-in [1-5]. In the author's estimation the most comprehensive review of MOVPE is the book by Stringfellow, the second edition of which was published in 1999 [2; 3].

1.1 Historical Perspective

Hal Manasevit and his group at Rockwell were the first to broadly implement the MOVPE technique in the 1960's [6-8]. Although there are earlier patents the initial publications by Manasevit and co-workers in the scientific literature are usually recognized by the MOVPE community as the beginning of this technique [3]. This technique was developed to simplify the apparatus for producing epitaxial films of semiconductors compared to the more complex set up required for vapor phase epitaxy (VPE) [3; 8].

Prior to the work at Rockwell, many of the III/V and II/VI compound semiconductors were grown either by liquid phase epitaxy (LPE) or vapor phase epitaxy (VPE), using hydride and chloride sources [3; 9]. While these techniques were adequate for many of the devices of this time period, they were not able to produce the complex structures commonly required today, that are enabled using MOVPE [1-3]. Also these techniques could not control the incorporation of In and Al for LPE and Al for VPE into the device structures [1-3].

LPE has been used for the growth of II-VI and III-V semiconductors since the early 1960's [9]. The technique was used for the growth of salts from aqueous solutions since the late 1800's to synthesize epitaxial orientations of various minerals on cleaved facets [9]. As Stringfellow mentions this technique has produced very high purity semiconductors with superior properties for materials such as AlGaAs and InP for active device layers from a very simple apparatus [3; 4]. One advantage of LPE is that it can easily produce thick layers, 10-100 μm, of high purity semiconductors. However, LPE is limited in its ability to produce complex structures with multiple layers of different composition. This limitation is due to the lack of thickness uniformity and inability to produce abrupt interfaces. Also, due to the large differences in solubility and liquid-solid distribution coefficients of In and Al, alloys of these materials are almost impossible to grow by LPE [3; 10]. Because of these limitations, LPE is not used for the production of most modern devices.

VPE, either hydride or chloride based chemistries (HVPE, ClVPE), has also been used in the past to produce high quality, thick epitaxial layers of compound semiconductors. These techniques were used in the early 1960's to produce some of the first III-V devices. It is nearly ideal for simple devices like GaAsP light emitting diodes (LEDs). However, unlike LPE the growth occurs in a rather complex apparatus [8]. Because of the system limitations for VPE it is rarely used to make some of the complex structures that are used in today advanced devices due to the difficulty in making thin layers or superlattices. Also, Al containing structures are difficult to prepare due to the stability of the Al-chlorides compared to other Group III chlorides such as Ga in these systems [3]. One advantage of VPE that is still utilized today is the very high growth rates that can be achieved, >100 μm/h. This allows for the growth of very thick crystals that are high quality with low dislocation density, $<10^6$ cm^{-2}. These crystals are utilized especially in the growth of GaN due to the current lack of sources of bulk GaN substrates [11].

High vacuum techniques like molecular beam epitaxy (MBE) and chemical beam epitaxy (CBE) as well as other similar mixed gas-metal source methods were developed in the same time frame and for similar reasons as MOVPE, yet these techniques were never widely adopted for the commercial production of compound semiconductor devices [12]. In spite of their relative simplicity, their capability to produce high quality superlattices, and high purity layers, these techniques have proven to be too expensive due to their ultra-high vacuum system requirements and their complex maintenance procedures. Furthermore, these systems also do not easily lend themselves to scaling up to larger sizes or multiple wafers for mass production.

Because of the limitations of both LPE and VPE in growing complex device structures and Al and In containing alloys, MOVPE developed rapidly in the 1970's and is now the primary production technique used in the compound semiconductor industry. Although initially explored as a simpler technique than VPE with a less complex apparatus, MOVPE can produce complex device structures of all of the III-V and II-VI semiconductors with high uniformity over large area substrates [12]. This technique has been shown to be capable of growing high purity materials as well as nearly atomically abrupt interfaces in numerous systems [3]. Due to this versatility and simplicity, MOVPE has been adopted throughout the world for the production of the vast majority of III-V and II-VI devices. Today large scale, multi-wafer MOVPE systems with state-of-the-art gas inlet systems designed to optimize uniformity and yield and in-situ diagnostics are available from several commercial system companies such as Veeco and Aixtron.

1.2 Overview of MOVPE for Materials Preparation and Device Applications

As mentioned in the previous section, MOVPE is the major production technique for the vast majority of compound semiconductor devices due to its relative simplicity and versatility. MOVPE is simple in that the apparatus consists of a heated substrate in a cold wall flow chamber; however the control of numerous flows of the sources and their distribution in the chamber as well as the temperature control can seem somewhat overwhelming to the uninitiated. Perhaps the most studied compound grown by MOVPE is GaAs [3; 4; 7; 13; 14; 15]. The growth of GaAs by MOVPE exhibits what may be considered classic growth rate behavior as illustrated in Figure 1. From about 550 to 850°C the growth rate of GaAs using

trimethylgallium (TMGa) and arsine has been found to be mass transport limited. This means that the growth rate of GaAs is directly proportional to the TMGa flow rate. Mass transport limited growth makes the growth rate nearly independent of the GaAs substrate orientation with no significant re-evaporation of the GaAs from the surface after it has been deposited. However, changes to the gas velocity, which directly affect the mass transport of reactants to the growth surface influence growth rate. The simplicity of mass transport limited growth disappears at higher and lower temperatures. At higher temperatures the growth rate is believed to be reduced by gas-phase reactant depletion and/or re-evaporation of growth species. At lower temperatures the growth rate decreases due to the incomplete decomposition of the TMGa and other kinetic factors [3; 4; 13; 16].One of the major advantages of MOVPE is that high quality AlGaAs and InGaAs alloys can be grown using conditions similar to GaAs[3; 4; 17]. It is because of these growth attributes that MOVPE has been widely adapted by industry to produce a large number of devices in the GaAs-based system.

It is beyond the scope of this chapter to exhaustively list all of the device types that are manufactured using MOVPE but some of these devices and references are listed in Table I. One major advance worth mentioning here is the explosion in the use of MOVPE for the production of GaN-based devices. Although Manasevit was able to deposit GaN and AlN in 1971 it was not until the work of Akasaki and separately Nakamura in the 1990's that the production of device quality GaN-based structures became a reality [8; 18-20]. Since that time MOVPE growth of LEDs progressed from low intensity indicator lamps to high intensity LEDs currently used in multiple applications such as signage, displays, TVs, and even solid state lighting. As demonstrated by numerous authors in the literature (see discussion below) and discussed in more detail in a separate chapter in this Handbook by Amano, the deposition chemistry of the three-nitrides is significantly more complex than that of the other III-V or II-VI compounds. This difficulty arises primarily for three reasons. First, there is no lattice matched substrate available for the growth of these materials and various nucleation layer schemes had to be invented to grow adequate epitaxial layers of GaN. Second, there are complex reactions that take place in the vapor phase to form adducts and other gas-phase products which inhibit the mass transport of the Group III elements to the surface. Third, there are no good p-type dopants with low ionization energy. The best p-type dopant for these devices is Mg which has a acceptor energy level of 170-250 meV from the valence band so that only about one to two percent of the Mg produces holes at room temperature in the device structures [20; 21]. AlGaN-based devices are also being developed for UV emitters and detectors, some of which are illustrated in Table I.

There are many other devices made from multiple materials by MOVPE especially InP-based devices for optical communications and III-Sb-based devices for use in the infrared (Table I). In addition there are many multi-layer devices such as vertical cavity surface emitting lasers that are still being developed for multiple applications. Again all of these materials and devices can be made using MOVPE which further demonstrates its versatility and usefulness in manufacturing.

2. The Science of MOVPE - Fundamental Aspects

Although the use of MOVPE to prepare GaAs and GaN based devices can seem rather straight forward and simple, the details of the reaction mechanisms are somewhat complicated. As Stringfellow, Kuech, and Creighton have pointed out the actual mechanisms can vary and depend on the growth conditions and the precursors used [1-5; 13; 16; 17; 22]. If MOVPE growth depended only on thermodynamic considerations, the chemical description for GaAs or GaN growth from their precursors (TMG and NH_3 or AsH_3) would be simple. However, since many other factors come into play during the deposition of these materials such as pre-reactions, surface orientation, and pressure and temperature effects, it is often important to know the details of the complex chemistry taking place during the deposition process in both the gas phase as well as on substrate surface. More detailed descriptions of these topics are found in Stringfellow's book and his review [2; 3]. Here, we will illustrate some of the complexities involved in GaAs and GaN growth as examples.

2.1 The Chemistry of MOVPE deposition (GaAs and GaN as illustrative cases)

The large free energy of formation of the three/five (III/V) semiconductors such as GaAs and InP results in a sufficient force to drive these reactions to completion as illustrated in equation (1). The phase diagrams for these materials show only a single phase over large ranges of temperature and composition [10], resulting in a wide choice of MOVPE growth conditions that all result in the desired semiconductor. Although a complete description of the details of the MOVPE growth mechanism for GaAs is very complex, the net result is that very pure, single crystal GaAs can be grown under a variety of conditions [1; 3; 23; 24].

For the growth of GaAs or GaP, a high V/III ratio is typically used. This condition is used because the Group V element (As or P), has a high vapor pressure and does not readily condense on the surface. If a low V/III ratio is used the Group III element condenses on the surface and introduces a second phase into the growing material. The use of a high ratio also helps to reduce the incorporation of impurities such as carbon and oxygen during growth [3; 17; 25]. Unlike the other III/V's the growth of the Sb containing III/V's is usually done at a V/III ratio close to one due to the relatively low vapor pressure of Sb under the normal growth conditions [26; 27].

$$(CH_3)_3Ga + AsH_3 = GaAs + 3CH_4 \qquad (1)$$

The efficiency of the MOVPE growth process is determined by several factors the most important of which are the transport of the source gases, e.g. TMGa and AsH_3, to the heated susceptor and the reaction of the sources gases at the susceptor. The transport of the gases is governed by hydrodynamic flow processes in the reactor, which depend on the system design. This type of hydrodynamic flow modeling has been described in detail by K. F. Jensen in the first edition of this Handbook for Crystal Growth as well as other authors [1; 28; 29]. The level of detail in this flow modeling varies from one dimensional to full 3D models used to design modern MOVPE systems [12]. Commercial software packages, such as ANSYS Fluent, are available to model MOVPE systems.

The other factor that governs the efficiency of the MOVPE growth process is the reaction of the source gases when they reach the hot susceptor. As shown in Figure 1, the growth rate of GaAs from TMGa and AsH_3 varies significantly with temperature [1; 3; 14]. The typical temperature range for growth is in the mass transport or diffusion limited regime where all of the TMGa is depleted at the surface and results in the growth of GaAs (T ~ 550-850 C). In this intermediate temperature range the growth rate is found to be directly proportional to the flow rate of the metal-organic compound. This type of behavior has been found for the growth of numerous III/V compounds besides GaAs (e.g. InP, AlAs, InP, InSb and InAs) [1; 3; 26; 30]. Almost all of the growth of III/Vs is carried out in this intermediate temperature range where the growth rate is easily controlled by the flow of the metalorganic.

At higher temperature the growth rate decreases (see Figure1). Although not completely understood even for GaAs, it appears that this reduced growth rate is due to the increased rate of evaporation of the III/V surface. In other words the vapor phase concentration is no longer high enough to cause a saturation of the constituents at the higher temperatures because the surface equilibrium evaporation rate is higher than the condensation or growth rate. Another explanation involves the depletion of reactants before they can reach the growth surface. This explanation is supported by the observation that lower system pressure changes the temperature behavior [3; 31].

At lower temperatures the growth rate also decreases dramatically. Through extensive studies of the growth mechanism and the GaAs surface structure it is known that at low temperatures the growth is inhibited by the incomplete decomposition of the metal–organic sources. For instance Creighton has shown that at low temperatures a surface reconstruction consisting of As-Ga-CH_3 units covers a complete layer of arsenic [16]. This surface reconstruction, designated as (1x2)-CH_3, illustrates the presence of surface Ga-CH_3 groups that must desorb the methyl group before growth can continue. Several research groups have independently observed that the surface reconstruction changes correspond to the changes in

growth rate behavior as a function of temperature and partial pressure of TMGa [16; 32; 33; 34; 35; 36; 37]. They all observe a high temperature, high arsenic partial pressure c(4x4) reconstruction that coincides with the normal, mass transport limited growth rate region. At intermediate temperatures and arsine partial pressures the presence of two controversial surface reconstructions are found. The temperature versus TMGa pressure phase diagram proposed by Creighton and Reinhardt *et al.* is shown in figure 2 [16; 32]. These surfaces are described as a mixture of c(4x4) and (1x6) with Ga-As or Ga dimers [32]. Kisker *et al*. describe them as a weak p(1x2) reconstruction [36]. Creighton, through a series of experiments believes the surface at the intermediate temperature to be closely related to a slightly disordered c(4x4) surface. Creighton has proposed that the low temperature surface reconstruction is an arsenic rich (1x2)-CH_3 phase [16; 38]. The presence of different surface reconstructions is direct evidence that at these lower temperatures the surface influences the growth reaction mechanism. Mountziaris postulated in their model that a limited number of adsorption sites for the TMGa exist on the surface due to the slow decomposition of monomethylgallium [24; 39]. Thus the decomposition of monomethylgallium at low temperatures as illustrated by equation (2) becomes the rate limiting step for the growth of GaAs from TMGa and AsH_3,

$$CH_3Ga_{(surface)} + AsH_{(surface)} = GaAs + CH_4 \qquad (2)$$

There is relative consensus as to the deposition reaction mechanism for the GaAs growth at all temperature and pressure regimes [1; 3]. The very early work of Schlyer and Ring in 1976 indicated that the reaction involved the adsorption of the reactants and their subsequent decomposition on the GaAs surface [40]. This conclusion has since been supported by numerous experimental and theoretical studies including the work of Reep and Ghandhi, Aspnes and Richter, Creighton, and others using numerous techniques such as growth rate studies versus temperature, in-situ grazing incidence x-ray diffraction, and reflectance difference spectroscopy [14; 16; 32; 33; 34; 35; 36; 37; 38]. All evidence supports a reaction mechanism described by a Langmuir-Hinshelwood (LH) mechanism in which the growth rate, $\mathbf{r_{GaA}}$, is proportional to the pressure of TMGa, $\mathbf{P_{TMGa}}$, modified by the adsorption processes according to equation (3),

$$r_{GaAs} \sim a\, P_{TMGa}/(1+b\, P_{TMGa}), \qquad (3)$$

where ***a*** and ***b*** are derived from the adsorption process. This LH mechanism is supported by the growth rate data of Kisker *et al*. obtained by in-situ grazing incidence x-ray diffraction experiments [41].

Compared to the work done on GaAs surface reconstructions, less work has been conducted on surface reconstructions during growth for the other III/V semiconductors. For example, reconstructions for InP surfaces are similar to those on GaAs surfaces [42]. The c(4x4) reconstruction is not found under normal growth conditions for InP probably due to the increased vapor pressure of P on the surface. The antimonides show a large number of other types of reconstructions compared to those of InP and GaAs [43]. Some work has also been done on InAs and GaP [44] and all of these compounds display surface reconstructions. Stringfellow has postulated that the presence of reconstructed surfaces for the III/Vs is the main reason complex and very thin layers for numerous device applications can be achieved [4]. If the surfaces were not reconstructed it is probable that layer by layer or step-flow growth modes might not be achieved.

During the growth of GaAs as well as other semiconductors the reduction or elimination of surface roughness is quite often a difficult objective to achieve. Surface roughness has been postulated to be related to a large number of phenomena with numerous causes [4]. The observed roughness can be related to surface preparation, surface orientation, growth rate, and several other sometimes hard to control factors such as particulate that is formed in the vapor phase during growth. Growth during epitaxy is known to occur through the attachment of atoms or molecules at steps or by the formation of two and/or three dimensional islands when the surface diffusion of the growth species is small compared to the step size. These two growth modes are step-flow or layer-by-layer when large 3D islands are not formed. These types of growth modes have been observed experimentally using both grazing incidence x-ray

spectroscopy (GIXS) and RDS [33; 36]. Roughness arises when the growth forms three dimensional islands or when step bunching occurs. Islands can also occur at impurities or defects that can act as preferential nucleation sites by lowering the energy barrier for attachment, while step bunching has been explained by both thermodynamic and kinetic effects [3; 4]. All of these conditions must be considered when optimizing the growth of smooth layers.

Unlike the other III/Vs the deposition chemistry of the Group III-nitride semiconductors can be heavily influenced by chemical reactions in the vapor phase. The MOVPE of GaN, InN, and AlN are usually done using TMGa, TMAl, TMIn with ammonia. The temperatures of three-nitride deposition (500-1000°C) cause multiple, source depleting, parasitic reactions to occur in the vapor phase [22; 45-49]. These reactions can ultimately lead to nanoparticle formation and consume a significant fraction of the Group III-growth precursor. These parasitic reactions produce strong temperature-dependent thin film growth rates and also cause the growth rates and alloy compositions to vary nonlinearly with precursor concentration [50; 51]. These nanoparticles have been shown to be suspended at some distance from the growing film by thermophoretic forces [46; 47]. The nanoparticles represent the end product of a sequence of gas-phase nucleation and particle growth reactions that are still not completely understood. The first step in the mechanism is believed to be adduct or Lewis acid-base complex formation between NH_3 and TMAl, TMGa,and/or TMIn, as in Reaction (4).

$$(CH_3)_3Al + NH_3 = (CH_3)_3Al : NH_3 \qquad (4)$$

The formation of this adduct seems unavoidable when the reactants are mixed in any conventional MOVPE system. Following adduct formation, a next likely step involves a CH_4 elimination which then forms the $(CH_3)_2M\text{-}NH_2$ species. Following this, dimers, trimmers, and extended oligomerization through possible further CH_4 elimination is proposed as the mechanism for particle formation. Other mechanisms are possible such as deposition on the small particles and further research is needed to elucidate the complete mechanism.

Even though vapor phase interactions decrease source and growth efficiency, the Group III nitrides have similar characteristics to the other III-V semiconductors. In a series of experiments using grazing incidence in-situ x-ray spectroscopy it has been shown that GaN exhibits step-flow, layer-by-layer, and three dimensional growth modes as the growth temperature is reduced [52]. This variation in the growth mode has enabled the preparation of quantum wells and superlattices that enable so many of the modern devices. The III-nitrides have also been shown to have a rather unique surface reconstruction which although not like the other III-Vs, still contains rows of gallium dimers under the growth conditions [53]. Again, this reconstructed, lower energy surface allows for the growth of complex layered structures enabling modern devices.

2.2 Alloy growth using MOVPE

As mentioned earlier in this review, facile growth of ternary and quaternary alloys by MOVPE such as AlGaAs, InGaAs, and InGaAsP, is one of the major advantages of the technique. The use of equilibrium thermodynamics usually allows for the composition of the solid phase to be accurately predicted from the appropriate equilibrium constants which are a function of the reactant temperature and vapor phase concentrations [2-4]. For alloys like AlGaAs where there is complete solubility across the AlAs-GaAs phase diagram and low enthalpy of mixing, the composition of the solid is directly related and practically equal to the vapor phase composition when grown with excess arsine. The AlGaAs alloy's composition is determined by the relative growth rates of the AlAs and GaAs binaries. However, for other alloys with more limited solubility and higher enthalpy of mixing, the composition is dependent more on the solubility and the relative activities of the solid phase components Stringfellow and others have shown that the enthalpy of mixing is related to the strain energy associated with the difference in the size of the components [10; 54]. Thus for systems such as AlInPSb a large miscibility gap is predicted. However, miscibility gaps are also known to occur for commercially important systems such as InGaAsP where the

size difference is not so great. In the following discussion we will briefly describe the MOVPE growth of several ternary systems. .

2.2.1 III-III'-V alloys (AlGaAs, InGaAs, InGaP)

For many of the III-III'-V alloys the composition is controlled by the relative concentrations in the vapor phase of the starting materials. Alloys such as AlGaAs, InGaAs, InGaP are grown under excess arsine or phosphine flows and the alloy composition is determined by the vapor phase concentrations and mass transport of the Group III gases to the growth surface. This is true for the growth of InGaP, AlGaAs and InGaAs [55; 56]. Another way to express this behavior is to indicate the solid-vapor distribution coefficients ($k_{III} = X_{III}(s)/X_{III}(v)$ where $X_{III}(s)$ is the mole fraction of the III-V in the solid and $X_{III}(v)$ is the Group III input partial pressure) which are close to or equal to one in all these cases. This ideal behavior is not always observed, especially in the Group III-III' nitrides as described below, where complex vapor phase interactions cause the incorporation of the group three metal to not be directly related or equal to the vapor phase partial pressure.

2.2.2 III-V-V' alloys

For the III-III' alloys which are grown under an excess Group V flow, mass transport and the thermodynamic stability of the resulting compound controls the composition. For the III-V-V' alloys, such as InAsSb, GaAsSb, or GaAsP the large difference in the thermodynamic stability of the binaries and the enthalpy of mixing are more likely to control the resulting composition.

InAsSb is of particular interest for long wavelength applications, such as infrared detectors and lasers. This semiconductor has the smallest bandgap of any of the more developed III-V materials with a value of 0.15 eV at room temperature [26]. Although there were many earlier reports of the synthesis of InAsSb, the first detailed study by Biefeld in 1986 described the composition dependence of InAsSb on the growth conditions and resultant bandgap [26; 57; 58]. In this paper a thermodynamic model previously applied by Stringfellow to the growth of InAsSb and GaAsSb was used to describe the solid composition dependence on temperature, V/III ratio, and vapor phase composition. The thermodynamic model considered was first used by Stringfellow to describe the results of Fukui and Horikoshi for InAsSb growth at 500°C [58]. The observed trends for the effects of input vapor concentrations on the resulting solid composition are illustrated in Figure 3 that depicts both the theoretical data by lines and selected alloy and superlattice data points. The model predicts that the thermodynamically more stable III-V compound will control the composition. For the InAsSb system when the V/III ratio > 1, arsenic is preferentially incorporated into the solid and the solid-vapor distribution coefficient of antimony (k_{Sb}) is < 1. This is because InAs is more stable, has a lower free energy of formation, than InSb at 475-525 C. For V/III ratios close to one, k_{Sb} approaches one and for V/III $\leq$ 1, $k_{Sb} = 1$. When V/III $\leq$ 1, all of the Group V materials, arsenic and antimony, will be incorporated into the solid. Under most normal growth situations the V/III ratio is close to or slightly greater than one and all of the arsenic is preferentially incorporated, with excess antimony rejected from the solid and segregated on the epitaxial surface.

For the results presented in Figure 3, there are some slight deviations from the predicted thermodynamic behavior. For some of the samples grown at 475 ^{o}C, k_{Sb} appears to be greater than one. This can be explained by assuming that not all of the arsine is decomposed at this temperature. This assumption is consistent with the reported incomplete decomposition of arsine at temperatures below 500° C [3]. The thermodynamic model assumes that all of the arsine and the TMSb are decomposed at the growth temperature into their stable elemental form such as As_4. This effect becomes more pronounced at lower temperatures as less arsine is decomposed and the resulting antimony content of the solid exceeds that predicted by the model [57]. The superlattices grown at 525° C had TMSb vapor fractions between 0.3 and 0.5, which is slightly less than that predicted by the thermodynamic model. This is illustrated in Figure 3 by the dashed and dotted lines that represent the predicted compositions for V/III ratios of 2.0 and 20, respectively. The compositions should fall between these two limits. This discrepancy can be explained by the formation of an arsenic-rich interface or diffusion of arsenic into the antimony-

containing layer during growth of the superlattice. The presence of this type of interface has been observed directly by both scanning tunneling microscopy (STM) and transmission electron microscopy (TEM) investigations of these materials [59].

The same type of thermodynamic model that was used to describe the composition control of InAsSb will accurately predict the composition for the MOCVD growth of GaAsSb using the standard trimethyl sources and arsine [26; 60-62]. Again, arsenic is preferentially incorporated into the solid and excess antimony is rejected and solidifies on the surface after growth. As for InAsSb, the effects of temperature and V/III ratio on the composition of GaAsSb are accurately predicted by the thermodynamic model [62]. As the V/III ratio is increased, less antimony is incorporated reducing the antimony distribution coefficient. More recent studies have been done using alternate sources such as TEGa and tertiarbutylarsine (TBAs) with TMSb [63]. In this study the authors reported that the model was accurate for a growth temperature of 550 C but not at 475 to 525 C. For these lower temperatures they observed an arsenic distribution coefficient less than one which contradicts the model. Although a difference in pyrolysis rates might be one explanation, it is generally accepted that TBAs pyrolyzes at a lower temperature that TMSb and so arsenic should still be preferentially incorporated. Other kinetic factors must be playing a role here such as surface processes or source interactions to cause the model to fail in this case. The contribution of these kinetic factors is further supported by the results of Kuech *et al*. in a recent study of the effect of different precursors on the growth of GaAsSb [27; 64].

The MOVPE growth of GaAsP as well as the quaternary InGaAsP have been extensively investigated primarily for their use in communications [61; 65-68]. The control of the As and P ratio in the resulting solid is extremely important as this ratio controls the lattice constant and the band gap. Early work by Stringfellow indicated that a thermodynamic model which assumed that arsine and phosphine were completely decomposed could not accurately predict the resulting compositions [61; 65]. The data indicated that even at high temperatures, 800-850 C, arsenic was preferentially incorporated into the solid. Therefore he proposed that the incomplete pyrolysis of phosphine was the explanation for the discrepancy. Smeets found that this discrepancy could be modeled by using an adjustable parameter in conjunction with the thermodynamic explanation to fit the experimental data [68]. Biefeld also showed that the data could be fit, as shown in figure 4, by using an analytical expression which depends on both the temperature and the partial pressures of the phosphine and arsine [67]. The growth of the As-P ternaries or quaternaries is controlled not only by the solid-phase thermodynamic stabilities, but also by the kinetics of decomposition of the source gases, in this case arsine and phosphine.

2.2.3 III-N alloys

Today, the majority of the Group III-nitride growth is focused on the production of blue wavelength LEDs for general lighting purposes. GaN growth was first initiated in the 1930's [69], and until the early 1980's GaN growth was only sporadically studied primarily using HVPE [70] on a variety of growth compatible substrates [71]. The largest advance in GaN growth on sapphire occurred with the invention low temperature AlN layers first by Amano and coworkers using low temperature AlN layers [18] and later GaN layers by Nakamura [72]. Later Weeks *et al.* demonstrated that high temperature AlN could be used to grow GaN on wurtzite SiC [73]. These nucleation layers orient the GaN wurtzite phase and control the GaN nucleation density and ultimately influences the GaN crystallinity. When GaN is grown at high temperature (> 1000 °C) on these low temperature nucleation layers, planar GaN is formed with dislocation densities of ~10^9 cm^{-2} [74]. Aiding in the planar growth is the fact that GaN has a large lateral growth rate at > 1000 °C [75] due to a gas-phase Ga transport mechanism [76]. MOVPE is the growth technique of choice for GaN-based devices because it can be used to grow the GaN template and associated active regions such as QWs and p-doped layers all within the same system.

Also important in the early 1990's was achieving p-type GaN using Mg doping. After growth p-type GaN films were typically found to be highly resistive, however post-growth exposures to electron beam (LEEBI) [77] or anneals in vacuum or N_2 [78] were found successful at activating p-type material through

the dissociation of the Mg-H complex [79]. After p-type GaN was available, high brightness LEDs soon followed [80], which could ultimately lead to the replacement of traditional incandescent and fluorescent lighting by white LEDs.

One major difference between MOVPE GaN growth and the growth of conventional III-V's is that V/III ratios exceeding 1,000 are required. The reason for the high V/III ratio has several possible explanations including the prevention of GaN decomposition [81], the catalytic dissociation of NH_3 [82; 83], the fluxes necessary to achieve Ga to N stoichiometry [84], and the stabilization of c-plane growth [85]. GaN decomposition has been studied in flowing H_2 and N_2, leading to the conclusion that the rate limiting decomposition step highly depends on the degree of adatom hydrogenation [81]. GaN decomposition in flowing H_2 + NH_3 showed that as the NH_3 density increases there is an initial 100x suppression of the decomposition rate followed by a slight increase in the decomposition rate [86]. All work suggests that during MOVPE GaN growth there is some degree of decomposition which possibly aids in bringing growth closer to equilibrium [84]. During GaN growth, the degree of NH_3 dissociation is not entirely understood, although based on the equilibrium rate constant, NH_3 should be fully dissociated above ~ 200 °C. Instead NH_3 dissociation is highly temperature sensitive and has been measured to be several percent at 900 °C and 40-50% at 1050 °C [82]. The high temperature sensitivity suggests that a catalyst such as metallic Ga or GaN surface is necessary for NH_3 dissociation. I If the N to Ga desorption rates from GaN are compared, at 1050 °C, the N to Ga desorption rate is x1000 times larger and decreases as the temperature decreases reaching a ratio of 1 near 780 ºC [84]. Following this consideration, it is believed that choosing the V/III ratio close to the N to Ga desorption rate aids in producing stoichiometric GaN [84]. Finally, at high temperatures and high V/III ratios the growth rate of c-plane GaN becomes less than the rates for facets with in-plane components, making c-plane the most stable facet [85] and leading to a high lateral GaN growth rate observed when GaN overgrows masked regions [75]. Growth factors that impact GaN morphology have been discussed recently by Koleske *et al.* [87], specifically how growth temperature influences mounding behavior.

2.2.3.1 InGaN growth

The MOVPE growth of InGaN is usually conducted at substantially lower temperatures than GaN, ranging from 600 to 900 °C and at even higher V/III ratios than GaN, often exceeding 10,000. The lower growth temperature is necessary to offset the high rate of indium desorption and the high NH_3 flow compensates for the suspected reduction in NH_3 dissociation on the InGaN surface. If the InGaN growth temperature is too low, metalorganic fluxes too high, or NH_3 dissociation too low, metallic clustering occurs leading to a grayish surface appearance. At higher temperatures, the indium desorption increases and the indium incorporation is solely dictated by the GaN growth rate [88]. Nitrogen carrier gas must be used for InGaN growth since even small amounts of H_2 have been shown to decrease indium incorporation [89].

For InGaN growth on c-plane GaN, the InGaN alloy is limited to about 20 to 25 % indium due to the coherency strain from the underlying GaN film, even if the gas-phase In/(In+Ga) ratio is larger than 0.25. If the InGaN film is grown thick enough, strain relaxation occurs resulting in InGaN alloys with higher indium concentrations [90]. In fact, InGaN alloys over most of the entire compositional range have been grown using MOVPE [91], however, the defect concentration in these higher indium concentration films is so large that the films have little or no optical emission. On some semi-polar GaN planes, higher indium incorporation has been observed, resulting in longer wavelength LEDs [92], however misfit dislocations formed by basal or non-basal plane slip systems can occur on these non-polar or semi-polar structures resulting in reduced emission efficiency [93]. Developing a strain-relaxed, low-defect density InGaN template [94] would facilitate indium concentrations over 25 % to possibly produce yellow and red wavelength LEDs.

Even with the high defect and dislocation densities in the underlying GaN template, InGaN QW LEDs can be grown [95] with internal quantum efficiencies reaching ~ 90% [96]. Several theories have been

proposed to explain how semiconductors with such high dislocation densities are even optically functional. These explanations primarily invoke localization within quantum dots [97] or composition fluctuations [98], well-width fluctuations coupled to the strong polarization fields [99], or on condensates of In-N [100]. Contrary to the proposed localization schemes, energetic screening of carriers away from dislocations via the creation of a higher energy landscape around the dislocation cores has also been proposed [101]. Complicating a concise explanation for the high optical efficiency is the use of low temperature GaN, or dilute indium concentration InGaN, or InGaN/GaN superlattices layers underneath the InGaN QWs which have been shown to dramatically increase the luminescence efficiency [102]. In addition, further improvements in hole concentration have been demonstrated in Mg doped $In_{0.14}Ga_{0.86}N$ films with measured hole concentrations up to $6.7x10^{18}$ cm^{-3} [103] and in InGaN/GaN superlattice structures up to $2x10^{19}$ cm^{-3} [104]. The advent of bulk GaN substrates with reduced dislocation densities have led to UV, blue, and green laser diodes on c-plane and some semipolar planes [105]. InGaN is also a promising material for photovoltaic applications [106; 107] provided the indium concentration can be increased to better cover the entire solar spectrum. InGaN growth above atmospheric pressure has been attempted to suppress InGaN thermal decomposition and improve InGaN quality [108], but this work is in the preliminary stages.

2.2.3.2 AlGaN growth

AlGaN structures were first grown by Khan *et al*. [109] and Itoh *et al*. [110] to produce LEDs with wavelengths shorted than GaN. Unlike InGaN films, AlGaN is usually grown at pressures ≤ 75 torr to minimize gas-phase parasitic particulate formation [22]. This particulate formation preferentially removes aluminum from the gas phase resulting in AlGaN alloys with reduced aluminum [51] To reduce the parasitic chemistry, lower pressure and reduced NH_3 and MO flow rates are used [51]. Later even lower NH_3 flow rates or modulation of the NH_3 flow during growth was considered to enhance Al adatom migration, resulting in improved AlGaN quality and smoother surfaces [111]. In addition, higher growth temperatures (up to 1300 °C) also improve material quality suggesting enhancing Al mobility on the surface is essential for materials improvement [112]. For deep UV LEDs, it has been difficult to make p-type AlGaN materials since the hole activation energy scales with the bandgap. However recent work of Kinoshita *et al.* [113] and Kawanishi *et al.* [114] show promise in achieving p-type character in high (Al > 0.5) AlGaN films. Deep UV LEDs have been recently produced emitting at 278 nm with EQE of 10% [115].

When thin AlGaN layers are grown on undoped GaN, high electron mobility transistors (HEMTs) can be produced with a two-dimension electron gas (2 DEG) induced in the GaN beneath the AlGaN layer [116]. The 2 DEG is a direct consequence of the strong polarization fields which create up to ~$1x10^{13}$ cm^{-2} carriers in the GaN without doping [117]. The introduction of a thin AlN layer between the AlGaN and GaN further enhances the polarization fields leading to even higher sheet carrier densities [118]. One key property of the GaN material used for HEMTs is that it needs to be resistive (or semi-insulating) enough to ensure device pinch-off and high frequency operation [119]. Highly resistive GaN can be produced by carefully controlling the dislocation density and carbon doping levels [119]or by intentionally pinning the Fermi level mid-bandgap through the use of Fe doping [120]similar to Fe doping of InP [121]. MOVPE growth pressure and GaN dislocation density have been directly related to the carbon concentrations and subsequent resistivity of the underlying GaN [119]. Unintentional carbon doping of GaN was found to decrease with increasing growth temperature, pressure, and ammonia flow and to increase with increasing TMGa flow [122]. Photoionization spectroscopy measurements of the trap concentrations suggests carbon and grain boundaries or dislocations produce trap states [123] that are responsible for current collapse [124]. Careful attention to reducing bulk trap states [125] and passivation of surface states [126] has led to the rapid development of these structures for RF power electronics [127].

2.2.4 II-VI alloy growth

Due to space limitations and the knowledge of the authors, we only mention some of the distinct growth characteristics of the more common II-VI semiconductors. Typically the volatilities of the Group II and VI elements are much greater than the Group III and even the Group V elements on the semiconductor surface after deposition. Thus, during growth of HgTe or CdTe as well as other II-VIs, the vapor pressure of the Group II metal is not zero at the growth interface. During the growth of the alloy, HgCdTe, special techniques are used to make sure that the appropriate amount of Hg is incorporated due to the very high vapor pressure of Hg compared to Cd. [128; 129]. Considerable re-evaporation can take place during growth. Also, depending on the source of the Group VI element, the precursor may not be completely decomposed due to the low temperature of deposition and the stability of the source material [1; 128]. In calculating the composition of the solid from a given vapor phase composition it is important to take into consideration the stabilities of the source materials as described by Kisker and Zawadzki [130], similar to the above discussion of GaAsP growth. Kisker and Zawadzki also have pointed out the II-VI-VI' composition dependence based on the carrier gas used [130]. The above differences are only some of the factors that must be considered when growing II-VI materials by MOVPE. The reader is referred to the references for this section for more details on the growth of II-VI semiconductors.

3. The role of impurities

Dopants or impurities allow control of the electronic properties of semiconductors. In MOVPE carbon is an example of an unintentional dopant or impurity that originates from metal-organic sources. Other elements from the periodic table are intentionally introduced and can behave as donors, introducing an extra electron, or as acceptors, capturing an electron and thereby generating a hole. The generation of electrons or holes controls the resistivity of the layer and introduces static electric fields that can be engineered for a specific device. Since the focus of this chapter has been III-V materials, this section considers only dopants in these materials. II-VI materials have their own selection of donor and acceptor dopants and chemical trends with growth. The goal is to provide a review of the literature, identifying successes as well as highlighting pitfalls that are not reasonable areas for progress. Previous publications have significantly influenced the material and its organization [2; 131] .

As illustrated in Figure 5, dopants can incorporate into the growing material in different ways. This figure shows two ways, one in a linear fashion which can be considered ideal, and the other in a sub-linear fashion. For the linear case the resulting carrier concentration, either electrons or holes, is directly proportional to the input vapor concentration of the dopant source material. In the other case the resulting carrier concentration is not directly proportional to the source concentration and in the illustrated case it is sub-linear. As discussed below, these two cases are typical of many results but examples of more complex behavior have also been found. We present some details for a fairly comprehensive list of dopants but due to space limitations we cannot present all of the published results.

3.1. Group 2 - Alkaline Earth Metals

Beryllium and magnesium are the only two elements from Group II of the periodic table that have been used as dopants in MOCVD. Both form acceptors by substituting on the Group III site. Beryllium was used early in the development of MOCVD, but ithas seen very limited use due to its toxicity. Magnesium was investigated as an alternative to beryllium. The reactivity of magnesium compounds leads to strong memory effects with interior reactor surfaces that make abrupt profiles challenging to achieve. Magnesium found limited application until the explosion of work on wide-bandgap semiconductors. In AlGaInP, magnesium is the preferred acceptor dopant because it has less temperature sensitivity and a high distribution coefficient. For nitride-based semiconductors magnesium is the only acceptor dopant capable of generating reliable p-type doping.

3.1.1. Beryllium

Beryllium was known to be a good acceptor in GaAs from pre-existing MBE work. The early work with atmospheric-pressure MOCVD demonstrated beryllium incorporation using diethylberyllium (DEBe)

capable of achieving acceptor concentrations over $1x10^{20}$ cm^{-3} and producing abrupt profiles in GaAs [132; 133]. The high incorporation was attributed to the very low vapor pressure of Be metal at the growth temperature (2×10^{-12} Torr at 800°C). DEBe use was successfully extended to p-type AlGaAs with acceptor densities over $1x10^{18}$ cm^{-3} using 76 Torr MOVPE.[134] This work highlighted the challenges associated with using a low vapor pressure metal-organic source like DEBe (1 mTorr at 18°C)

DEBe was used to prepare p-type $In_{0.53}Ga_{0.47}As$ with acceptor densities approaching $8x10^{19}$ cm^{-3} using 70 Torr MOCVD. At growth temperatures of 500°C, Be produces abrupt doping profiles. At very high DEBe inlet partial pressure there are some indications of compensation associated with Be, potentially due to the transport of oxygen to the growth front [135]. Other work demonstrated nearly complete activation of incorporated beryllium to over $1x10^{19}$ cm^{-3} [136].

More recent work has utilized bismethyl cyclopentadienyl beryllium for the preparation of p-type InP. [137] For InP the acceptor concentration is limited to $4x10^{18}$ cm^{-3}, presumably due to the formation of inactive interstitial Be in the lattice [138]. While future device applications may require development of beryllium sources, no commercial sources of beryllium compounds are readily available perhaps due to their toxicity.

3.1.2. Magnesium

The earliest demonstration of the use of magnesium as an acceptor dopant in MOVPE was in GaAs. This report used bis-(cyclopentadienyl) magnesium (Cp_2Mg) and demonstrated four orders of magnitude of acceptor concentration before saturation of the carrier density was observed. At an acceptor density of $1x10^{19}$ cm^{-3}, pyramidal defects formed on the surface, probably associated with a magnesium-rich phase. [139] While magnesium can easily achieve high acceptor concentrations, it has strong turn-on and turn-off transients [140; 141; 142]. These temporal transients cause spatial variations in acceptor density through the doped layer and make abrupt dopant profiles challenging to achieve. In some cases these transients represent a non-ideality that must be accounted for, but in other cases it makes device fabrication impossible. Higher growth temperatures and higher Cp_2Mg gas phase concentrations reduce the turn-off transient [143]. It was speculated that Cp_2Mg adsorbs on the cooler surfaces of the reactor. By introducing baffles to vary the surface area of the growth chamber Kuech, *et al.* were able to show that quartz was the source of the adsorption sites, not the stainless steel of the gas injection manifold.[142] Cp_2Mg had similar challenges with InGaAs and InP. In InP the acceptor concentration is limited to $1x10^{18}$ cm^{-3}, even though atomic densities over $3x10^{19}$ cm^{-3} could be incorporated into the film [144]. InGaAs does not suffer the same deficiency and acceptor densities of over $1x10^{19}$ cm^{-3} were achieved [145].

For all of the deficiencies associated with Cp_2Mg and the alkyl-substituted analogs, it has found extensive application wide band gap semiconductors for light emitters. Magnesium is a much more efficient dopant than Zn in the AlGaInP alloy system. The elemental vapor pressure of Zn is over 0.1 Torr at 700°C, compared to Mg which is under 0.01 Torr at the same temperature. This effect was shown dramatically for doping $(Al_{0.4}Ga_{0.6})_{0.5}In_{0.5}P$ where it takes 200 times more Zn to achieve the same acceptor concentration [146]. This result is also supported by other researchers, suggesting that magnesium can be an efficient dopant for AlGaInP [147]. The turn-on transient was shown to be less severe in Al-containing materials and postulated that Al compounds compete with Mg compounds for adsorption sites in the MOCVD chamber [148] Reactive Si-O bonds could serve as adsorption sites for both Mg and Al leading to competitive absorption.

Achieving p-type doping in nitride semiconductors was a challenging problem. The earliest demonstration of p-conductivity in GaN was achieved by Amano and coworkers [77] P-type conductivity is not achieved in the as-grown film. Subjecting Mg:GaN to a low energy electron beam irradiation dissociated the as-grown Mg-H complex and produced modest p-type conductivity [77] This procedure was later replicated and extended to achieve record high acceptor densities of $3x10^{18}$ cm^{-3} in

GaN [149]. Later work by Nakamura *et al.*, showed that the Mg-H complex could be dissociated by thermal annealing [78].

An early vexing problem in GaN concerned why the acceptor density was limited to $1x10^{18}$ cm^{-3} or less. Temperature-dependent Hall measurements and defect spectroscopy identified energy levels in Mg-doped GaN that were 170 meV [150], 135-155 meV [151], and 112-190 eV [21] above the valance band depending on doping level. While this seems very deep when compared to other III-V materials, these experimental results are consistent with theory [152]. Results on AlGaN and InGaN also suggest that the acceptor level gets deeper as the band gap increases and shallower as it decreases [153]. Also, Mg seems to self-compensate if the atomic concentration exceeds $2x10^{19}$ cm^{-3}, [21; 154], which has been proposed to be associated with nitrogen vacancy complexes with magnesium [154]. These large Mg concentrations in GaN have been suspected to produce Mg-rich planar defects [155] and inversion domains [156].

The proprietary nature of nitride semiconductor technology keeps detailed reports out of the literature. The need to activate Mg:GaN complicates evaluation of doping trends in this system and makes identification of chemical trends difficult. This is because the wrong activation recipe can dominate the results [157]. Until very recently, GaN development has required heteroepitaxial growth on mismatched substrates, further influencing chemical trends. Kozodoy, *et al*., performed an early evaluation of magnesium incorporation into GaN on sapphire [158]. Near atmospheric-pressure atomic magnesium concentrations of $1x10^{19}$ cm^{-3} were obtained, producing acceptor concentrations of $8x10^{17}$ cm-3. The amount of Mg incorporated was independent of the growth rate or V/III ratio. Growth at 76 Torr resulted in an order of magnitude more magnesium incorporated into the film. The increase in magnesium concentration was attributed to reduced parasitic adduct formation at low pressures [159]. At low pressure, the acceptor concentration increased at low growth rates and higher V/III ratios, but the maximum concentration obtained was only one-quarter of the concentration obtained using atmospheric pressure growth. The increase in acceptor concentration was assigned to reduced compensation of the GaN film by residual donor defects, most likely nitrogen vacancies.[158]. The transient effects identified in cubic III-V materials are still present in GaN materials [160]. Magnesium redistribution appears to be more extreme due to the high temperatures required for GaN growth [161].

Magnesium sources such as bis(cyclopentadienyl) magnesium and dis(methylcyclopentadienyl) magnesium are readily available. Alkyl-substituted cyclopentadienyl ligands increases the vapor pressure of the source and in this case raise the melting point enough to produce a liquid at room temperature.

3.2. Group 12 - Volatile Metals

Zinc and cadmium were some of the first dopants used to achieve p-type GaAs. Both elements incorporate at the growth front as weakly bonded atoms making their incorporation sensitive to growth temperature through thermal desorption. Acceptors are formed when they replace a Group III element in the lattice. The vapor pressure of cadmium is over ten times larger than zinc at 700°C. Cadmium has found limited applications, while zinc is widely used for p-doping InGaAsP materials.

3.2.1. Cadmium

Cadmium was used to prepare p-type GaAs using atmospheric pressure MOVPE. The high vapor pressure of elemental Cd limits incorporation.[8; 162] Thermal desorption of cadmium was shown to be active in InP also. Only at temperatures below 550°C is desorption sufficiently low that saturation of the acceptor concentration could be observed. [163] Early reports identified cadmium incorporation to be proportional to the partial pressure of dopant in the reactor chamber for InP growth. [163; 164] This partial pressure can be high during atmospheric pressure growth leading to efficient incorporation, but is reduced significantly for low pressure growth. Raising the flow of dopant source solves this problem, but now produces the case where the dopant partial pressure is comparable to the partial pressure of the metal-organic source. Since the dopant is no longer a small perturbation on the undoped system, undesirable surface morphologies result. [164] While cadmium has limitations when applied to InP and GaAs

materials, it did find application in achieving controlled doping levels during atmospheric pressure MOVPE of InAsSb materials for p-n junction photodetectors.[165] Dimethylcadmium is readily available with a vapor pressure of about 30 Torr at 20°C.

3.2.2. Zinc

Zinc has a lower vapor pressure than cadmium making it a more viable acceptor dopant. The challenge zinc presents is its mobility once incorporated in the lattice. This is especially true for InP and to a lesser extent GaAs, and a great deal of effort was spent understanding the diffusion of Zn during layer growth and processing. Early work established the ionization energy of Zn acceptors at 25 to 30 meV in agreement with theoretical calculations. The acceptor ionization energy increases as the band gap increases in AlGaAs alloys. [166] The most thorough evaluation of zinc doping in GaAs was performed by Glew, who compared dimethyl zinc and diethyl zinc in 50 Torr MOVPE [167]. Acceptor concentrations in excess of $1x10^{20}$ cm^{-3} were achieved at dopant source partial pressures comparable to the TMGa partial pressure. Both zinc sources have similar thermal dependences. Below 575°C, zinc incorporation is independent of growth temperature. At higher temperatures, the doping concentration decreases with activation energies between 2 and 4 eV. [167] A more recent study of zinc doping reports a linear dependence with DMZn for acceptor densities less than $3x10^{18}$ cm^{-3}. This work reported a desorption energy of 3.2 eV. [168].

Zinc doping was extended to AlGaAs alloys using 100 Torr MOVPE with DEZn, showing no impact of alloying on zinc incorporation[169] Hageman, *et al*., extended the work on AlGaAs by performing a thorough evaluation of the effect of temperature and reactor pressure on zinc incorporation using DEZn. Linear incorporation for both GaAs and $Al_{0.45}Ga_{0.55}As$ were obtained. They confirmed that alloying aluminum has no impact on zinc incorporation. This work experimentally showed that higher partial pressures possible in atmospheric MOVPE leads to more zinc incorporation than in reduced pressure MOVPE. The activation energies for zinc desorption ranged from 2.6 to 4.1 eV. The authors go on to develop a kinetic model for zinc incorporation which is consistent with their observations [170].

Hsu investigated InP and $In_{0.5}Ga_{0.5}P$ using DMZn with atmospheric MOVPE reporting acceptor concentrations approaching $1x10^{19}$ cm^{-3} for both materials [171]. Kurtz, *et al*., evaluated the impact of growth conditions on zinc incorporation from DEZn into InGaP lattice-matched to GaAs using atmospheric pressure MOVPE. These studies were limited to the linear region for zinc incorporation, below $2x10^{18}$ cm^{-3}. They developed a kinetic model of the doping process that considered the attachment of zinc atoms at step edges and found the zinc concentration to be proportional to the product of the Group V surface coverage and the zinc partial pressure. The model explains some of the apparent inconsistencies in growth rate dependence for both InGaP and GaAs. The partial pressure of Group III species has very little effect on zinc incorporation. The Group V partial pressure controls the density of Group V terminated sites. This kinetic model is consistent with a thermodynamic mass action model [172].

Logan, *et al*., considered zinc doping of InP in depth. Specifically they were interested in understanding the saturation of zinc incorporation at high zinc source partial pressures. Using atmospheric pressure MOVPE they evaluated not only the typical (100) surface orientation, but considered the much less developed (110), (111)In, and (111)P surfaces. All surfaces show saturation of incorporated zinc, with levels for the (110) and (111)In surfaces exceeding $1x10^{19}$ cm^{-3}, compared to the $4x10^{18}$ cm^{-3} for (100) and the $1x10^{18}$ cm^{-3} for (111)P. The model developed was a surface-adsorption-trapping description that takes into account the dynamic nature of epitaxy, which is not accurately described by a static Langmuir surface-adsorption-desorption model. The conclusion is that zinc adsorption is limited to only a fraction of chemical adsorption sites on the surface as indium. When these limited sites are filled, no further zinc can be incorporated.[173] The model also shows how a wide range of apparent desorption energies can be obtained for even a simple chemical system. This work emphasizes the complexity of the MOVPE

process, but begins to show that fundamental understanding can be gained through careful experimentation and modeling.

Eisenbach, *et al*., investigated the growth of zinc doped $In_{0.53}Ga_{0.47}As$ on InP with low-pressure MOVPE. They identified conditions that produced acceptor concentrations in excess of $1x10^{19}$ cm^{-3} and that would limit diffusion of the grown-in Zn profile. Lower growth temperatures and higher growth pressures raised the saturation level, but also shifted the DMZn partial pressure where saturation was observed at the "knee point". To avoid zinc redistribution, it was necessary to keep the partial pressure below the "knee point". Higher growth temperatures are associated with indium vacancy formation during growth [174]. Zn doping of InGaAsP materials is largely independent of material composition. Doping is more efficient at higher chamber pressure, as established for GaAs. At 700 Torr, InP shows saturation at $1x10^{18}$ cm^{-3}, while InGaAs does not show saturation. Zinc incorporates linearly in InP and InGaAs below $1x10^{18}$ cm^{-3}. Zn doping is more efficient in InGaAs than in InP.[175]

Zinc has also been used as an acceptor in GaSb and its alloys with indium or aluminum. For GaSb, zinc incorporation over $1x10^{19}$ cm-3 has been demonstrated by both atmospheric pressure and 120 Torr MOVPE.[176; 177] The extension of zinc incorporation into InGaAsSb alloys has been performed [178].

3.3. Group 14 – Tetragens

It is ironic that some of the most important dopants for III-V materials come from this Group of the periodic table. Carbon is nearly the ideal acceptor dopant for GaAs and its alloys; silicon has many desirable characteristics as a donor. Germanium and tin have seen less application.

3.3.1 Carbon

The fate of carbon has been an important question for all materials deposited by MOVPE, especially when direct metal-carbon bonds are part of the source molecules. While carbon is a contaminant in MOVPE, the concentration is typically very low (under $1x10^{15}$ cm^{-3}) and can be controlled by the choice of growth conditions and precursor selection. The low concentration of unintentional carbon made analytical evaluation challenging. Still the device results obtained with MOCVD suggest that some carbon contamination is not detrimental. Carbon is the best intentional acceptor for GaAs and AlGaAs; truly a case where a liability has been made strength [179].

3.3.1.1. Unintentional carbon incorporation

Some of the earliest work looked at the impact that growth parameters have on carbon-related optical transitions in low temperature photoluminescence (PL). While PL is not rigorously correlated to acceptor concentration, when care is taken it can be a powerful comparative technique. PL is a semi-qualitative probe of the amount of carbon in films grown under different conditions. While the total integrated PL intensity increased as the growth temperature was increased from 600 to 800°C, the intensity of carbon-related emission increased as well, coinciding with increased carbon in GaAs layers. Increasing the AsH_3 partial pressure at a fixed TMGa partial pressure resulted in reduced carbon incorporation. Replacing H_2 with He resulted in no change in carbon-related PL or background acceptor densities. This suggests that atomic hydrogen from AsH_3 decomposition helps eliminate carbon, but molecular hydrogen does not participate in carbon elimination.[17] The source of unintentional carbon was further narrowed by experiments that introduced isotopically labelled hydrocarbons, like methane, into the growth ambient. No isotopically labeled carbon was found in the film produced, indicating strongly that carbon does not come from stable by-product decomposition, but from reactive intermediates.[180] The speculation at the time was that methyl groups decorate the growth surface. Atomic hydrogen or AsH_2 from AsH_3 decomposition combines with the methyl groups to form methane. To increase the concentration of AsH_3 decomposition products azo-t-butane was added to the growth ambient. The speculation was that azo-methane or t-butane, results in alkyl radicals that attack AsH_3 and produce AsH_2 and alkanes. The AsH_2 goes on to react with methyl groups to remove carbon from the growth front [181].

The addition of aluminum alkyls to form AlGaAs introduces a new wrinkle. The Al-C bond energy is slightly larger than the Ga-C bond energy. Carbon incorporation strongly increases with AlAs composition, increasing more than an order of magnitude from $Al_{0.1}Ga_{0.9}As$ to $Al_{0.75}Ga_{0.25}As$ at a growth temperature of 700°C and a fixed AsH_3 partial pressure. Carbon concentration increased an order of magnitude from 600°C to 700°C for $Al_{0.75}Ga_{0.25}As$. Hole densities show a maximum with temperature between 700 and 750°C [182].

Further insight into carbon incorporation came from examining the limits of the growth conditions. This work was motivated by an interest in high carbon concentrations for device applications. Carbon incorporation of $6x10^{19}$ cm^{-3} was demonstrated using AsH_3 and TMGa and low temperatures and very low V/III ratios. The carbon concentration dropped rapidly going from V/III = 1 to V/III = 2. Under these conditions significant hydrogen incorporation was observed. This result suggests that carbon is not incorporated as an atomic species, but rather from methyl radical decomposition to a carbene species. [183] Similar investigations examined the temperature dependence between 560 and 700°C under very low V/III ratio using TMGa and AsH_3 , achieving $1x10^{20}$ cm^{-3}. At V/III = 1.6, the acceptor concentration increased with increased temperature, but at V/III = 2.7 the acceptor concentration decreased monotonically as the temperature increased. The acceptor density decreased as the V/III increased from 1 to 4 at a fixed temperature [184].

The trends established for intrinsic carbon incorporation into GaAs were extended to $Al_{0.5}Ga_{0.5}As$ with the goal of forming p-type AlGaAs without the need for extrinsic doping. The study considered the effect of Al composition, growth temperature, and V/III ratio as parameters. For a V/III = 4.3 and a growth temperature of 600°C a linear increase in carbon with Al composition occurred. Carbon incorporation is a strong function of temperature and a V/III between 1 and 10. The growth rate in this regime is activated. Low V/III ratios between 1 and 2.6 produce acceptor concentrations approaching $1x10^{20}$ cm^{-3}. At V/III ratios of 5.2 and 10.4 carbon concentrations decreased at high temperatures. Carbon incorporation increases at lower V/III, but saturates below a V/III = 2, for temperatures between 550 and 650°C [185].Unintentional carbon doping of GaN has been mentioned in Section 2.2.3.2.

3.3.1.2. Alternative AsH_3 sources

The use of AsH_3 for MOVPE of arsenides is a significant liability due to its high toxicity. The impact of metal-organic arsenic sources has been investigated, not only for hydride replacement, but as a way to modify the growth ambient to incorporate more carbon. Trimethyl arsenic (TMAs) was investigated for controlled carbon incorporation. An extended study of the thermochemistry of alkyl substituted arsine sources was performed at atmospheric pressure using mass spectrometry to evaluate source stability and the reaction products [186]. This study determined that tertiarybutyl arsine (TBAS) was the most likely AsH_3 replacement, because it generates AsH_2 intermediates. The tri- and di-alkyl substituted arsenic metal-organics generated products with As-C bonds which likely lead to carbon incorporation.

Intentional carbon incorporation in Group III arsenide materials has also been examined using TMAs or mixtures of TMAs and AsH_3. Carbon incorporation using TMAs and TMGa has a strong temperature dependence, with the hole concentration decreasing two orders of magnitude going from 600 to 700°C. The addition of small amounts of AsH_3 to the growth ambient, resulted in a progressive decrease in the hole concentration. This study highlights the importance of active hydrogen from AsH_3 decomposition in eliminating methyl radicals from the growth surface. Both TMAs and TMGa are nearly fully decomposed at growth temperatures, suggesting that the decomposition products are responsible for carbon incorporation [187]. In a separate study using low pressure MOVPE with TMAs and TMGa it was found that carbon incorporation increases as total chamber pressure decreases. Carbon incorporation increased with growth rate (TMGa partial pressure) at fixed TMAs partial pressure, but decreased slightly for increased TMAs at a fixed TMGa partial pressure. Carbon incorporation decreased with increased growth temperature for both growth with AsH_3 and with TMAs between 500 and 600°C. Little change in carbon concentration occurs at higher V/III ratios for growth with TMAs, while for AsH_3 the carbon

concentration is reduced at higher V/III [188] When TMAs is used as the arsenic source the only sources of atomic hydrogen are from the carrier gas and hydrocarbon decomposition.

In conjunction with experimental efforts on carbon incorporation significant computational work was performed in an effort to understand the microscopic processes that contribute to carbon incorporation. This work reproduced doping trends with temperature, V/III ratio, and the additions of AsH_3 to TMAs-TMGa. The proposed reaction set, for both gas phase and surface is exhaustive, but the conclusion of the work is that $GaCH_2$, gallium carbene, is the species responsible for carbon incorporation into GaAs. This work represents a milestone in the chemical understanding of MOVPE [189].

The only metal-organic arsenic source to show significant promise for AsH_3 replacement was TBAs. Early demonstrations showed that high purity GaAs with carbon concentration similar to obtained with AsH_3 could be obtained using both atmospheric pressure and low pressure MOVPE with either TMGa or TEGa [190]. While TBAs reduces the toxicity hazard represented by AsH_3 it does not eliminate the hazard as TBAs is a high vapor pressure liquid with many of the same concerns. In addition, concerns over the commercial availability of TBAs has limited wide spread adoption. Carbon incorporation into GaAs using TMGa and TBAs is limited for V/III > 10. For lower V/III, the acceptor concentration increases with decreasing V/III. For V/III of 2.5 and 1.6, the carbon concentration decreases with increased temperature. For a V/III ratio of 2.5, carbon concentrations of over $1x10^{18}$ cm-3 were obtained at 500°C, while for V/III = 1.6, $7x10^{18}$ cm^{-3} is obtained at the same temperature. Temperatures below 560°C were needed to get good morphology for V/III < 2.5 [191].

3.3.1.3. Halocarbon sources

Experimental confirmation that alkane hydrocarbons are stable at MOVPE growth conditions eliminates them as intentional carbon sources. Fluoride forms a molecule with similar chemical stability to alkanes and has not been successfully used as a carbon source. Chloride, bromide, and iodide substituted hydrocarbons have been used successfully. Iodide substituted hydrocarbons were some of the first to be used as intentional carbon sources. Methane diiodide (CH_2I_2) was a successful carbon source, but methane monoiodide (CH_3I) was not. Decomposition of CH_2I_2 produces a carbene group bonded to the surface gallium atom. CH_3I leads to methyl groups on the surface that can be hydrogenated completely by atomic hydrogen. The removal of the carbene is more difficult and leads to carbon incorporation [192]. CH_2I_2 is not an ideal source for MOVPE as it has a low vapor pressure (0.7 Torr at 20°). Carbon tetrachloride (CCl_4) has a much higher vapor pressure, nearly 100 Torr at 20°C. Early work showed that carbon concentrations over $1x10^{19}$ cm^{-3} were possible. Carbon incorporation was linear with the CCl_4 partial pressure in the chamber. This work showed that while carbon incorporation decreases with increased growth temperature in GaAs, $Al_xGa_{1-x}As$ showed progressively less temperature dependence as the Al composition increased. The authors suggest that CCl_4 undergoes homolytic fission of the C-Cl bond leaving a reactive CCl_y, where y < 3. It was speculated that the difference in incorporation for AlGaAs compared to GaAs is due to the increased Al-C bond strength compared to Ga-C on the surface [193]. The exploration of CCl_4 was extended to atmospheric pressure MOVPE, which showed a sub-linear incorporation out to $1x10^{20}$ cm^{-3}. The sub-linear trend is suggestive of surface site saturation at higher CCl_4 partial pressures. The authors were the first to report on the etching effect of CCl_4, reporting a 20% growth rate reduction when the TMGa/CCl_4 ratio > 10 [194]

The seminal work on use of halomethane for carbon incorporation into GaAs considered many of the tetra, tri, and di substituted sources [195]. The work developed several trends that are important for selecting carbon doping precursors. Using 78 Torr MOVPE over a wide range of temperatures (600 to 750 C) and V/III ratios (30 to 100), the authors compared CCl_4, $CHCl_3$, CH_2Cl_2; CBr_4 and $CHBr_3$; CI_4, CHI_3, and CH_2I_2. Carbon incorporation decreases with higher growth temperature and higher V/III for all sources. The activation energy for carbon is between 1.3 and 2.6 eV. The dependence on V/III is generally $C \sim (V/III)^k$, where k < -1. Carbon incorporation was conclusively identified as being from the halomethane and not from a concerted reaction with TMGa, by using ^{13}C-labeled TMGa. The efficiency

of the halomethane source goes like $CH_3X < CH_2X_2 < CHX_3 < CX_4$. The proposed reaction mechanism for carbon incorporation from halomethanes is a competition between decomposition of the adsorbed species and desorption. $CHCl_3$ is a less efficient carbon source than CCl_4 in GaAs. Brominated methane has a similar efficiency. CCl_4 and CBr_4 are the most efficient carbon sources while other sources are less efficient [195].

The saturation of carbon acceptor concentration was investigated in GaAs grown with 60 Torr MOVPE using a vertical rotating disk reactor at 700 rpm. The work investigated temperatures of 430 to 540 °C at a V/III of 8 to 230. Lower acceptor concentrations show a linear dependence on CCl_4 partial pressure, but for higher acceptor densities sub-linear incorporation is observed. This work eliminated carbon donor deactivation by hydrogenation as the source of the sub-linear acceptor incorporation. The work also rejected the compensation of carbon acceptors by carbon donors based because there was no indication of hold mobility reduction. Saturation of carbon incorporation in SIMS measurements is the source of acceptor saturation. The results are consistent with surface site saturation due to competitive adsorption of C and As a saturation limit of $2x10^{20}$ cm^{-3} [196].

Extending the earlier work on intrinsic carbon incorporation on different substrate orientations, early trends for carbon incorporation with CCl_4 into GaAs grown on substrates different from (100) gave fundamental insight. Carbon incorporation is enhanced for growth on (111)A surfaces and reduced for (111)B surface.[197] Kondo, *et al*. report the same trend, but followed the trend with much finer resolution. For miscuts from (100) toward (111)A or (111)B, carbon incorporation initially drops. The origin of this drop is attributed to enhanced AsH_3 decomposition. For the (311)A surface carbon incorporation increases dramatically. For the (311)B surface further decrease in carbon incorporation is reported. In the case of (111)B, the carbon density increases slightly compared to the (311) surface, but is still significantly less than the (100) surface. Similar trends were reported for $Al_{0.35}Ga_{0.65}As$ [198].

One persistent issue with using CCl_4 to obtain high carrier densities over $1x10^{19}$ cm^{-3} is that the growth rate obtained is always less than the one obtained for undoped GaAs or AlGaAs. Early demonstrations using 80 Torr MOVPE found that the growth rate decreased linearly with the partial pressure of CCl_4 with a maximum reduction of 40% at a growth temperature of 600°C.[199] Quantitative investigations of GaAs etching were performed using gravimetric measurement of GaAs deposited on quartz tubes. Since this is only an etching experiment, without film growth to incorporate carbon GaAs was etched to form $GaCl_3$ the more fully oxidized state of gallium. For growth experiments surface science techniques coupled with the gravimetric analysis indicated that a less oxidized GaCl was formed consistent with chloride reaction with less strongly bonded surface Ga. GaCl is expected to form during MOVPE conditions [200].

Efforts to find a halogen-carbon source that does not lower growth rates as much as CCl_4 have led researchers to consider other halomethane sources. CBr_4 has been investigated for this purpose using 52 Torr MOVPE with TMGa and AsH_3. No impact on growth rate was identified at temperatures of 600 or 670°C. Higher growth temperatures led to reduced carbon incorporation. Increasing the V/III ratio at fixed growth rate led to reduced carbon incorporation as expected, but no change in growth rate was identified. At low V/III, some growth rate reduction was found, believed to be associated with limited As partial pressure [201]. Investigations were undertaken of carbon incorporation into GaAs and AlGaAs on (100), (311)A, and (311)B using 76 Torr MOVPE with TMGa, TMAl, AsH_3, and CBr_4. Carbon incorporation is linear for CBr_4 flows investigated. For GaAs the (100) and (311)A had the largest incorporation, while the (311)B had less incorporation, consistent with results for CCl_4 . AlAs followed the same trends only the magnitude of the reduction for (311)B was larger. For both GaAs and AlAs, carbon incorporation decreased with increased temperature for both (100) and (311)A. For (311)B, carbon in GaAs decreased as well, but for AlAs on (311)B the carbon increased. Carbon decreased with increased V/III for all surfaces.[202] Another alternative carbon source is $CClBr_3$. [203].

3.3.1.4. In alloys – InGaAs, InAlAs, InAs – problems with carbon doping

In spite of the good characteristics carbon displays in GaAs and AlGaAs it generates serious problems with indium containing materials. Carbon can form compensating donors by incorporating on the Group III site [204]. Some of the most dramatic problems came from trying to use CCl_4 in the atmospheric pressure MOVPE of $In_{0.53}Ga_{0.47}As$ on InP and $In_{0.5}Ga_{0.5}P$ on GaAs. For InGaP, CCl_4 leads to InP etching and deterioration of the film surface due to loss of lattice-matching. InP doped with CCl_4 has a dopant level comparable to the undoped background level, suggesting no carbon was incorporated. This early result suggests that carbon incorporation will be challenging for indium containing compounds [205]. For InGaAs, p-type InGaAs, was possible only for InAs compositions of 0.1 or less, otherwise n-type conduction was obtained. The addition of CCl_4 to the growth chamber resulted in the depletion of indium in the film. In general CCl_4 is not a viable source for atmospheric MOVPE of In-containing compounds [206].

The motivation to use carbon with $In_{0.53}Ga_{0.47}As$ on InP is driven in part by the desire to use it in the base layer of npn HBT structures for high-speed electronics. Other applications would use this, but much of the literature reports focus on this use. For low pressure MOVPE carbon incorporation is possible at higher In composition. No degradations were identified out to $In_{0.12}Ga_{0.88}As$ on GaAs, and hole concentrations of $1x10^{20}$ cm-3 were obtained. Additional InAs resulted in a decline in the maximum acceptor density. $1\ x10^{18}\ cm^{-3}$ was achieved in $In_{0.53}Ga_{0.47}As$ on InP. All of this work required low temperature (500 to 550°C) and low V/III ratios (5 to 15). The hole concentration decreased going from V/III = 3 to V/III = 15 [207]. Another issue with InGaAs is that InCl is formed preferentially over GaCl, requiring the gas phase TMIn/Group III ratio to be adjusted to maintain lattice match. Under these conditions hydrogen passivation of carbon becomes an issue and carbon may form inactive clusters. [208]. Following the trends with GaAs and AlGaAs, CBr_4 was used to achieve p-type $In_{0.53}Ga_{0.47}As$ on InP. While this was achieved the conditions used were not optimal and hydrogen passivation remained a problem [209]. Efforts to get carbon on the right site in InGaAs led to the use of TMAs as had been done for GaAs. Reports using 15 Torr MOVPE with TMIn, TEGa and TMAs with CBr_4 could not get InGaAs to grow. The replacement of TMAs with AsH_3 allowed growth to occur [210]. The lack of growth with TMAs is attributed to limited TMAs decomposition. Growth was performed at both atmospheric and 200 Torr MOVPE using TMGa, TMIn, and TMAs. InGaAs grown with TMAs was n-type, just like with AsH_3, but the mobilities are much lower suggesting significant compensation [211].

While the use of CBr_4 with InGaAs can be considered only a marginal improvement compared to CCl_4, it has been used to good effect for other In-containing alloys. CBr_4 was used to incorporate carbon into AlInAs using 60 Torr MOVPE with TMIn and TMAl and AsH_3. A growth temperature of 530°C and V/III ratio of 20 lead to significant carbon incorporation, $3\ x10^{19}\ cm^{-3}$. Higher temperatures or V/III ratios resulted in less carbon being incorporated. With these conditions one gets a nearly linear incorporation of carbon, but increasing the CBr_4 resulted in a decreased growth rate. The composition of the film was not affected by the increased flow of CBr_4, suggesting that Br etches both Al and In equally. [212] This is very strange as one would expect In to etch more readily than Al. Activation of carbon is still an issue in AlInAs. The acceptor density is one order of magnitude less than the carbon concentration determined by SIMS. Annealing the sample in N_2 either in situ or in RTA resulted in hydrogen removal and up to 60 % of the carbon being activated.

3.3.1.5 GaAsSb and GaSb – possible solutions

While the efforts to incorporate carbon into $In_{0.53}Ga_{0.47}As$ met with limited success an alternative material was being developed for the npn HBT application. GaAsSb can be lattice matched to InP. While there are issues associated with GaAsSb that can make it challenging to grow, it can be easily doped with both CCl_4 and CBr_4. The earliest efforts to use p-type GaAsSb showed the potential for InP/GaAsSb/InP HBTs [213]. Subsequent work investigated the growth of carbon-doped GaAsSb on InP using 100 Torr MOVPE with TEGa, TMSb, and TBAs. This work compared CBr_4 to CCl_4. The hole mobilities obtained were much lower than expected and this was attributed to the high scattering potential. Little variation in hole mobility with carrier density was observed, further indicating the importance of alloy

scattering compared to ionized impurity scattering. There is an observed linear increase in conductivity with carrier density up to $1x10^{20}$ cm^{-3}. The carrier density is slightly sub-linear at the conditions investigated. The Sb composition decreases with increased CCl_4 flow and the growth rate is reduced by a factor of two at the highest CCl_4 flows consistent with GaCl formation. The Sb composition decreased and the acceptor density decreased with increased V/III. [214] Interest in GaAsSb as an alternative base layer led to evaluation of carbon incorporation into GaAsSb using CBr_4. Using 60 Torr MOVPE with TEGa, TMSb, and AsH_3 and growth temperatures between 470 to 500°C, this work identified that with increasing CBr_4 partial pressure both the growth rate and the GaSb composition decrease. This is associated with preferential etching of GaSb compared to GaAs. The etch rate of GaSb is estimated to be three times larger than that for GaAs. The growth rate is independent of V/III, but the GaSb composition decreases with higher V/III [215]. A further advantage of C:GaAsSb is that there appears to be less hydrogen passivation of carbon acceptors for growth temperatures above 530°C.

The natural extension of this work was to incorporate carbon into GaSb. Using conditions similar to those used for GaAsSb, linear incorporation over four orders of magnitude were observed. There is a larger strain effect for GaSb than for GaAs due the size difference between Sb and C, compared to As and C. Acceptor densities over $1x10^{19}$ cm^{-3} could easily be obtained [216] Subsequent work established that carbon has an ionization energy of between 8 and 13 meV in GaSb [217].

3.3.2 Silicon

In contrast to carbon, silicon is a donor in most III-V materials. Typical MOVPE sources are silicon hydrides diluted in a high pressure gas mixture. The simplest hydride source is silane (SiH_4), which decomposes into silylene and hydrogen according to the reaction $SiH_4 = SiH_2 + H_2$. The decomposition of silane is a thermally activated process [218]. Early investigations produced activation energies that varied widely with chamber conditions from 0.5 to 2 eV [219-222]. This wide variation in activation energy has been assigned to various sources; the most likely one being coupled kinetics of silicon incorporation to the diffusion to the wafer surface of a rate limiting species. For silane, the temperature dependence was imposed on the modest temperature nonuniformity in early MOVPE systems which resulted in significant spatial variation in dopant concentration. In the early development of MOVPE, silane was the only convenient source for silicon. Silicon incorporation into GaAs and AlGaAs is proportional to the input silane partial pressure and no significant memory effect is observed [219; 223]. Silicon incorporation goes down with both increased TMGa partial pressure and increased AsH_3 partial pressure. The dependence on the TMGa partial pressure is consistent with prediction from mass action, but the hydride dependence is suggestive of the role hydrides play in silicon incorporation. The decrease with increased AsH_3 is associated with either AsH_3 displacing SiH_2 on surface or the heterogeneous formation of monosilyarsine (SiH_3AsH_2) formation and removal from chamber [224].

Silicon typically incorporates on the Group III site. At very high carrier densities compensation mechanisms start to become active. An evaluation of these mechanisms was performed in atmospheric MOVPE using TMGa, AsH_3, and silane. Linear incorporation of donors from silicon up to $1x10^{19}$ cm^{-3} is achieved, but is followed by a decline. Atomic silicon incorporation is linear above $1x10^{19}$ cm^{-3}, as determined by SIMS. Below $1x10^{19}$ cm^{-3} the main compensation mechanism is Si_{As} acceptors, but above $1x10^{19}$ cm^{-3} Si-V_{Ga} complex defects start to form. Only at silane partial pressures of 0.1 Torr, much above the compensation point does the lattice constant of epitaxial GaAs change measurably. It was noted that no memory effect was identified with silicon, even for conditions that produce lattice dilation [225]. In general atmospheric MOVPE can get higher donor densities, $1x10^{19}$ cm^{-3}, where low pressure MOVPE is limited to $5x10^{18}$ cm^{-3}. This is probably due to the higher Group V partial pressure and lower Group III partial pressure used in low pressure MOVPE that favors Si-V_{Ga} defects leading to compensation.

A potential solution to the thermal sensitivity of silicon incorporation came from development of lower temperature sources for silicon epitaxy. Disilane was developed for this purpose and readily applied to

III-V growth. The earliest demonstration of disilane as a dopant in 78 Torr MOVPE showed that silicon incorporation was independent of growth temperature over a range of temperatures between 600 and 800°C. As with silane, incorporation is linear with source partial pressure up to a carrier density of 5E18 cm^{-3} [226]. This early work was extended to look at the effect of surface orientations other than (100) on silicon incorporation. Silane has a strong surface orientation dependence with more silicon being incorporated on the (111)B surface than on the (100) and even less silicon being incorporated on the (111)A. This sensitivity was not observed with disilane. This result indicates that while silane decomposition is heterogeneous and depends on the density of surface sites, disilane decomposition likely occurs in the gas phase and does not have the same incorporation mechanism [227].

More thorough evaluation of the effect of pressure and reactor residence time on silicon incorporation from disilane highlights the complex phenomena present. Low pressures (1 to 10 Torr) display thermally activated decomposition with activation energies similar to what had been observed for silane. At higher pressures (10 to 100 Torr) a temperature independent region can be identified. Shorter residence times reduce disilane decomposition [220]. Other investigations indicate that the design and operation of the growth chamber can impact silicon incorporation from disilane. The use of disilane with atmospheric pressure horizontal MOVPE displays reactor dependent results [222], while atmospheric vertical rotating disk systems report regimes of temperature independent incorporation [228]. This strongly suggests coupled mass transfer and kinetics as the source of variable behavior. The importance of silylene in silicon incorporation was identified and the formation of monosilylarsine was advanced as the critical species for silicon incorporation [229]. A later result presented a simplified analytical evaluation of the pressure effect [230]. These analysis explain why variable activation energies are obtained. The analytical treatments suggest that reactor design and operating conditions can strongly influence doping incorporation in MOVPE systems.

As identified previously TBAs is an alternative source for arsenic. TBAs also positively impacts silicon incorporation because it readily forms AsH_2. The temperature dependence of silicon incorporation from TBAs and silane is less and the efficiency of silicon incorporation is higher than with AsH_3. This work determined that the increased efficiency is not due to tertiarybutyl silane formation, but due to enhanced formation of monosilyarsine [231]. Residence time studies further suggested that silicon incorporation with silane and TBAs is not limited by gas phase reaction, but by heterogeneous reaction on the wafer surface. Additions of AsH_3 to TBAs and silane leads to reduced incorporation efficiency. [232].

While a great deal of work has been done unraveling the chemistry of silicon incorporation into GaAs, silicon has been investigated for other III-V materials as well. Significant investigations have been performed with silane and disilane for InP and lattice matched $In_{0.53}Ga_{0.47}As$. A linear dependence on silane partial pressure was determined for atmospheric pressure MOVPE of InP[171]. In the case of GaAs there is a slight decrease in silicon incorporation with increased AsH_3 partial pressure. This was not identified for InP and might be due to the lower rate of decomposition for PH_3 compared to AsH_3 [233]. A comparison of InP to $In_{0.53}Ga_{0.47}As$ with atmospheric pressure MOVPE identified that silicon incorporation is more efficient in InP. This work established linear trends with disilane partial pressure. Below 600°C silicon incorporation from disilane exhibits thermally activated incorporation into InP, but above this temperature the temperature dependence is weak. This work also supported the claim that no hydride partial pressure dependence was observed [234]. Results from 75 Torr MOVPE also confirmed the transition from activated incorporation, with an energy of 2.6 eV, to temperature independent silicon incorporation at 620°C. The key observation from this study was that while only 50% of the silicon incorporated produces a donor while the solubility of silicon in InP is very high allowing carrier densities of $1x10^{19}$ cm^{-3} to be obtained[235]. Silicon incorporation into $In_{0.53}Ga_{0.47}As$ using disilane and TBAs shows coupled kinetics and mass transport effects. As with GaAs, using TBAs instead of AsH_3 leads to more efficient silicon incorporation presumably to easier formation of monosilyarsine. The challenge with $In_{0.53}Ga_{0.47}As$ is that no temperature independent incorporation regime could be identified. Xu, 1997 #538}. InGaP lattice matched to GaAs grown with 15 Torr MOVPE has many of the characteristics of

InP. A linear incorporation with disilane partial pressure and higher incorporation efficiency was observed. Carrier densities of 8E18 cm^{-3} were obtained. The key result for InGaP was that no donor-related DX center could be identified, making this alloy a viable replacement for AlGaAs that is plagued by DX centers.

Silicon is the most widely used donor in GaN, allowing carrier densities over $1x10^{19}$ cm^{-3} to be obtained [236]. Silicon incorporation into GaN and $Al_{0.1}Ga_9N$ are linear in silane partial pressure. Other studies produced lower carrier densities of $5x10^{18}$ cm^{-3} for Si:GaN and $1x10^{18}$ cm^{-3} for Si: $Al_{0.1}Ga_9N$. Silane partial pressures above these limits resulted in degradation in surface morphology, presumably due to SiN formation. [237] The incorporation of silicon from silane increases with reactor pressure and decreases with increased NH_3 partial pressure. While these trends are similar to what has been observed for cubic systems at lower growth temperature, it is difficult to believe that the same mechanisms are operative in GaN that is grown at temperatures 300°C warmer. Silicon incorporation into AlGaN alloys is critical for light emitters. While this alloy can be doped with silane, there is an increase in the ionization energy with composition. It is unclear if this is similar to the DX center that plagued AlGaAs or if it has a different origin, unique to the nitride semiconductors. [238] The energies of the silicon donor in AlGaN may be associated with higher ionization states of the V_{Al} defect [239].The use of disilane, which was an important discovery for cubic III-V, was evaluated for GaN. Because GaN is grown at such a high temperature the use of disilane presented limited advantage. High carrier densities over $1x10^{19}$ cm^{-3} are obtained with linear incorporation [240].

The theme with the use of silicon as a donor dopant is that it interacts strongly with hydrides to incorporate efficiently with little compensation. GaSb presents a challenge for silicon as there is no hydride to direct incorporation because metal-organic antimony is used. Studies that have attempted to incorporate silicon into GaSb have identified it as an acceptor [241]. In addition, silicon has been used as an acceptor in $In_{0.2}Ga_{0.8}Sb$ [242].

3.3.3 Germanium

Germanium has similar source chemistry as silicon. In contrast to silicon, little work has been done. Germanium is a donor in GaAs and GaN grown by MOVPE, which were the only studies identified in our review of the literature. The result from these investigations was not encouraging. Unlike silane, germane decomposes completely at MOCVD growth temperatures to elemental Ge and hydrogen gas. Germanium is a low vapor pressure element and once it deposits on the surface there are few opportunities for reconfiguration into the lattice into a specific site. This leads to significant compensation, resulting in low carrier mobility when compared to silicon doped material [221]. Germanium was investigated for n-type doping of GaN and showed that germanium does form a donor in GaN that can achieve carrier concentrations of $1x10^{19}$ cm^{-3}. At the temperatures used for GaN growth both SiH_4 and GeH_4 are completely decomposed to elemental Ge or Si and hydrogen and the higher temperature increases the elemental vapor pressure enough that there is opportunity for germanium to incorporate into correct sites for donor formation. The problem identified with germanium is that above $1x10^{19}$ cm^{-3}, pits formed in the film. The other issue with Ge in GaN is that about an order of magnitude more GeH_4 was needed than SiH_4 to achieve the same carrier density [236]. This could be due to germanium re-evaporation or GeN formation.

3.3.4 Tin

Tin was investigated early in GaAs MOVPE development using both atmospheric and low pressure systems. Carrier concentrations above $1x10^{19}$ cm^{-3} were easily demonstrated with linear incorporation up to $1x10^{19}$ cm^{-3}. Tetrametyl tin (TMSn) was used in these early demonstrations [132; 243-245] TMSn has very high vapor pressure (100 Torr at 20°C). Tetraethyl tin (TESn) was demonstrated for doping InP and InGaAs with atmospheric MOCVD [246]. Carrier concentrations of $3x10^{19}$ cm^{-3} in InP and $6x10^{19}$ cm^{-3} in lattice-matched InGaAs were demonstrated. Similar results were obtained by low pressure MOCVD [247]. TESn has a significantly lower vapor pressure (0.5 Torr at 20°C) than TMSn making partial

pressure control easier. In addition to these traditional materials, tin has been used in low band gap materials such as InAs and InSb [248]. It has also been used to demonstrate n-type conductivity in AlAsSb for use as electron barriers [249].

While tin does produce higher carrier densities than Si, it does have a thermal dependence associated with TESn decomposition. Tin may form a segregation layer on the film surface when trying to achieve high carrier densities. Segregation layers impact the profile abruptness leading to turn-on and turn-off transients. A problematic segregation layer occurs when Sn is used in MBE. Investigations performed at atmospheric pressure strongly suggest that no segregation layer forms [243; 246]. However, results using low pressure MOVPE hint that some segregation layer is present for carrier densities over $3x10^{19}$ cm^{-3} [245]; [244]; [247] The source of the segregation layer is not shown in the literature, but comparison of the different results suggests that the low pressure results use a larger metal-organic tin partial pressure, which may lead to segregation layer formation that can be avoided at the lower partial pressures used in atmospheric pressure MOVPE.

3.4 Group 16 – Chalcogens

Chalcogen donor dopants are unique to MOVPE. They incorporate on the Group V site in high concentrations. Their high elemental vapor pressure makes them difficult to control in MBE applications, but chemical sources are readily available for MOVPE. Hydrides of sulfur and selenium, H_2S and H_2Se are used in quantity for the fabrication of ZnS and ZnSe optical materials. These gases are highly toxic, a familiar hazard in MOVPE technology. H_2Te is unstable under most conditions leading to the development of tellurium metal-organics. For cubic III-V materials, oxygen forms several energetically deep levels in the band gap. This makes it unsuitable for any applications, except generating high-resistivity layers and generating films with low carrier lifetimes for ultrafast optoelectronics. Oxygen has been shown to be a shallow donor in GaN [250].

3.4.1 Sulfur

Hydrogen sulfide (H_2S) was investigated for doping GaAs using atmospheric MOVPE. Sulfur displaces atoms from the Group V sublattice. The incorporation increases linearly with H_2S partial pressure and decreases with increased AsH_3 partial pressure. This behavior is consistent with what would be expected from mass action. The decrease in carrier density at a fixed H_2S partial pressure with increased growth temperature is consistent with the evaporation of sulfur from the growth surface [251]. While this is a kinetic process it can be controlled by diffusion leading to variable activation energies, between 0.9 to 1.5 eV, as in the case of silane [219]. The linear incorporation of donors with H_2S partial pressure becomes sub-linear at high temperature and high H_2S partial pressure. Since the atomic concentration of sulfur continues to increase linearly with H_2S partial pressure it is concluded that the sub-linear carrier density is associated with compensating defect formation. The sub-linear increase in carrier density with increased TMGa partial pressure was associated with the competition between forming simple sulfur donors, that replaced As in the lattice, and compensating S_{As}-V_{Ga} acceptor complexes. As the TMGa partial pressure is raised the quantity of V_{Ga} centers is reduced. The amount of sulfur incorporated changes little, but the activation of the sulfur incorporated is increased [225]. Consistent with the theme of a kinetically limited doping process, sulfur is strongly dependent on the density of surface sites generated by the substrate miscut for both GaAs and InP. In both cases the sulfur incorporation is strongly enhanced by miscuts toward the (111)B. Incorporation was suppressed slightly for miscuts toward (111)A [252].

In addition to GaAs, H_2S was investigated for InP compounds. Using 100 Torr MOVPE at 600°C and a V/III = 100 linear incorporation was shown. Carrier densities of $3x10^{18}$ cm^{-3} were demonstrated with linear incorporation. At the partial pressures required some memory effect was reported [253]. Sulfur doping was extended to InGaAs and InGaAsP alloys using both 76 Torr and atmospheric MOVPE. At 76 Torr InP shows saturation of the carrier density at $3x10^{18}$ cm^{-3}, but InGaAs and InGaAsP don't show the same behavior. Atmospheric pressure has higher efficiency; less H_2S is needed to achieve the same carrier density [175].

3.4.3 Selenium

While the chemistry of hydrogen selenide (H_2Se) is similar to H_2S it does not have the same kinetic problems that impact incorporation. H_2Se is fifty times more efficient than H_2S for incorporating donors into GaAs [254]. H_2Se does have significant memory effects related to its reaction with stainless steel that has hampered its adoption as an n-type dopant [140; 255]. Kinetic models for Se incorporation from H_2Se in GaAs correctly predict selenium incorporation should be linear with H_2Se partial pressure, independent of Group III partial pressure, and scales inversely with Group V partial pressure. These predictions are supported by Se:GaAs grown at atmospheric pressure. The outgrowth of this model was the determination that Se atoms are not accumulated while dosing the surface with a background Group V partial pressure making delta doping with H_2Se impossible [256]. The thermal dependence of Se incorporation is independent of temperature above 650°C, but increases slightly at lower temperatures. This is inconsistent with evaporation of volatile Se atoms from the surface and suggests the formation of strongly bonded surface species [257].

A similar evaluation was performed using 20 Torr MOVPE, showing a linear increase in incorporation as the partial pressure of H_2Se was increased and a sub-linear increase in the carrier density with increased TEGa partial pressure. The authors speculate that the TEGa dependence comes from the increased density of V_{As} with increased gallium partial pressure. A more likely source of the increase is reduced compensation due to the formation of V_{Ga}-Se complexes similar to what has been shown to be active with sulfur doping, as the partial pressure of Ga goes up the density of V_{Ga} should decrease and the incorporation of Se donors should increase. The temperature dependence of selenium incorporation was evaluated and shows a significant activation energy similar to what has been observed for SiH_4. While the authors speculate that this is attributed to shifts in bulk stoichiometry, it is more likely associated with reduced gas phase kinetics associated with the chamber pressure used [258].

Early demonstrations used H_2Se in atmospheric pressure MOVPE of AlGaAs over most of the composition range. This work identified the increase in ionization energy of the donor increasing to 300 meV at the midpoint of the alloy system [259]. The memory effects identified with GaAs are also present in AlGaAs, although the transients are less severe due to either the reaction of H_2Se with TMAl or the displacement by adsorbed TMAl on internal reactor surfaces. H_2Se was shown to adsorb on any internal surface by using graphite baffles to increase the internal surface area [223]. H_2Se was also used to dope GaAsP and GaP grown by atmospheric MOVPE, which identified a sub-linear variation of carrier density with H_2Se partial pressure. Carrier densities approaching $1x10^{19}$ cm^{-3} were achieved [249]. H_2Se was also used to dope $In_{0.5}Ga_{0.5}P$ with linear incorporation achieving carrier densities approaching $1x10^{19}$ cm^{-3} with 50 Torr MOVPE. In this case Se incorporation is four orders of magnitude less efficient than in GaAs grown under the same conditions [260].

The n-type doping of antimony materials is an area that selenium (and tellurium) has a unique application. Se is linearly incorporated into GaSb and the atomic density is inversely dependent on the TMSb partial pressure consistent with prediction from mass action in 100 Torr MOVPE. Carrier density measurements on GaSb films are complicated by the small energy separating the Γ and L conduction band minimum. This effect leads to saturation of the carrier density measured by Hall effect measurements. Hall effect measurements on GaSb film are also complicated because most Hall effect measurements are performed on films grown heteroepitaxially on GaAs or InP. The structural defects introduced can interfere with the carrier density measurements. The maximum carrier density was $4x10^{17}$ cm-3 [177; 261; 262].

While the high vapor pressure of selenium precludes its use as a donor in GaN growth, it has been identified as a donor in GaN, but only modest carrier densities of $7x10^{17}$ to $1.5x10^{18}$ cm^{-3} could be obtained before Se impacts the growth leading to pits. At high surface concentration, grooves and cracks appear in the GaN film [263].

Some problems with using selenium come from the reactivity of H_2Se, which is the most widely investigated source compound. Metal-organic selenium compounds are alternative source. Ditertiarybutyl

selenium was recently investigated in GaAs using 76 Torr MOVPE. Carrier densities of $8x10^{18}$ cm^{-3} were produced at 560°C [264].

3.4.4 Tellurium

Unlike sulfur and selenium, H_2Te is not a stable compound. Some of the problems associated with the reactivity of hydrides are eliminated when metal-organics sources are used. Diethyl tellurium (DETe) is a common metal-organic source, but dimethyl tellurium (DMTe) and diisopropyl tellurium (DIPTe) have also been used. DIPTe and DETe can be obtained as liquid sources in conventional bubblers. Alternatively DMTe and DETe can be mixed with inert gases and supplied from high pressure cylinders.

One of the earliest studies use 76 Torr MOVPE to investigate Te incorporation into AlGaAs cited its low diffusion coefficient: two orders of magnitude lower than S, Si, or Sn, and one order of magnitude lower than Se. Linear incorporation of donors with increased DETe partial pressure was observed and decreased tellurium incorporation with increased AsH_3 partial pressure for GaAs, both consistent with mass action for donors incorporating on the Group V sublattice. Carrier densities approaching $1x10^{19}$ cm^{-3} were obtained. The carrier concentration goes down with increased temperature which is consistent with evaporation of Te, but the activation energy depends on the DETe partial pressure in chamber. The authors speculate that a high DETe partial pressure compensates for evaporation by adsorption from the gas phase. For AlGaAs the ionization energy for the Te donor starts to increase at x = 0.22 and rises to 100 meV at x = 0.4 consistent with DX center formation. This is much lower than the 300 meV for Si donors in AlGaAs. Modest memory effects are reported that can be reduced by minimizing exposed surface area and heating dopant lines to 60°C [265]. Other reports investigating only GaAs using 60 Torr MOVPE reproduce many of the observations [224].

Tellurium appears to be superior to sulfur for doping InP. DETe is a more efficient, achieving carrier densities of $5x10^{19}$ cm^{-3} where in comparision H_2S achieved only 2 $x10^{18}$ cm^{-3}. DETe is sublinear at the highest carrier densities. Carrier densities as high as $1x10^{20}$ cm^{-3} were reported in InP using 152 Torr MOVPE, but above $1x10^{19}$ cm^{-3} lattice dilation was observed, believed to be associated with the formation of V_{Ga}-Te_{As} defects. The activation of tellurium donors in InP is very high, over 60% at $1x10^{20}$ cm^{-3} [233; 266].

The high carrier densities achieved in InP motivated interest in looking at tellurium incorporation into other phosphide materials. DETe was used to dope $In_{0.5}Ga_{0.5}P$ with76 Torr MOVPE at 675°C to achieve $5x10^{18}$ cm^{-3}. Under these conditions, strong memory effects were observed that are assigned to the build-up of a Te segregation layer on the surface and its depletion when the DETe is switched to vent. A surface segregation model is likely because transients in alloy composition are observed [267]. These memory effects can be compensated by dosing the surface prior to growing the doped layer and purging the surface after the heavily doped layer. Using this approach carrier densities of $1x10^{19}$ cm^{-3} with abrupt profiles were obtained at 580°C with 39 Torr MOVPE [268]. Carrier densities over $1x10^{19}$ cm^{-3} are necessary for tunnel junctions used in multi-junction solar cells. A demonstration of the very high carrier densities possible with tellurium in $Al_{0.1}Ga_{0.4}In_{0.5}P$ was reported by preparing tunnel junctions with C:AlGaAs. While junctions using tellurium could achieve low resistance tunneling behavior, similar Si:AlGaInP/C:AlGaAs junctions could not. This indicates some of the specialized applications where tellurium might be used [269]. DETe has also been used to heavily dope InPAs alloys [270].

As mentioned in the previous section on selenium doping, tellurium is used to incorporate donors efficiently into GaSb and Sb-based alloys. DMTe was used to doped GaSb using atmospheric MOVPE, achieving carrier densities of $4x10^{17}$ cm^{-3} [271]. Higher carrier densities, over $1x10^{18}$ cm^{-3}, were achieved in GaSb with 100 Torr MOVPE with DETe. The troubling observation was that for DETe partial pressures above the value that gave $1x10^{18}$ cm^{-3} donors the carrier density goes down, even though the atomic Te concentration in the film increased [261]. Even higher carrier densities of $2x10^{18}$ cm^{-3} were demonstrated in $In_{0.2}Ga_{0.8}Sb$ with DETe using 100 Torr MOVPE. This work reported that the activation of Te donors decreased as larger concentrations of Te were incorporated into the film. The activation

varies from 75 to 35%, with activation as low as 1% at Te concentrations of $1x10^{19}$ cm-3. The authors attributed the reduction due to second phase formation. Alternatively this could be a population of the L conduction band minimum that underestimates the carrier density when using Hall effect measurements. Other reports support the low activations at high tellurium concentrations for GaSb [272] A significant achievement for antimonide devices was the demonstration of n-type doping in AlGaSb using DETe in 150 Torr MOVPE. This demonstration shows that doping was possible out to $Al_{0.4}Ga_{0.6}Sb$. The important issue for achieving significant n-type doping into AlGaSb was lowering the background carbon and oxygen concentration. To achieve this condition alternative aluminum and gallium metal-organic sources were used [273]. This was extended to achieve n-type AlAsSb using DETe [274].

4. Growth system considerations

In this section, we discuss several necessary aspects of MOVPE that evolved during the practice of this growth technique. This includes requirements for the operational aspects of MOVPE and how well essential growth variables need to be controlled to improve growth reproducibility. Later modeling of MOVPE growth using computational fluid dynamics allowed improved reactor design and increased utility of chemical reactants. Obtaining information during growth has also become essential to not only control but also rapid evaluation of the material properties, leading to more rapid advancement of the desired materials. Finally, in this section we discuss how MOVPE systems evolved from simple laboratory systems for growth to immense reactors capable of industrial production.

4.1 Operational aspects of MOVPE: Equipment, sources, and purity

For MOVPE growth, ways to introduce the reagents into a growth chamber, heat a substrate to drive the chemical reactions, and remove reaction byproducts are required. The equipment required for these processes can be quite modest for simple depositions or quite complex as might be expected in a production environment. In this section we describe the equipment absolutely necessary for MOVPE growth of compound semiconductors and later list other less essential items that may improve quality, purity, or enable growth of sophisticated device structures.

Essential equipment required for MOVPE are; 1) a growth chamber, 2) a substrate holder that can be heated, 3) chemical sources (both MO and hydrides), and 4) inlet to and exhaust from the growth chamber. For the growth chamber the flow across the substrate can either be horizontal, vertical, or a combination of both [275]. Typically, the growth chamber is constructed of a non-reacting material such as quartz or stainless steel, usually chosen to reduce impurity incorporation. Means to heat the substrate include radio-frequency induction, IR lamps, or resistance heating. Chemical reagents are plumbed into the growth chamber through electro-polished stainless steel tubing with seals comprised of o-ring or metal gaskets that are compatible with the hydride gases used. To guarantee safe operation and the material purity, helium leak checking of all parts of the MOVPE system is essential.

The substrate holder is composed of a high temperature material such as Mo, graphite, SiC-coated graphite or other material that is resilient to the growth process. In addition, the substrate holder must couple heat from the source to the wafer surface loaded on top of it, uniformly. Rotation of the wafer improves growth uniformity, and high rotation speeds provide an additional benefit of directing gas flow across the growth surface. Rotation of the wafer can be accomplished by coupling an external motor to the substrate holder using a ferrofluidic feed-through or a portion of the process gas.

The source chemicals introduced into the growth chamber are thermally decomposed on the substrate surface resulting in growth of the desired semiconductor film. For III-V compounds, the source chemicals typically consist of hydrocarbon ligand substituted Group III metals and Group V hydrides (AsH_3, PH_3, and NH_3), although a variety of custom or single source molecules have also been used, as discussed by A. C. Jones [276]. The metal-organics (MOs) are delivered in vendor supplied, stainless-steel “bubblers” which contain a longer dip tube for a carrier gas (typically H_2 or N_2) to bubble through the MO and out

the shorter tube to the growth chamber. The MO molar flow rate is controlled through bubbler temperature, which is fixed using a fluid bath, carrier gas flow rate controlled by a mass flow controller (MFC), and bubbler pressure held constant using a pressure control valve (PCV) on the bubbler outlet. For liquid MOs with reasonable vapor pressures (such as TMGa and TMAl), this combination of MFC and PCV provides steady, reliable molar flow rates into the growth chamber. For solid MOs (such as TMIn and Cp_2Mg), additional low-vapor-pressure hydrocarbon molecules are added to prevent MO sintering and keep the MO surface area in the bubbler constant. The MOs are delivered to the growth chamber in an inert carrier gas flow, typically N_2 or H_2 although He and Kr have been used [277]. Over the years, the chemical producers have worked very closely with MOVPE practitioners to quantify and reduce the impurity concentrations in their chemicals from ppm to ppb levels.

In addition to these essential features, MOVPE systems have other desired features including, 1) toxic gas monitoring equipment to warn uses when Permissible Exposure Limits (PEL) are exceeded, 2) oil-free pumps, needle valves, and throttle valves for controlling pressure, 3) gas manifolds with separate run and vent lines welded from electropolished stainless steel tubing to quickly switch gases in and out of the chamber to avoid large pressure fluctuations, 4) treatment of exhaust to neutralize, treat, or capture spent reaction products, 5) load lock for rapid sample loading and reducing atmospheric contamination of the growth chamber, 6) temperature monitoring and control (using pyrometry or thermocouples) to ensure reproducible material properties, 7) in-situ monitoring of wafer curvature and optical reflectance, 8) computer control of the entire growth process driven by operator written recipes, 9) dilution loops to produce smaller MO molar flows for doping and thin layers such as quantum wells, and 10) gas purifiers to remove impurities from hydride, H_2, and N_2 gases. These features are commonly found on commercially purchased MOVPE systems and aid the user in achieving consistent material quality, especially in production environments.

4.2. MOVPE control variables

We highlight the most relevant parameters as it pertains to control of the MOVPE process. A detailed analysis of control variables was discussed by Betsch as it related to gas manifold design [278]. Since the vapor pressure of the MO depends exponentially on temperature, control of the bubbler temperature is extremely critical to obtain constant molar flow rate. Early on, a low pressure of the gas manifold was shown to reduce adduct formation in the chamber delivery tubing compared to atmospheric operation [278]. (Adduct formation can be easily overcome by using separate run and vent lines and keeping the alkyl and hydride sources as separate as possible inside the growth chamber). For short MO switching times (for example QWs), the time response of the gas manifold needs to be considered [278], however if the run and vent manifolds are pressure balanced and working in a pressure control mode, the time delay in switching MOs in and out of the run line is less of an issue. Other more elaborate changes to the gas manifold have provided the ability to vary the MO concentration switching time to within a few hundred milliseconds [279]. The MFCs should also be operated near midrange so that the set point repeatability of this flow are less than the smallest tolerance acceptable for the given layer [278].

A second consideration is precise temperature control and stability which can be more or less important depending on the material system. Temperature control is especially necessary for InGaN growth since the indium desorption rate is heavily temperature dependent. This makes accurate temperature control essential for reproducibility of InGaN QW LEDs, since the LED wavelength can shift by ~2 nm per °C due to differences in the amount of indium incorporated [280; 281]. This effect also makes across wafer temperature uniformity essential for increasing LED yield [282].

A third source of process deviation during MOVPE growth is the MO pick-up rate out of the bubbler. The traditional assumption is that the MO vapor pressure is constant; however during long growth runs or when high flow rates of the MO are required this assumption is less valid. This issue can be alleviated by directly sensing the MO concentration in the gas phase using optical [283; 284] or ultrasonic [285] monitoring. The use of direct sensing of the MO concentration can then be fed back to the MFC to

maintain constant MO concentrations [286]. Solid source MOs, such as trimethylindium, can be mixed with a less volatile organic molecule to prevent source sintering within the bubbler. For example TMIn has been mixed with N,N-dimethyldodecylamine to increase MO usage and delivery consistency [287]. Improvements in bubbler design have also demonstrated improved MO usage and increased maximum bubbler output [288]. For even higher flow rates (grams/min) required by industrial sized MOVPE systems, the heat of vaporization of the MO [289] needs to be considered as cooling of the MO within the bubbler can be more than 1 °C leading to a TMGa delivery error of more than 6% [290]. Ideally, in-situ monitoring and feedback control can alleviate these issues with MO delivery [286].

4.3. Effects of fluid flow on control of MOVPE

Hydrogen was traditionally used as the push and carrier gas since it could be purified using a heated Pd membrane to produce high purity H_2 with impurity concentrations measured in parts per billion (ppb)[291]. Later with advances in resin-bed purifiers [292], ppb purity N_2 also became available and resin-bed purification of H_2 and the hydride gases soon followed. The advantages of using N_2 carrier gas compared to H_2 is that N_2 is less flammable, less reactive to the chemicals that are being transported, requires less waste treatment, laminar gas flow can be more easily achieved, and reduced gas-phase parasitic reactions during Group III-N growth [22; 47; 49]. In addition the thermal conductivity of H_2 is 7 times that of N_2 which must be considered when conducting flow modeling at the growth temperature.

Also, for the growth of some materials by MOVPE the hydride precursor constitutes a significantly large fraction of the total flow. This is truest for III-N growth as the NH_3 flow rate can reach 60 to 70 % of the total flow through the system, especially for InGaN growth. Since N_2 and NH_3 have nearly identical thermal conductivities, N_2 and NH_3 can be substituted for each other without severely disrupting the fluid flow dynamics. In many commercial reactors, a combination of H_2 and N_2 are used to better control the flow dynamics.

Advances in detailed modeling of the flow dynamics and possible growth chemistries have gradually led to advances in MOVPE reactor design [28; 293-296; 297-300]. Initially only fluid flows through the MOVPE system was considered due to the complexity of the growth chemistry and the fact that in many cases the exact nature of the growth chemistry was not entirely known. One of the first studies of flow dynamics was for a rotating disk reactor (RDR) by Olander [293]. For the vertical RDR the boundary layer formed at the disk surface was found to be caused by shear forces arising from the disk rotation and the gas viscosity [294]. With the RDR geometry the growth uniformity then depends on the depletion of the MO when the boundary layer is thicker and from diffusion limited delivery of the MO to the surface when the boundary layer is thinner [294]. Later work recognized how buoyancy rolls affect growth non-uniformities, especially at low flow rates [28; 295]. 2D and 3D reactor modeling led to suggestions on how to reduce the influence of buoyancy rolls such as cooling the surface opposite the heated sample, increasing flow rates, using H_2 or He as the carrier gas instead of N_2 or Ar, and reactors with small heights between the reagent injection and growth surface [28; 295]. Later it was shown that buoyancy rolls could be controlled when the Grashoff number divided by the Reynolds number was well below 60 [296]. Also important to these early flow modeling studies was visual verification of the flow dynamics using TiO_2 particle injection [296; 297]. From the TiO_2 particle studies, thickness uniformity was shown to be influenced by the shape of the susceptor edge and the reactor wall geometry [296]. One of the first studies that coupled fluid flow dynamics and Si growth chemistry is discussed by Coltrin and coworkers for an RDR [298]. Much of this early work on understanding reactor flow dynamics in various geometries is discussed by Holstein [299] and by Breiland and coworkers for RDR geometries [300].

As the reactor geometries became more established, flow modeling of specific reactor types was studied along with the relevant growth chemistries [45; 301-303; 304; 305; 306]. This work allowed further reactor design modifications to improve thickness uniformity, increase reactor size, and help in the selection of optimal gas flows. For example operating conditions were found to follow RDR scaling laws for an established 180 mm RDR as the reactor diameter was increased to 300 and 420 mm [301].

Modeling of close-spaced [302], high-speed RDR [303; 304], and horizontal systems [305] all allowed further reactor geometry refinement, specifically the MO and hydride injection schemes and optimization of the flow dynamics. Developing accurate and predictive growth chemistries is still ongoing, however early work coupling growth chemistries to flow dynamics has shown promise [45; 306]. The main issue with adding growth chemistries to the reactor flow dynamics is that the major contributing gas-phase, gas-surface, and cluster growth [22] chemistries are only partially understood for some materials, or require so many coupled chemical reactions as to make computation intractable.

4.4 In situ process control

For MBE growth at low pressure, electron diffraction techniques (RHEED) are ideally suited for monitoring and controlling growth since these techniques provide information on the atomic scale ordering. For MOVPE growth these electron diffraction techniques cannot be used because of the higher operating pressures. Instead photons must be relied upon to convey growth information to the operator. Photons at x-ray wavelengths would convey atomic scale information similar to RHEED, however, commercial x-ray beam intensities are several orders of magnitude too low to continuously survey the necessary diffraction features with sufficient time resolution. This leaves IR to UV wavelength photons as the best conveyers of information.

As a practical matter, direct viewing the emitted radiation is essential. This requirement leads to placing optical access on the top of the MOVPE system. To keep the windows clean, purge flows of inert gases are required which may contribute to the overall flow pattern in the MOVPE system. Other in-situ techniques require a glancing geometry which may influence fluid flow within the MOVPE system and may be more difficult to keep clean during growth. This may be one of the reasons why these more glancing geometry techniques have not been as widely implemented as the surface normal techniques have been as discussed below.

4.4.1. Optical Reflectance

Optical reflectance is the most widely used in-situ diagnostic used during MOVPE growth, because it is easy to implement and interpret. Typically a single wavelength is monitored and information such as growth rate and optical constants of the growing material can be identified [307]. The measurement consists of using a chopped light source (laser or tungsten bulb) and measuring the reflected light from the surface in a near normal incidence geometry [307]. Such an approach can usually be combined with temperature measurement to produce an emissivty corrected pyrometer [307]. Breiland and coworkers developed a virtual interface model and an automated procedure for extracting information that requires no prior knowledge other than the starting reflectance of the substrate [308]. Even if full interpretation of the reflectance waveform is not required, optical reflectance can be used to “finger-print” each growth run, thereby providing a check of growth run reproducibility. Moving this technique from single wafer to multi-wafer reactors requires computerized indexing of each wafer to track individual wafers throughout the entire growth [309].

The use of optical reflectance has guided Group III-nitride growth since the early days of developing planar GaN. Nakamura first described film optimization obtained using low temperature GaN nucleation layers (NL) and guided by reflectance measurements [310]. Later work was conducted to identify and quantify various features in the GaN reflectance waveform [311]. For example, intentional extension of the 3D roughened growth stage prior to coalescence was shown to lead to films with reduced dislocation densities and higher output power UV LEDs [122]. In-situ measurements of GaN NL decomposition showed similar activation energies as bulk GaN layers, however the NL decomposition rates were a factor of four to nine times larger depending on the annealing conditions [312]. Ex-situ AFM analysis of annealed GaN NLs showed that the reflectance waveform signal first decreases due to NL decomposition followed by NL roughening [313]. Later an analytical model was developed to fit the reflectance waveforms during NL annealing which included the temperature dependence of refraction indices and the decomposition rates measured under varying or constant temperature [314].

4.4.2. Spectroscopic reflectance

The spectral reflectance can also be measured at multiple wavelengths, producing a wealth of information during growth [307]. The method has proven to be a real-time "wellness" monitor during deposition as the run-to-run reflectance "finger-print" can be compared to previously grown films [307]. Since multiple wavelengths are measured, optical constants may be extracted from the reflectance spectra of growing thin films. Lum *et al.* showed how wavelengths between 400–2500 nm could be attained using a spectrometer and Si/PbS dual detector, allowing the monitoring of InP/InGaAs/InP double heterostructures and 1.3 μm InGaAsP MQW lasers [315]. Using multiple wavelengths allows the measurement of the optical constants of the growing film [316] and using the virtual interface model of Breiland *et al.* [308], allowing determination of the alloy concentration.

4.4.3. Surface photo-adsorption

Developed by Kobayashi [317-321], surface photo-absorption (SPA) provides information on the formation and disappearance of surface bonds during growth. The method uses p-polarized near ultra-violet and visible light at the Brewster-angle to measure reflectivity changes that correspond to the surface bond electronic adsorption spectrum. Under typical conditions, the reflectivity from a GaAs surface is only ~5% of the incident, yet this condition is sufficient to detect a monolayer of adsorbed Ga atoms which changes the reflectivity by 2.2% [318]. Since this technique requires more glancing angles with respect to the surface normal, the walls and chamber must be purged to prevent deposition which would block optical access. While not a common in-situ measurement, this technique has been used to gain information on surface coverage [320], [321]. , reconstructions [319], exchange of Group V atoms [317], as well as monitor growth [322].

4.4.4 Spectroscopic Ellipsometry

Ellipsometry measures the amplitude ratio and phase difference of the p- and s-polarized light waves after they are reflected from the surface [323]. Its increased usage has coincided with the advent of computer models needed to calculate the layer properties to match to the ellipsometric signals. There are two constraints on the ellipsometric measurement namely that the surface roughness remains low and the incident and reflected light beams are measured at angles of typically 70-80º to the surface normal [323]. The first of these requirements can be met during most MOVPE growth; however the requirement for oblique angles makes this technique somewhat difficult to implement and may be the main reason why ellipsometry is not routinely used to monitor MOVPE growth of thin films.

Spectroscopic ellipsometry (SE) has been used to measure a number of parameters for MOVPE including real-time layer thickness and compositions for InGaAs and InAlAs layers grown on InP [324]. surface stoichiometry during GaN [325]. }, Al concentrations in AlGaN, [326] andS a growth mode transition from smooth to rougher layers allowing determination of the InGaN strain relaxation thickness [327].

4.4.5. Reflectance Difference Spectroscopy (RDS)/Reflectance Anisotropy Spectroscopy (RAS)

Both RDS and RAS may be regarded as a further development of spectroscopic ellipsometry (SE) pioneered by Aspnes and coworkers at Bellcore in the mid 1980's [37; 328; 329-331]. Originally the technique was called reflectance difference spectroscopy (RDS), but was later renamed reflectance anisotropy spectroscopy (RAS) to differentiate it from the 'static' spectroscopic methods of surface differential reflectance and electroreflectance [331]. In contrast to SE, RAS uses linearly polarized light which is introduced at near normal incidence, making the optical access for RAS more practical than SE. Interpretation of RAS signals is non-trivial since the signal depends on the complex dielectric function of both the surface and bulk and typically the dielectric function must be calculated from first principles [332]. For RAS to work, the surface has to be optically anisotropic which is true for FCC and BCC (110) surfaces, (001) semiconductor reconstructed surfaces, and non-polar surfaces of cubic and wurtzite

wideband gap semiconductors [332]. This requirement of optical anisotropy is a serious drawback to more routine implementation of this technique for MOVPE..

The first use of RAS by Colas *et al.* suggested that relative surface coverage could be monitored during MOVPE similarly as done during MBE growth [330]. Noting that the RAS signals reach extreme values at a wavelength of 2.5 eV, they were able to show that this maximum signal closely follows the TMGa decomposition kinetics confirming the RAS signal is sensitive to the relative As and Ga coverage [330]. RAS studies have shown irreversible TMGa decomposition on an AsH_3 stabilized surface [329] and that the wide range of activation energies reported for TMGa dissociation is the result of the fractional-occupancy and decomposition-probability effects on TMGa decomposition[329]. RAS has shown intensity oscillations similar to RHEED oscillations of steps during island growth [35] and doping profiles deviations during HBT and DBRs for vertical-cavity surface-emitting lasers [333].

4.4.6 Temperature sensing

At a first glance temperature sensing might not be thought of as an in-situ technique for growth. Yet, it is essential to both accurately measure and precisely control the temperature at which material growth occurs. Usually, growth temperature is determined using close-proximity thermocouples or optically by measuring the light intensity emitted by the substrate, so called pyrometry. More typically, a combination of both temperature measurement techniques are used with thermocouples used to set the temperature and pyrometers used to verify the correct operating temperature. In this section, we discuss pyrometry especially emissivity-correcting pyrometry and a more specialized technique that uses the band edge adsorption to determine the temperature.

4.4.6.1 Emissivity-correcting pyrometry

Pyrometry is commonly used outside the field of MOVPE growth, so here we will only elaborate on a few features as they apply to temperature measurement in a MOVPE reactor and for further details refer the reader to a thorough review by Breiland [334]. For pyrometry, the usual assumptions are that the semiconductor wafer is opaque at the measuring wavelength and that the wafer remains smooth during deposition. While the first assumption is valid for most compound semiconductors at growth temperature, wide band gap semiconductors are typically transparent at the traditional wavelengths used for optical pyrometry (~500-1000 nm). The second assumption of wafer flatness is valid for most growth situations, except during the initial stage of GaN growth on sapphire [122]. Emissivity changes can occur during thin film growth especially if it is semitransparent [334] or if multiple wafers are viewed on a carrier with different emissivity characteristics [335]. Finally, the pyrometer must also be calibrated either against a black body or via some other self-consistent means [334]. To overcome these issues with changes to emissivity and optical reflectance effects, emissivity-correcting pyrometers (ECPs) were developed [334].

Fordham and coworkers first report the use of emissivity correction during pyrometric measurements by chopping collected sample light and reflecting back off the sample and onto into the detector [336]. Later implementations of this same general scheme used an emission-stable, external light source such as laser or halogen bulb [334]. By adding the emissivity correction and sorting algorithms Ramer *et al.* demonstrated such pyrometers could be used to measure wafer temperature in a high speed RDR with disk sizes up to 400 mm [335]. One additional advantage of these ECPs is that the normalized reflectance is also measured during growth as described in Section 4.4.1.

For optically transparent materials, such as GaN and sapphire, traditional pyrometers measure the radiation emitted from the wafer carrier and not the wafer surface. To resolve this issue, UV [280] and mid-IR [281] wavelength pyrometers have been developed. The UV wavelength (~405 nm) pyrometer exploits the fact that the high-temperature GaN at a thickness of ~1 μm becomes opaque [280]. One difficulty of this approach is the low signal intensity at this wavelength especially at InGaN growth temperatures. Above 1000 °C the temperature noise is less than 0.1 °C, however as the temperature is lowered to temperatures between 700 to 800 °C for InGaN growth, the temperature noise is ~ 1 °C which

is important since indium incorporation in this alloy can be very temperature sensitive [280]. The mid-IR pyrometer relies on the fact that sapphire substrates are opaque and the reactant gases are transparent near ~7–8 μm [281]. A mid-IR pyrometer developed by Creighton was installed on a multiwafer system and used to control the surface temperature during InGaN MQW deposition, resulting in improved control of the photoluminescence wavelength [281].

4.4.6.2 Adsorption edge pyrometry

Another temperature method gaining acceptance is to use the temperature dependence of the optical absorption edge that is inherent in semiconductor materials. This temperature measuring technique was first mentioned by Shanabrook *et al.* [337] and Johnson *et al.* [338] who showed better than 1 ºC sensitivity of this technique [338]. The band-gap thermometry is sensitive to thin film interference, which causes the apparent temperature to oscillate [339]. This interference oscillation can be removed from the temperature measurement by using the width of the adsorption knee to correct temperature errors [339]. This temperature measurement technique has been used in the IR to measure GaAs and InP [340] and wide bandgap materials such as GaN and SiC [341]. Commercial instruments based on this technique are available from k-Space Associates [342].

4.4.7 Strain sensing

For films with large differences in lattice constants or coefficients of thermal expansion (COE) compared to the substrates, management of film strain is extremely important. If not properly managed, film strain can lead to cracks, delamination, or wafers so warped that cannot be lithographically patterned or processed. To measure the wafer curvature during growth, the deflection of a single [343] or multiple [344; 345] laser beams can be measured along with application of the Stoney equation to determine in-situ the strain state [346]. The single laser beam technique relies on detecting the reflected beam with a position sensitive detector as the rotating wafer passes through the sampling beam [343]. For the multiple beam technique, a laser beam is converted into multiple parallel beams using an etalon [345; 347] and the distance between the beams can be independently tracked by a CCD camera to obtain the wafer curvature [345]. Commercial instruments are current available from several vendors.

Early applications of this technique in an MOVPE environment centered on measuring the stress evolution for GaN films growth on sapphire [348; 349]. Hearne *et al.* found that even though GaN has a 16% compressive lattice mismatch to sapphire, GaN consistently grows in tension at high temperature and is only put into compress upon cooling to room temperature [349]. The strain state of GaN could also be controlled by inserting AlN interlayers which prevented wafer cracking by reducing tensile stress [348]. Later the critical layer thicknesses for strain relaxation for AlGaN/GaN heterostructures were measured with AFM analysis showing that the onset of AlGaN relaxation occurs through surface fracture [350]. One anomalous feature of this technique on transparent films and substrates is that the reflection is susceptible to thickness gradients which steer the laser beam away from the ideal specular condition [351]. Strain measurements during growth have also been conducted on InGaAs/GaAs heterostructures [352] and multi-junction solar cells [353] to control the resultant strain the film.

The most significant application of in-situ strain measurement has been in the development of GaN growth on Si(111) spearheaded by Dadgar and Krost [354; 355; 356], ultimately leading to crack free LED wafers up to 150 mm diameter [356; 357]. Using the in situ curvature measurement technique at perpendicular incidence, the impact of 3D-island coalescence, layer thermal mismatch, and doping on the collective film/substrate strain state could be monitored and controlled through the insertion of AlN and AlGaN strain relieving layers [354]. With the aid of the in-situ strain measurement system, the strain state of the Group III-nitride film on the Si(111) substrate can be engineered so that the final strain state is near zero, which is ideal for wafer processing.

4.4.8 Gas phase analytical techniques

In addition to monitoring the growth surface, measuring the gas phase precursor and reactant concentrations can provide additional control of the MOVPE process. Monitoring the gas phase precursor concentration is especially important for MO's with low vapor pressures (such as TMIn), or that have a tendency to sinter in the bubbler [358], or to determine when a bubbler is empty. Monitoring the exhaust allows determination of the extent of the chemical reactions [359]. The techniques described below are primarily optically based, but also include mass spectrometry and piezo-acoustic sensors.

The optically based techniques involve either UV absorbance measurements or IR sensing of the molecular vibrations. For the UV approach the molecular concentration the absorbance is measured and the gas phase concentration is obtained using Beers' Law [284; 358; 360]. Using this approach Baucom and coworkers explained discrepancies for TMA1 delivery were due to the monomer to dimer equilibrium [284]. Using a remote fiber-optic based dual-wavelength detection scheme, DeSisto and Rappolli were able to make chemical specific measurements of YBCO precursors allowing determination of extremely dilute concentrations of these low volatility MOCVD sources [358]. Fourier transform infrared (FTIR) methods have been developed to detect molecular vibrations [361; 362; 363]. Using FTIR, Sywe *et al.* studied TMGa and NH_3 predeposition reactions and measured the IR absorption bands of the gaseous TMGa:NH_3 adduct formation [361]. FTIR was also used to study the high temperature thermal decomposition of the TMGa:NH_3 adduct, where the liberation of a -CH_3 radical was observed above 500 ºC followed by abstraction of a hydrogen from NH_3 [363]. Raman active modes can be measured using Coherent anti-Stokes Raman Scattering (CARS) [364]and this technique has been used to study the thermal decomposition of AsH_3, PH_3, TMGa and $C_4H_9PH_2$ [365].

Finally, mass spectroscopy, normally a vacuum-based technique, has been used during growth to analyze small amounts of the siphoned-off gas stream. What makes this technique valuable is that both precursors and spent reactants in the exhaust can be simultaneously evaluated [366]. For example Davies *et al.* sampled the concentration of DMZn entering the reactor and its decomposition product, methane, to determine the extent of DMZn decomposition in the presence and absence of H_2Se [366]. The gas phase pyrolysis of MO and hydride precursors were studied to determine the precursor decomposition pathways from the hydrocarbon product distributions [367]. In-situ mass spectrometry has also been demonstrated as a real-time metrology tool for the growth of AlGaN/GaN/AlN/SiC HEMT structures [359]. Measurement of the methane and ethane reaction byproducts showed that the methane to ethane ratio related to the GaN epilayer crystal quality [359]. Piezo acoustic sensors have also been developed to monitor MO gas-phase concentration under the name Epison [285] and Piezocon [368].

4.5. Evolution of reactor designs: Fundamental Studies to Manufacturing.

While simple MOVPE reactor designs were initially used for fundamental growth studies and developing device prototypes, more advanced reactor designs have led to improved material quality and device manufacturability. Initial reactors consisted of reactants flowing through simple quartz tubes onto a heated substrate holder, with the wafer holder held either parallel or perpendicular to the main gas flow. The development of rotating disk reactor provided an additional viscous drag on the gas flow, pulling the gas flow down and redirecting it outward over the wafer surface [301; 369]. Later work by Nakamura used high flows of N_2 to thin the boundary layer, resulting in increased GaN growth rate at atmospheric pressure [275]. Wafer rotation was also shown to improve growth uniformity especially when implemented in multi-wafer systems using a gas-foil rotation scheme for each individual wafer [370]. Later reactor designs involved improving injection of the Group III and V reactants to reduce pre-reaction, including the showerhead [371], jetted slots [303], two-flow [372] and three-flow [373] reactor designs.

With these developments and improved flow modeling capability as discussed in Section 4.3, large scale MOVPE machines have been developed capable of growth on 12-4" wafers with 90% yield for blue wavelength LEDs [368]. Clusters of 2 to 4 MOVPE tools are also available for increased tool utilization and reduced footprint [368]. MOVPE systems in the horizontal flow mode or with a close coupled

showerhead are also available [374]. Blue InGaN-based LEDs have been produced on eight inch sapphire wafers [375], however for LED growth on these larger wafers special care must be taken reduce wafer curvature [376]. Also of interest is GaN device growth on Si due to low cost and availability of larger area wafers [357] and reduced cost for processing each individual wafer. As discussed in section 4.4.7, GaN growth on Si has been made possible through the development of strain relief layers and dislocation density reducing layers [377] which was enabled by the development of in situ diagnostics as summarized by Zhu *et al*.[357].

5. Conclusions

As presented in this review the use of MOVPE is extensively used to develop new materials and device structures. As first developed by Manasevit and coworkers, MOVPE systems have grown in size and complexity to meet the stringent demands of production environments. Over the years, improvements in source purity, reactor design, fluid flow modeling, in-situ diagnostics, and computer interfacing have led to exquisite control of thickness and composition in even the thinnest layers, allowing for complex device architectures to be grown in at most a couple of hours. Future improvements in reactor designs should further increase up-time between maintenance cycles and improved utilization of chemical precursors, allowing further reduction in the cost of ownership.

6. Acknowledgement

This work was funded by Sandia National Laboratories. Sandia National Laboratories is a multi-program laboratory managed and operated by Sandia Corporation, a wholly owned subsidiary of Lockheed Martin Corporation, for the U.S. Department of Energy's National Nuclear Security Administration under contract DE-AC04-94AL85000.

7. References

[1] D.W. Kisker, T.F. Kuech, in: D. Hurle (Ed.), Handbook of Crystal Growth, Elsevier, Amsterdam, 1994.
[2] G.B. Stringfellow, Organometallic vapor-phase epitaxy: theory and practice, Academic Press, 1989.
[3] G.B. Stringfellow, Organometallic Vapor-Phase Epitaxy: Theory and Practice, Second Edition, Academic Press, Boston, 1999.
[4] G.B. Stringfellow, Mater. Sci. Eng. B-Solid State Mater. Adv. Technol. 87 (2001) 97-116.
[5] T.F. Kuech, K.F. Jensen, in: V.J. L., K. W. (Eds.), Thin Film Processes II, Academic Press, Orlando, 1991,M.A. Tischler, IBM J. Res. Dev. 34 (1990) 828.
[6] Manasevi.Hm, Applied Physics Letters 12 (1968) 156-&.
[7] Manasevi.Hm, F.M. Erdmann, W.I. Simpson, J. Electrochem. Soc. 118 (1971) 1864-&.
[8] H.M. Manasevit, J. Cryst. Growth 13-14 (1972) 306-314.
[9] L.R. Dawson, Progress in Solid State Chemistry 7 (1972) 117-139.
[10] M.B. Panish, M. Ilegems, Progress in Solid State Chemistry 7 (1972) 39-83.
[11] M.J. Cich, R.I. Aldaz, A. Chakraborty, A. David, M.J. Grundmann, A. Tyagi, M. Zhang, F.M. Steranka, M.R. Krames, Applied Physics Letters 101 (2012).
[12] W. Quinn, Driving Down HB-LED Costs: Implementation of Process Simulation Tools and Temperature Control Methods of High Yield MOCVD Growth, 2012, Medium: ED.
[13] J.R. Creighton, J. Cryst. Growth 147 (1995) 64-73.
[14] D.H. Reep, S.K. Ghandhi, J. Electrochem. Soc. 130 (1983) 675-680,D.H. Reep, S.K. Ghandhi, J. Electrochem. Soc. 131 (1984) 2697-2702.
[15] C. Plass, H. Heinecke, O. Kayser, H. Luth, P. Balk, J. Cryst. Growth 88 (1988) 455-464,H. Krautle, H. Roehle, A. Escobosa, H. Beneking, J. Electron. Mater. 12 (1983) 215-222.
[16] J.R. Creighton, K.C. Baucom, Surf. Sci. 409 (1998) 372-383.
[17] T.F. Kuech, E. Veuhoff, J. Cryst. Growth 68 (1984) 148-156.
[18] H. Amano, N. Sawaki, I. Akasaki, Y. Toyoda, Applied Physics Letters 48 (1986) 353-355.
[19] H. Amano, I. Akasaki, K. Hiramatsu, N. Koide, N. Sawaki, Thin Solid Films 163 (1988) 415-420.
[20] S. Nakamura, Jpn. J. Appl. Phys. Part 1 - Regul. Pap. Short Notes Rev. Pap. 30 (1991) 1620-1627.
[21] P. Kozodoy, H.L. Xing, S.P. DenBaars, U.K. Mishra, A. Saxler, R. Perrin, S. Elhamri, W.C. Mitchel, J. Appl. Phys. 87 (2000) 1832-1835.
[22] J.R. Creighton, G.T. Wang, M.E. Coltrin, J. Cryst. Growth 298 (2007) 2-7.
[23] T.J. Mountziaris, K.F. Jensen, J. Electrochem. Soc. 138 (1991) 2426-2439,K.F. Jensen, D.I. Fotiadis, T.J. Mountziaris, J. Cryst. Growth 107 (1991) 1-11.
[24] N.K. Ingle, C. Theodoropoulos, T.J. Mountziaris, R.M. Wexler, F.T.J. Smith, J. Cryst. Growth 167 (1996) 543-556.
[25] T.F. Kuech, M.A. Tischler, R. Potemski, F. Cardone, G. Scilla, J. Cryst. Growth 98 (1989) 174-187.
[26] R.M. Biefeld, Mater. Sci. Eng. R-Rep. 36 (2002) 105-142.
[27] M.K. Rathi, B.E. Hawkins, T.F. Kuech, J. Cryst. Growth 296 (2006) 117-128.
[28] H. Moffat, K.F. Jensen, J. Cryst. Growth 77 (1986) 108-119.
[29] R.J. Kee, M.E. Coltrin, P. Glaborg, Chemically Reacting Flow: Theory and Practice, Wiley Interscience, John Wiley and Sons, Inc., Hoboken, New Jersey, 2003.
[30] R.M. Biefeld, K.C. Baucom, S.R. Kurtz, J. Cryst. Growth 137 (1994) 231-234.
[31] R.J. Field, S.K. Ghandhi, J. Cryst. Growth 69 (1984) 581-588,Y. Takahashi, T. Soga, S. Sakai, M. Umeno, S. Hattori, Jpn. J. Appl. Phys. Part 1 - Regul. Pap. Short Notes Rev. Pap. 22 (1983) 1357-1360.
[32] F. Reinhardt, J. Jonsson, M. Zorn, W. Richter, K. Ploska, J. Rumberg, P. Kurpas, J. Vac. Sci. Technol. B 12 (1994) 2541-2546.
[33] K. Ploska, J.T. Zettler, W. Richter, J. Jonsson, F. Reinhardt, J. Rumberg, M. Pristovsek, M. Zorn, D. Westwood, R.H. Williams, J. Cryst. Growth 145 (1994) 44-52,K. Ploska, M. Pristovsek, W. Richter, J. Jonsson, I. Kamiya, J.T. Zettler, Phys. Status Solidi A-Appl. Res. 152 (1995) 49-59.
[34] W. Richter, J.T. Zettler, Appl. Surf. Sci. 100 (1996) 465-477,A.P. Payne, P.H. Fuoss, D.W. Kisker, G.B. Stephenson, S. Brennan, Physical Review B 49 (1994) 14427-14434,F.J. Lamelas, P.H. Fuoss, P. Imperatori, D.W. Kisker, G.B. Stephenson, S. Brennan, Applied Physics Letters 60 (1992) 2610-2612,P.H. Fuoss, D.W. Kisker, F.J. Lamelas, G.B. Stephenson, P. Imperatori, S. Brennan, Physical Review Letters 69 (1992) 2791-2794,D.W. Kisker, G.B. Stephenson, P.H. Fuoss, S. Brennan, J. Cryst. Growth 146 (1995) 104-111,I. Kamiya, L. Mantese, D.E. Aspnes, D.W. Kisker, P.H. Fuoss, G.B. Stephenson, S. Brennan, J. Cryst. Growth 163 (1996) 67-77.

[35] J.T. Zettler, J. Rumberg, K. Ploska, K. Stahrenberg, M. Pristovsek, W. Richter, M. Wassermeier, P. Schutzendube, J. Behrend, L. Daweritz, Phys. Status Solidi A-Appl. Res. 152 (1995) 35-47.
[36] D.W. Kisker, G.B. Stephenson, J. Tersoff, P.H. Fuoss, S. Brennan, J. Cryst. Growth 163 (1996) 54-59,D.W. Kisker, G.B. Stephenson, I. Kamiya, P.H. Fuoss, D.E. Aspnes, L. Mantese, S. Brennan, Phys. Status Solidi A-Appl. Res. 152 (1995) 9-21.
[37] I. Kamiya, D.E. Aspnes, H. Tanaka, L.T. Florez, J.P. Harbison, R. Bhat, Physical Review Letters 68 (1992) 627-630,I. Kamiya, D.E. Aspnes, L.T. Florez, J.P. Harbison, Physical Review B 46 (1992) 15894-15904.
[38] J.R. Creighton, H.K. Moffat, K.C. Baucom, Proceedings of Symposium on Fundamental Gas-Phase and Surface Chemistry of Vapor-Phase Materials Synthesis (1999) 75-88.
[39] T.J. Mountziaris, S. Kalyanasundaram, N.K. Ingle, J. Cryst. Growth 131 (1993) 283-299.
[40] D.J. Schlyer, M.A. Ring, Journal of Organometallic Chemistry 114 (1976) 9-19.
[41] D.W. Kisker, G.B. Stephenson, P.H. Fuoss, F.J. Lamelas, S. Brennan, P. Imperatori, J. Cryst. Growth 124 (1992) 1-9.
[42] W.G. Schmidt, P.H. Hahn, F. Bechstedt, N. Esser, P. Vogt, A. Wange, W. Richter, Physical Review Letters 90 (2003),L. Li, B.K. Han, Q. Fu, R.F. Hicks, Physical Review Letters 82 (1999) 1879-1882,L. Li, Q. Fu, C.H. Li, B.K. Han, R.F. Hicks, Physical Review B 61 (2000) 10223-10228,R.L. Woo, U. Das, S.F. Cheng, G. Chen, K. Raghavachari, R.F. Hicks, Surf. Sci. 600 (2006) 4888-4895,M.J. Begarney, C.H. Li, D.C. Law, S.B. Visbeck, Y. Sun, R.F. Hicks, Applied Physics Letters 78 (2001) 55-57,P. Vogt, T. Hannappel, S. Visbeck, K. Knorr, N. Esser, W. Richter, Physical Review B 60 (1999) R5117-R5120,P. Vogt, K. Lüdge, M. Zorn, M. Pristovsek, W. Braun, W. Richter, N. Esser, Physical Review B 62 (2000) 12601-12604,W.G. Schmidt, et al., Physical Review B 61 (2000) 16335-16338,H. Doescher, K. Moeller, T. Hannappel, J. Cryst. Growth 318 (2011) 372-378.
[43] K. Yong, J.G. Ekerdt, Surf. Sci. 448 (2000) 108-116.
[44] L. Töben, T. Hannappel, K. Möller, H.J. Crawack, C. Pettenkofer, F. Willig, Surf. Sci. 494 (2001) L755-L760,L. Li, B.K. Han, R.F. Hicks, Applied Physics Letters 73 (1998) 1239-1241.
[45] T.G. Mihopoulos, V. Gupta, K.F. Jensen, J. Cryst. Growth 195 (1998) 733-739.
[46] J.R. Creighton, W.G. Breiland, M.E. Coltrin, Sources of the parasitic chemical reactions during AlGaNOMVPE, 2002.
[47] J.R. Creighton, W.G. Breiland, M.E. Coltrin, R.P. Pawlowski, Applied Physics Letters 81 (2002) 2626-2628.
[48] J.R. Creighton, G.T. Wang, W.G. Breiland, M.E. Coltrin, J. Cryst. Growth 261 (2004) 204-213.
[49] M.E. Coltrin, J.R. Creighton, C.C. Mitchell, J. Cryst. Growth 287 (2006) 566-571.
[50] J. Han, T.B. Ng, R.M. Biefeld, M.H. Crawford, D.M. Follstaedt, Applied Physics Letters 71 (1997) 3114-3116.
[51] A.A. Allerman, M.H. Crawford, A.J. Fischer, K.H.A. Bogart, S.R. Lee, D.M. Follstaedt, P.P. Provencio, D.D. Koleske, J. Cryst. Growth 272 (2004) 227-241.
[52] G.B. Stephenson, J.A. Eastman, C. Thompson, O. Auciello, L.J. Thompson, A. Munkholm, P. Fini, S.P. DenBaars, J.S. Speck, Applied Physics Letters 74 (1999) 3326-3328,M.I. Richard, M.J. Highland, T.T. Fister, A. Munkholm, J. Mei, S.K. Streiffer, C. Thompson, P.H. Fuoss, G.B. Stephenson, Applied Physics Letters 96 (2010).
[53] A.R. Smith, R.M. Feenstra, D.W. Greve, M.S. Shin, M. Skowronski, J. Neugebauer, J.E. Northrup, Applied Physics Letters 72 (1998) 2114-2116,A. Munkholm, G.B. Stephenson, J.A. Eastman, C. Thompson, P. Fini, J.S. Speck, O. Auciello, P.H. Fuoss, S.P. DenBaars, Physical Review Letters 83 (1999) 741-744.
[54] G.B. Stringfellow, J. Cryst. Growth 27 (1974) 21-34,S.K. Duan, D.C. Lu, J. Cryst. Growth 170 (1997) 514-517,I.H. Ho, G.B. Stringfellow, J. Cryst. Growth 178 (1997) 1-7,S.H. Wei, A. Zunger, Physical Review B 39 (1989) 3279-3304.
[55] J.S. Yuan, C.H. Chen, R.M. Cohen, G.B. Stringfellow, J. Cryst. Growth 78 (1986) 63-68,C.C. Hsu, R.M. Cohen, G.B. Stringfellow, J. Cryst. Growth 62 (1983) 648-650,J. Komeno, J. Cryst. Growth 145 (1994) 468-472,M.J. Ludowise, C.B. Cooper, R.R. Saxena, J. Electron. Mater. 10 (1981) 1051-1068.
[56] Y. Mori, N. Watanabe, J. Appl. Phys. 52 (1981) 2792-2798.
[57] R.M. Biefeld, J. Cryst. Growth 77 (1986) 392-399.
[58] T. Fukui, Y. Horikoshi, Japanese Journal of Applied Physics 19 (1980) L551-L554,G.B. Stringfellow, J. Cryst. Growth 62 (1983) 225-229.
[59] D.M. Follstaedt, R.M. Biefeld, S.R. Kurtz, K.C. Baucom, J. Electron. Mater. 24 (1995) 819-825,E.T. Yu, S.L. Zuo, W.G. Bi, C.W. Tu, A.A. Allerman, R.M. Biefeld, Journal of Vacuum Science & Technology a-Vacuum Surfaces and Films 17 (1999) 2246-2250.

[60] C.B. Cooper, R.R. Saxena, M.J. Ludowise, J. Electron. Mater. 11 (1982) 1001-1010.
[61] G.B. Stringfellow, M.J. Cherng, J. Cryst. Growth 64 (1983) 413-415.
[62] M.J. Cherng, R.M. Cohen, G.B. Stringfellow, J. Electron. Mater. 13 (1984) 799-813.
[63] Y. Iwamura, T. Takeuchi, N. Watanabe, J. Cryst. Growth 145 (1994) 82-86.
[64] A.A. Khandekar, J.Y. Yeh, L.J. Mawst, X. Song, S.E. Babcock, T.F. Kuech, J. Cryst. Growth 303 (2007) 456-465.
[65] G.B. Stringfellow, J. Cryst. Growth 68 (1984) 111-122.
[66] A.S. Jordan, J. Electron. Mater. 24 (1995) 1649-1654.
[67] R.M. Biefeld, J. Electron. Mater. 15 (1986) 193-199.
[68] E. Smeets, J. Cryst. Growth 82 (1987) 385-395.
[69] W.C. Johnson, J.B. Parsons, M.C. Crew, J. Phys. Chem. 36 (1932) 2651-2654.
[70] M. Ilegems, J. Cryst. Growth 13-14 (1972) 360-4,Wickende.Dk, K.R. Faulkner, R.W. Brander, Isherwoo.J, J. Cryst. Growth 9 (1971) 158-&.
[71] L. Liu, J.H. Edgar, Mater. Sci. Eng. R-Rep. 37 (2002) 61-127.
[72] S. Nakamura, Jpn. J. Appl. Phys. Part 2 - Lett. 30 (1991) L1705-L1707.
[73] T.W. Weeks, M.D. Bremser, K.S. Ailey, E. Carlson, W.G. Perry, R.F. Davis, Applied Physics Letters 67 (1995) 401-403.
[74] K. Hiramatsu, S. Itoh, H. Amano, I. Akasaki, N. Kuwano, T. Shiraishi, K. Oki, J. Cryst. Growth 115 (1991) 628-633.
[75] O.H. Nam, M.D. Bremser, T.S. Zheleva, R.F. Davis, Applied Physics Letters 71 (1997) 2638-2640.
[76] C.C. Mitchell, M.E. Coltrin, J. Han, J. Cryst. Growth 222 (2001) 144-153.
[77] H. Amano, M. Kito, K. Hiramatsu, I. Akasaki, Jpn. J. Appl. Phys. Part 2 - Lett. 28 (1989) L2112-L2114.
[78] S. Nakamura, T. Mukai, M. Senoh, N. Iwasa, Jpn. J. Appl. Phys. Part 2 - Lett. 31 (1992) L139-L142.
[79] S.M. Myers, A.F. Wright, G.A. Petersen, W.R. Wampler, C.H. Seager, M.H. Crawford, J. Han, J. Appl. Phys. 89 (2001) 3195-3202.
[80] S. Nakamura, T. Mukai, M. Senoh, Applied Physics Letters 64 (1994) 1687-1689.
[81] D.D. Koleske, A.E. Wickenden, R.L. Henry, J.C. Culbertson, M.E. Twigg, J. Cryst. Growth 223 (2001) 466.
[82] S.S. Liu, D.A. Stevenson, J. Electrochem. Soc. 125 (1978) 1161-1169.
[83] V.S. Ban, J. Electrochem. Soc. 119 (1972) 761-&.
[84] D.D. Koleske, A.E. Wickenden, R.L. Henry, W.J. DeSisto, R.J. Gorman, J. Appl. Phys. 84 (1998) 1998.
[85] M.E. Coltrin, C.C. Mitchell, J. Cryst. Growth 254 (2003) 35-45.
[86] D.D. Koleske, A.E. Wickenden, R.L. Henry, Mrs. Internet J. Nitride Semicond. Res. 5 (2000) art. no.-W3.64.
[87] D.D. Koleske, S.R. Lee, M.H. Crawford, K.C. Cross, M.E. Coltrin, J.M. Kempisty, J. Cryst. Growth 391 (2014) 85-96.
[88] D.D. Koleske, J.J. Wierer Jr, A.J. Fischer, S.R. Lee, J. Cryst. Growth 390 (2014) 38-45.
[89] E.L. Piner, M.K. Behbehani, N.A. ElMasry, F.G. McIntosh, J.C. Roberts, K.S. Boutros, S.M. Bedair, Applied Physics Letters 70 (1997) 461.
[90] Z. Liliental-Weber, M. Benamara, J. Washburn, J.Z. Domagala, J. Bak-Misiuk, E.L. Piner, J.C. Roberts, S.M. Bedair, J. Electron. Mater. 30 (2001) 439-444,S. Pereira, M.R. Correia, E. Pereira, K.P. O'Donnell, E. Alves, A.D. Sequeira, N. Franco, I.M. Watson, C.J. Deatcher, Applied Physics Letters 80 (2002) 3913-3915.
[91] B.N. Pantha, J. Li, J.Y. Lin, H.X. Jiang, Applied Physics Letters 93 (2008),A. Yamamoto, T. Tanaka, K. Koide, A. Hashimoto, Phys. Status Solidi A-Appl. Res. 194 (2002) 510-514.
[92] H. Masui, S. Nakamura, S.P. DenBaars, U.K. Mishra, Ieee Transactions on Electron Devices 57 (2010) 88-100,H. Sato, et al., Applied Physics Letters 92 (2008).
[93] P. Shan Hsu, M.T. Hardy, E.C. Young, A.E. Romanov, S.P. DenBaars, S. Nakamura, J.S. Speck, Applied Physics Letters 100 (2012) -.
[94] A. Miura, T. Nagai, R. Senda, T. Kawashima, M. Iwaya, S. Kamiyama, H. Amano, I. Akasaki, J. Cryst. Growth 310 (2008) 3308-3312.
[95] S. Nakamura, M.R. Krames, Proceedings of the Ieee 101 (2013) 2211-2220.
[96] Y. Narukawa, M. Ichikawa, D. Sanga, M. Sano, T. Mukai, Journal of Physics D-Applied Physics 43 (2010),T. Sano, T. Doi, S.A. Inada, T. Sugiyama, Y. Honda, H. Amano, T. Yoshino, Japanese Journal of Applied Physics 52 (2013).

[97] Y. Narukawa, Y. Kawakami, M. Funato, S. Fujita, S. Fujita, S. Nakamura, Applied Physics Letters 70 (1997) 981-983.
[98] D. Gerthsen, E. Hahn, B. Neubauer, A. Rosenauer, O. Schon, M. Heuken, A. Rizzi, Physica Status Solidi a-Applications and Materials Science 177 (2000) 145-155.
[99] D.M. Graham, A. Soltani-Vala, P. Dawson, M.J. Godfrey, T.M. Smeeton, J.S. Barnard, M.J. Kappers, C.J. Humphreys, E.J. Thrush, J. Appl. Phys. 97 (2005).
[100] S.F. Chichibu, et al., Nature Materials 5 (2006) 810-816.
[101] A. Hangleiter, F. Hitzel, C. Netzel, D. Fuhrmann, U. Rossow, G. Ade, P. Hinze, Physical Review Letters 95 (2005).
[102] T. Akasaka, H. Gotoh, T. Saito, T. Makimoto, Applied Physics Letters 85 (2004) 3089-3091,J.K. Son, S.N. Lee, T. Sakong, H.S. Paek, O. Nam, Y. Park, J.S. Hwang, J.Y. Kim, Y.H. Cho, J. Cryst. Growth 287 (2006) 558-561.
[103] K. Kumakura, T. Makimoto, N. Kobayashi, Jpn. J. Appl. Phys. Part 2 - Lett. 39 (2000) L337-L339.
[104] K. Kumakura, T. Makimoto, N. Kobayashi, Jpn. J. Appl. Phys. Part 2 - Lett. 39 (2000) L195-L196.
[105] M.T. Hardy, D.F. Feezell, S.P. DenBaars, S. Nakamura, Materials Today 14 (2011) 408-415,S. Takagi, et al., Applied Physics Express 5 (2012),D. Sizov, R. Bhat, C.-E. Zah, Journal of Lightwave Technology 30 (2012) 679-699,K. Yanashima, et al., Applied Physics Express 5 (2012).
[106] R. Dahal, B. Pantha, J. Li, J.Y. Lin, H.X. Jiang, Applied Physics Letters 94 (2009),C.J. Neufeld, N.G. Toledo, S.C. Cruz, M. Iza, S.P. DenBaars, U.K. Mishra, Applied Physics Letters 93 (2008),J.J. Wierer, Jr., Q. Li, D.D. Koleske, S.R. Lee, G.T. Wang, Nanotechnology 23 (2012).
[107] J.J. Wierer, Jr., D.D. Koleske, S.R. Lee, Applied Physics Letters 100 (2012).
[108] V. Woods, N. Dietz, Mater. Sci. Eng. B-Solid State Mater. Adv. Technol. 127 (2006) 239-250,D. Iida, K. Nagata, T. Makino, M. Iwaya, S. Kamiyama, H. Amano, I. Akasaki, A. Bandoh, T. Udagawa, Applied Physics Express 3 (2010).
[109] M.A. Khan, R.A. Skogman, J.M. Vanhove, S. Krishnankutty, R.M. Kolbas, Applied Physics Letters 56 (1990) 1257-1259.
[110] K. Itoh, T. Kawamoto, H. Amano, K. Hiramatsu, I. Akasaki, Jpn. J. Appl. Phys. Part 1 - Regul. Pap. Short Notes Rev. Pap. 30 (1991) 1924-1927.
[111] R.S.Q. Fareed, J.P. Zhang, R. Gaska, G. Tamulaitis, J. Mickevicius, R. Aleksiejunas, M.S. Shur, M.A. Khan, in: M. Stutzmann (Ed.), Physica Status Solidi C - Conferences and Critical Reviews, Vol 2, No 7, 2005, pp. 2095-2098,S. Choi, H.J. Kim, J.-H. Ryou, R.D. Dupuis, J. Cryst. Growth 311 (2009) 3252-3256.
[112] N. Fujimoto, et al., in: S. Hildebrandt, M. Stutzmann (Eds.), Physica Status Solidi C - Current Topics in Solid State Physics, Vol 3, No 6, 2006, pp. 1617-1619,M. Imura, et al., Japanese Journal of Applied Physics Part 1-Regular Papers Brief Communications & Review Papers 45 (2006) 8639-8643,H. Amano, Iop, in: T. Walther, P.A. Midgley (Eds.), 17th International Conference on Microscopy of Semiconducting Materials 2011, 2011.
[113] T. Kinoshita, T. Obata, H. Yanagi, S.-i. Inoue, Applied Physics Letters 102 (2013).
[114] H. Kawanishi, T. Tomizawa, Physica Status Solidi B-Basic Solid State Physics 249 (2012) 459-463.
[115] M. Shatalov, et al., Applied Physics Express 5 (2012).
[116] M.A. Khan, A. Bhattarai, J.N. Kuznia, D.T. Olson, Applied Physics Letters 63 (1993) 1214-1215,J. Pankove, S.S. Chang, H.C. Lee, R.J. Molnar, T.D. Moustakas, B. Vanzeghbroeck, E.D.S. Ieee, HIGH-TEMPERATURE GAN/SIC HETEROJUNCTION BIPOLAR TRANSISTOR WITH HIGH GAIN, 1994.
[117] J.P. Ibbetson, P.T. Fini, K.D. Ness, S.P. DenBaars, J.S. Speck, U.K. Mishra, Applied Physics Letters 77 (2000) 250-252,I.P. Smorchkova, C.R. Elsass, J.P. Ibbetson, R. Vetury, B. Heying, P. Fini, E. Haus, S.P. DenBaars, J.S. Speck, U.K. Mishra, J. Appl. Phys. 86 (1999) 4520-4526.
[118] I.P. Smorchkova, L. Chen, T. Mates, L. Shen, S. Heikman, B. Moran, S. Keller, S.P. DenBaars, J.S. Speck, U.K. Mishra, J. Appl. Phys. 90 (2001) 5196-5201.
[119] A.E. Wickenden, D.D. Koleske, R.L. Henry, M.E. Twigg, M. Fatemi, J. Cryst. Growth 260 (2004) 54-62.
[120] S. Heikman, S. Keller, S.P. DenBaars, U.K. Mishra, Applied Physics Letters 81 (2002) 439-441.
[121] O. Mizuno, H. Watanabe, Electronics Letters 11 (1975) 118-119,J.A. Long, V.G. Riggs, W.D. Johnston, J. Cryst. Growth 69 (1984) 10-14.
[122] D.D. Koleske, A.J. Fischer, A.A. Allerman, C.C. Mitchell, K.C. Cross, S.R. Kurtz, J.J. Figiel, K.W. Fullmer, W.G. Breiland, Applied Physics Letters 81 (2002) 1940-1942.
[123] P.B. Klein, S.C. Binari, K. Ikossi, A.E. Wickenden, D.D. Koleske, R.L. Henry, Applied Physics Letters 79 (2001) 3527-3529.

[124] S.C. Binari, K. Ikossi, J.A. Roussos, W. Kruppa, D. Park, H.B. Dietrich, D.D. Koleske, A.E. Wickenden, R.L. Henry, Ieee Transactions on Electron Devices 48 (2001) 465-471.
[125] S. Arulkumaran, T. Hibino, T. Egawa, H. Ishikawa, Applied Physics Letters 85 (2004) 5745-5747,W. Lanford, V. Kumar, R. Schwindt, A. Kuliev, I. Adesida, A.M. Dabiran, A.M. Wowchak, P. Chow, J.W. Lee, Electronics Letters 40 (2004) 771-772.
[126] B.P. Gila, F. Ren, C.R. Abernathy, Mater. Sci. Eng. R-Rep. 44 (2004) 151-184.
[127] U.K. Mishra, L. Shen, T.E. Kazior, Y.-F. Wu, Proceedings of the Ieee 96 (2008) 287-305.
[128] D.W. Kisker, J. Cryst. Growth 98 (1989) 127-139.
[129] S.J.C. Irvine, J.B. Mullin, J. Cryst. Growth 55 (1981) 107-115.
[130] D.W. Kisker, A.G. Zawadzki, J. Cryst. Growth 89 (1988) 378-390.
[131] E.F. Schubert, Doping in III-V Semiconductors, Cambridge University Press, 2005.
[132] J.D. Parsons, F.G. Krajenbrink, J. Electrochem. Soc. 130 (1983) 1782-1783.
[133] J.D. Parsons, L.S. Lichtmann, F.G. Krajenbrink, D.W. Brown, J. Cryst. Growth 77 (1986) 32-36.
[134] R.S. Sillmon, S.M. Hues, D.K. Gaskill, N. Bottka, P.E. Thompson, J. Electron. Mater. 18 (1989) 501-504.
[135] B.T. McDermott, C.W. Seabury, C.W. Farley, J.A. Higgins, J. Electron. Mater. 22 (1993) 555-558.
[136] T. Kobayashi, K. Kurishima, T. Ishibashi, J. Cryst. Growth 142 (1994) 1-4.
[137] Y. Miyazaki, Y. Hanamaki, H. Tada, K. Takagi, M. Takemi, T. Aoyagi, Y. Mihashi, Y. Mitsui, J. Appl. Phys. 93 (2003) 3823-3826.
[138] T. Kimura, T. Ishida, T. Sonoda, Y. Mihashi, S. Takamiya, S. Mitsui, Jpn. J. Appl. Phys. Part 1 - Regul. Pap. Short Notes Rev. Pap. 34 (1995) 1106-1108.
[139] C.R. Lewis, W.T. Dietze, M.J. Ludowise, J. Electron. Mater. 12 (1983) 507-524.
[140] J.S. Roberts, N.J. Mason, M. Robinson, J. Cryst. Growth 68 (1984) 422-430.
[141] M.L. Timmons, P.K. Chiang, S.V. Hattangady, J. Cryst. Growth 77 (1986) 37-41,H. Tews, R. Neumann, T. Humerhager, R. Treichler, J. Appl. Phys. 68 (1990) 1318-1323.
[142] T.F. Kuech, P.J. Wang, M.A. Tischler, R. Potemski, G.J. Scilla, F. Cardone, J. Cryst. Growth 93 (1988) 624-630.
[143] M. Rask, G. Landgren, S.G. Andersson, A. Lundberg, J. Electron. Mater. 17 (1988) 311-314.
[144] C. Blaauw, R.A. Bruce, C.J. Miner, A.J. Howard, B. Emmerstorfer, A.J. Springthorpe, J. Electron. Mater. 18 (1989) 567-572.
[145] M. Ohkubo, J. Osabe, T. Shiojima, T. Yamaguchi, T. Ninomiya, J. Cryst. Growth 170 (1997) 177-181.
[146] C.C. Wu, C.Y. Chang, P.A. Chen, H.D. Chen, K.C. Lin, S.H. Chan, Applied Physics Letters 65 (1994) 1269-1271.
[147] G.J. Bauhuis, P.R. Hageman, P.K. Larsen, J. Cryst. Growth 191 (1998) 313-318,P. Roentgen, W. Heuberger, G.L. Bona, P. Unger, J. Cryst. Growth 107 (1991) 724-730,M. Kondo, C. Anayama, T. Tanahashi, S. Yamazaki, J. Cryst. Growth 124 (1992) 449-456,S.A. Stockman, et al., J. Electron. Mater. 28 (1999) 916-925.
[148] Y. Nishikawa, H. Sugawara, Y. Kokubun, J. Cryst. Growth 119 (1992) 292-296,M. Kondo, C. Anayama, H. Sekiguchi, T. Tanahashi, J. Cryst. Growth 141 (1994) 1-10,T. Onishi, K. Inoue, K. Onozawa, T. Takayama, M. Yuri, Ieee Journal of Quantum Electronics 40 (2004) 1634-1638.
[149] S. Nakamura, M. Senoh, T. Mukai, Japanese Journal of Applied Physics, Part 2 (Letters) 30 (1991) L1708-11.
[150] W. Gotz, N.M. Johnson, J. Walker, D.P. Bour, R.A. Street, Applied Physics Letters 68 (1996) 667-669.
[151] D.J. Kim, D.Y. Ryu, N.A. Bojarczuk, J. Karasinski, S. Guha, S.H. Lee, J.H. Lee, J. Appl. Phys. 88 (2000) 2564-2569.
[152] C.G. Van de Walle, C. Stampfl, J. Neugebauer, J. Cryst. Growth 189 (1998) 505-510.
[153] S.N. Lee, J. Son, T. Sakong, W. Lee, H. Paek, E. Yoon, J. Kim, Y.H. Cho, O. Nam, Y. Park, J. Cryst. Growth 272 (2004) 455-459.
[154] U. Kaufmann, P. Schlotter, H. Obloh, K. Kohler, M. Maier, Physical Review B 62 (2000) 10867-10872.
[155] Z. Liliental-Weber, M. Benamara, W. Swider, J. Washburn, I. Grzegory, S. Porowski, R.D. Dupuis, C.J. Eiting, Physica B-Condensed Matter 273-4 (1999) 124-129.
[156] P. Vennegues, M. Benaissa, B. Beaumont, E. Feltin, P. De Mierry, S. Dalmasso, M. Leroux, P. Gibart, Applied Physics Letters 77 (2000) 880-882,L.T. Romano, J.E. Northrup, M.A. Okeefe, Applied Physics Letters 69 (1996) 2394-2396,L.T. Romano, T.H. Myers, Applied Physics Letters 71 (1997) 3486-3488.
[157] Y. Doo-Hyeb, M. Lachab, M. Hao, T. Sugahara, H. Takenaka, Y. Naoi, S. Sakai, Japanese Journal of Applied Physics, Part 1 (Regular Papers, Short Notes & Review Papers) 38 (1999) 631-4,H. Harima, T. Inoue, S. Nakashima, M. Ishida, M. Taneya, Applied Physics Letters 75 (1999) 1383-1385,O. Svensk, S.

Suihkonen, T. Lang, H. Lipsanen, M. Sopanen, M.A. Odnoblyudov, V.E. Bougrov, J. Cryst. Growth 298 (2007) 811-814.
[158] P. Kozodoy, S. Keller, S. DenBaars, U.K. Mishra, J. Cryst. Growth 195 (1998) 265-269.
[159] G.T. Wang, J.R. Creighton, Journal of Physical Chemistry A 108 (2004) 4873-4877.
[160] A. Chakraborty, H. Xing, M.D. Craven, S. Keller, T. Mates, J.S. Speck, S.P. DenBaars, U.K. Mishra, J. Appl. Phys. 96 (2004) 4494-4499.
[161] X. Huili, D.S. Green, Y. Haijiang, T. Mates, P. Kozodoy, S. Keller, S.P. Denbaars, U.K. Mishra, Japanese Journal of Applied Physics, Part 1 (Regular Papers, Short Notes & Review Papers) 42 (2003) 50-3.
[162] K. Matsumoto, J. Hidaka, K. Uchida, J. Appl. Phys. 65 (1989) 3849-3851.
[163] A.W. Nelson, L.D. Westbrook, J. Cryst. Growth 68 (1984) 102-110.
[164] C. Blaauw, B. Emmerstorfer, A.J. Springthorpe, J. Cryst. Growth 84 (1987) 431-435.
[165] R.M. Biefeld, S.R. Kurtz, I.J. Fritz, J. Electron. Mater. 18 (1989) 775-780,V. Wagener, M.C. Wagener, J.R. Botha, J. Appl. Phys. 111 (2012).
[166] J.J. Yang, W.I. Simpson, L.A. Moudy, J. Appl. Phys. 53 (1982) 771-773.
[167] R.W. Glew, J. Cryst. Growth 68 (1984) 44-47.
[168] M.K. Hudait, P. Modak, S. Hardikar, S.B. Krupanidhi, J. Appl. Phys. 82 (1997) 4931-4937.
[169] S.Z. Sun, E.A. Armour, K. Zheng, C.F. Schaus, J. Cryst. Growth 113 (1991) 103-112.
[170] P.R. Hageman, M. Decroon, X. Tang, L.J. Giling, J. Cryst. Growth 129 (1993) 281-288,M.J. Anders, P.R. Hageman, L.J. Giling, J. Cryst. Growth 142 (1994) 292-297.
[171] C.C. Hsu, J.S. Yuan, R.M. Cohen, G.B. Stringfellow, J. Cryst. Growth 74 (1986) 535-542.
[172] S.R. Kurtz, J.M. Olson, A.E. Kibbler, K.A. Bertness, J. Cryst. Growth 124 (1992) 463-469.
[173] R.A. Logan, S.N.G. Chu, M. Geva, N.T. Ha, C.D. Thurmond, J. Appl. Phys. 79 (1996) 1371-1377.
[174] A. Eisenbach, A. Goldhorn, E. Kuphal, K. Mause, J. Cryst. Growth 170 (1997) 451-455.
[175] I. Moerman, G. Coudenys, P. Demeester, J. Crawley, Ieee, CHARACTERIZATION OF INP/INGAAS/INGAASP USING ATMOSPHERIC AND LOW-PRESSURE MOVPE, 1991.
[176] K. Hjelt, T. Tuomi, J. Cryst. Growth 170 (1997) 794-798.
[177] Y.K. Su, H. Kuan, P.H. Chang, J. Appl. Phys. 73 (1993) 56-59.
[178] C.A. Wang, J. Cryst. Growth 191 (1998) 631-640,C.A. Wang, H.K. Choi, D.C. Oakley, G.W. Charache, J. Cryst. Growth 195 (1998) 346-355.
[179] T.F. Kuech, J.M. Redwing, J. Cryst. Growth 145 (1994) 382-389.
[180] T.F. Kuech, M.A. Tischler, P.J. Wang, G. Scilla, R. Potemski, F. Cardone, Applied Physics Letters 53 (1988) 1317-1319,G.J. Scilla, T.F. Kuech, F. Cardone, Applied Physics Letters 52 (1988) 1704-1706.
[181] N.I. Buchan, T.F. Kuech, G. Scilla, F. Cardone, J. Cryst. Growth 110 (1991) 405-414.
[182] T.F. Kuech, D.J. Wolford, E. Veuhoff, V. Deline, P.M. Mooney, R. Potemski, J. Bradley, J. Appl. Phys. 62 (1987) 632-643.
[183] Y. Ashizawa, T. Noda, K. Morizuka, M. Asaka, M. Obara, J. Cryst. Growth 107 (1991) 903-908.
[184] S.I. Kim, K.S. Eom, Y. Kim, M.S. Kim, S.K. Min, C. Lee, M.H. Kwak, D.S. Ma, J. Cryst. Growth 126 (1993) 441-446,M. Pristovsek, B. Han, J.-T. Zettler, W. Richter, J. Cryst. Growth 221 (2000) 149-155.
[185] J. van Deelen, G.J. Bauhuis, J.J. Schermer, P.K. Larsen, J. Cryst. Growth 271 (2004) 376-384.
[186] R.M. Lum, J.K. Klingert, J. Appl. Phys. 66 (1989) 3820-3823.
[187] T.F. Kuech, M.A. Tischler, P.J. Wang, G. Scilla, R. Potemski, F. Cardone, Applied Physics Letters 53 (1988) 1317-1319.
[188] H.J. Moon, T.G. Stoebe, B.K. Chadwick, J. Electron. Mater. 19 (1990) 1351-1355.
[189] M. Masi, H. Simka, K.F. Jensen, T.F. Kuech, R. Potemski, J. Cryst. Growth 124 (1992) 483-492.
[190] G. Haacke, S.P. Watkins, H. Burkhard, J. Cryst. Growth 107 (1991) 342-347,S.P. Watkins, G. Haacke, Applied Physics Letters 59 (1991) 2263-2265.
[191] M. Longo, R. Magnanini, A. Parisini, L. Tarricone, A. Carbognani, C. Bocchi, E. Gombia, J. Cryst. Growth 248 (2003) 119-123.
[192] N.I. Buchan, T.F. Kuech, G. Scilla, F. Cardone, R. Potemski, J. Electron. Mater. 19 (1990) 277-281.
[193] B.T. Cunningham, J.E. Baker, G.E. Stillman, J. Electron. Mater. 19 (1990) 331-335.
[194] M.C. Hanna, Z.H. Lu, A. Majerfeld, Applied Physics Letters 58 (1991) 164-166.
[195] N.I. Buchan, T.F. Kuech, G. Scilla, F. Cardone, J. Cryst. Growth 110 (1991) 405-414.
[196] N. Watanabe, H. Ito, J. Cryst. Growth 182 (1997) 30-36,N. Watanabe, H. Ito, J. Cryst. Growth 178 (1997) 213-219.
[197] C. Caneau, R. Bhat, M.A. Koza, J. Cryst. Growth 118 (1992) 467-469.
[198] M. Kondo, T. Tanahashi, J. Cryst. Growth 145 (1994) 390-396.

[199] L.W. Yang, P.D. Wright, V. Eu, Z.H. Lu, A. Majerfeld, J. Appl. Phys. 72 (1992) 2063-2065.
[200] M.L. Warddrip, M.J. Kappers, L. Li, H. Qi, B.K. Han, S. Gan, R.F. Hicks, J. Electron. Mater. 26 (1997) 1189-1193,M.J. Begarney, M.L. Warddrip, M.J. Kappers, R.F. Hicks, J. Cryst. Growth 193 (1998) 305-315.
[201] E. Richter, P. Kurpas, D. Gutsche, M. Weyers, J. Electron. Mater. 24 (1995) 1719-1722.
[202] K. Tateno, C. Amano, J. Cryst. Growth 181 (1997) 33-40.
[203] K. Uchida, S. Bhunia, N. Sugiyama, M. Furiya, M. Katoh, S. Katoh, S. Nozaki, H. Morisaki, J. Cryst. Growth 248 (2003) 124-129.
[204] M. Weyers, K. Shiraishi, Jpn. J. Appl. Phys. Part 1 - Regul. Pap. Short Notes Rev. Pap. 31 (1992) 2483-2487.
[205] A.E. Kibbler, S.R. Kurtz, J.M. Olson, J. Cryst. Growth 109 (1991) 258-263.
[206] S.J. Taylor, B. Beaumont, R. Herberholz, J. Cryst. Growth 132 (1993) 61-70.
[207] S.A. Stockman, A.W. Hanson, A.P. Curtis, G.E. Stillman, Ieee, CARBON DOPING OF INXGA1-XAS BY MOCVD USING CCL4, 1992.
[208] C. Caneau, R. Bhat, S. Goswami, M.A. Koza, J. Electron. Mater. 25 (1996) 491-495,K.S. Hong, D. Pavlidis, J. Electron. Mater. 25 (1996) 449-455.
[209] H. Ito, S. Yamahata, N. Shigekawa, K. Kurishima, Jpn. J. Appl. Phys. Part 1 - Regul. Pap. Short Notes Rev. Pap. 35 (1996) 6139-6144,D. Keiper, R. Westphalen, G. Landgren, J. Cryst. Growth 197 (1999) 25-30.
[210] A. Lindner, P. Velling, W. Prost, A. Wiersch, E. Kuphal, A. Burchard, R. Magerle, M. Deicher, F.J. Tegude, J. Cryst. Growth 170 (1997) 287-291.
[211] H. Dumont, L. Auvray, J. Dazord, Y. Monteil, J. Bouix, A. Ougazzaden, J. Cryst. Growth 204 (1999) 1-9,H. Dumont, L. Auvray, J. Dazord, V. Souliere, Y. Monteil, J. Bouix, A. Ougazzaden, J. Cryst. Growth 197 (1999) 755-761.
[212] A. Ougazzaden, J. Holavanahalli, M. Geva, L.E. Smith, J. Cryst. Growth 221 (2000) 66-69.
[213] R. Bhat, W.P. Hong, C. Caneau, M.A. Koza, C.K. Nguyen, S. Goswami, Applied Physics Letters 68 (1996) 985-987.
[214] S.P. Watkins, O.J. Pitts, C. Dale, X.G. Xu, M.W. Dvorak, N. Matine, C.R. Bolognesi, J. Cryst. Growth 221 (2000) 59-65.
[215] Y. Oda, N. Watanabe, H. Yokoyama, T. Kobayashi, Appl. Surf. Sci. 216 (2003) 532-536.
[216] R. Wiersma, J.A.H. Stotz, O.J. Pitts, C.X. Wang, M.L.W. Thewalt, S.P. Watkins, J. Electron. Mater. 30 (2001) 1429-1432.
[217] R.D. Wiersma, J.A.H. Stotz, O.J. Pitts, C.X. Wang, M.L.W. Thewalt, S.P. Watkins, Physical Review B 67 (2003).
[218] J.P. Duchemin, M. Bonnet, F. Koelsch, D. Huyghe, J. Electrochem. Soc. 126 (1979) 1134-1149.
[219] R.J. Field, S.K. Ghandhi, J. Cryst. Growth 74 (1986) 551-558.
[220] M. Shimazu, K. Kamon, K. Kimura, M. Mashita, M. Mihara, M. Ishii, J. Cryst. Growth 83 (1987) 327-333.
[221] S.J. Bass, J. Cryst. Growth 47 (1979) 613-618.
[222] P.R. Hageman, X. Tang, M. Decroon, L.J. Giling, J. Cryst. Growth 98 (1989) 249-254.
[223] R. Azoulay, L. Dugrand, D. Ankri, E.V.K. Rao, J. Cryst. Growth 68 (1984) 453-460.
[224] A.G. Thompson, V.S. Sundaram, G.R. Girard, L.M. Fraas, J. Cryst. Growth 94 (1989) 901-910.
[225] R. Venkatasubramanian, S.K. Ghandhi, T.F. Kuech, J. Cryst. Growth 97 (1989) 827-832.
[226] T.F. Kuech, E. Veuhoff, B.S. Meyerson, J. Cryst. Growth 68 (1984) 48-53.
[227] E. Veuhoff, T.F. Kuech, B.S. Meyerson, J. Electrochem. Soc. 132 (1985) 1958-1961.
[228] N. Furuhata, K. Kakimoto, M. Yoshida, T. Kamejima, J. Appl. Phys. 64 (1988) 4692-4695.
[229] H.K. Moffat, T.F. Kuech, K.F. Jensen, P.J. Wang, J. Cryst. Growth 93 (1988) 594-601.
[230] P.R. Hageman, M. Decroon, J.N.H. Reek, L.J. Giling, J. Cryst. Growth 116 (1992) 169-177.
[231] J.M. Redwing, T.F. Kuech, D. Saulys, D.F. Gaines, J. Cryst. Growth 135 (1994) 423-433.
[232] J.M. Redwing, H. Simka, K.F. Jensen, T.F. Kuech, J. Cryst. Growth 145 (1994) 397-402.
[233] A.R. Clawson, T.T. Vu, D.I. Elder, J. Cryst. Growth 83 (1987) 211-218.
[234] E. Woelk, H. Beneking, J. Appl. Phys. 63 (1988) 2874-2876.
[235] C. Blaauw, F.R. Shepherd, C.J. Miner, A.J. Springthorpe, J. Electron. Mater. 19 (1990) 1-6.
[236] S. Nakamura, T. Mukai, M. Senoh, Jpn. J. Appl. Phys. Part 1 - Regul. Pap. Short Notes Rev. Pap. 31 (1992) 2883-2888.
[237] H. Murakami, T. Asahi, H. Amano, K. Hiramatsu, N. Sawaki, I. Akasaki, J. Cryst. Growth 115 (1991) 648-651,N. Koide, H. Kato, M. Sassa, S. Yamasaki, K. Manabe, M. Hashimoto, H. Amano, K. Hiramatsu, I. Akasaki, J. Cryst. Growth 115 (1991) 639-642.

[238] K.B. Nam, J. Li, M.L. Nakarmi, J.Y. Lin, H.X. Jiang, Applied Physics Letters 81 (2002) 1038-1040,Y. Taniyasu, M. Kasu, N. Kobayashi, Applied Physics Letters 81 (2002) 1255-1257.
[239] M.C. Wagener, G.R. James, F. Omnes, Applied Physics Letters 83 (2003) 4193-4195.
[240] L.B. Rowland, K. Doverspike, D.K. Gaskill, Applied Physics Letters 66 (1995) 1495-1497.
[241] C. Agert, P.S. Gladkov, A.W. Bett, Semiconductor Science and Technology 17 (2002) 39-46.
[242] H. Ehsani, I. Bhat, C. Hitchcock, R.J. Gutmann, G. Charache, M. Freeman, J. Cryst. Growth 195 (1998) 385-390.
[243] J.D. Parsons, F.G. Krajenbrink, J. Cryst. Growth 68 (1984) 60-64.
[244] R. Yakimova, A.P. Roth, D.F. Williams, V.S. Sundaram, J. Cryst. Growth 68 (1984) 71-77.
[245] V.S. Sundaram, A.P. Roth, D.F. Williams, R. Yakimova, Applied Physics Letters 45 (1984) 1196-1198.
[246] C.J. Pinzone, N.D. Gerrard, R.D. Dupuis, N.T. Ha, H.S. Luftman, J. Appl. Phys. 67 (1990) 6823-6829.
[247] A.R. Clawson, C.M. Hanson, J. Electron. Mater. 20 (1991) 365-372,A. Eisenbach, E. Kuphal, K. Miethe, H.L. Hartnagel, J. Cryst. Growth 135 (1994) 129-134.
[248] R.M. Biefeld, J.R. Wendt, S.R. Kurtz, J. Cryst. Growth 107 (1991) 836-839,P. Shamba, L. Botha, T. Krug, A. Venter, J.R. Botha, in: M. Saarinen, A. Leitch, R. Botha (Eds.), Physica Status Solidi C - Current Topics in Solid State Physics, Vol 5, No 2 2008, 2008, pp. 577-579.
[249] R.M. Biefeld, A.A. Allerman, M.W. Pelczynski, Applied Physics Letters 68 (1996) 932-934.
[250] R. Niebuhr, K.H. Bachem, U. Kaufmann, M. Maier, C. Merz, B. Santic, P. Schlotter, H. Jurgensen, J. Electron. Mater. 26 (1997) 1127-1130.
[251] M. Ikeda, S. Kojima, Y. Kashiwayanagi, J. Cryst. Growth 77 (1986) 157-162.
[252] R. Bhat, C. Caneau, C.E. Zah, M.A. Koza, W.A. Bonner, D.M. Hwang, S.A. Schwarz, S.G. Menocal, F.G. Favire, J. Cryst. Growth 107 (1991) 772-778.
[253] R. Saxena, V. Sardi, J. Oberstar, L. Hodge, M. Keever, G. Trott, K.L. Chen, R. Moon, J. Cryst. Growth 77 (1986) 591-597.
[254] V. Aebi, C.B. Cooper, R.L. Moon, R.R. Saxena, J. Cryst. Growth 55 (1981) 517-525.
[255] C.R. Lewis, M.J. Ludowise, W.T. Dietze, J. Electron. Mater. 13 (1984) 447-461.
[256] H. Asai, H. Sugiura, Jpn. J. Appl. Phys. Part 2 - Lett. 24 (1985) L815-L817.
[257] H. Sakaguchi, R. Suzuki, T. Meguro, J. Cryst. Growth 93 (1988) 602-606.
[258] Y.K. Su, Y.C. Chou, C.Y. Chang, Journal of Physics and Chemistry of Solids 47 (1986) 105-108.
[259] J.J. Yang, L.A. Moudy, W.I. Simpson, Applied Physics Letters 40 (1982) 244-246.
[260] C.C. Wu, K.C. Lin, S.H. Chan, M.S. Feng, C.Y. Chang, Mater. Sci. Eng. B-Solid State Mater. Adv. Technol. 19 (1993) 234-239.
[261] F. Nakamura, K. Taira, K. Funato, H. Kawai, J. Cryst. Growth 115 (1991) 474-478.
[262] Y.K. Su, H. Kuan, P.H. Chang, Solid-State Electronics 36 (1993) 1773-1778.
[263] J.D. Guo, M.S. Feng, F.M. Pan, Jpn. J. Appl. Phys. Part 1 - Regul. Pap. Short Notes Rev. Pap. 34 (1995) 5510-5514.
[264] A. Maassdorf, M. Hoffmann, M. Weyers, J. Cryst. Growth 315 (2011) 57-60.
[265] Y.M. Houng, T.S. Low, J. Cryst. Growth 77 (1986) 272-280.
[266] F.G. Kellert, K.T. Chan, J.E. Turner, V.M. Robbins, J. Electron. Mater. 19 (1990) 1425-1428.
[267] I. Garcia, I. Rey-Stolle, B. Galiana, C. Algora, J. Cryst. Growth 298 (2007) 794-799.
[268] C. Ebert, Z. Pulwin, D. Byrnes, A. Paranjpe, W. Zhang, J. Cryst. Growth 315 (2011) 61-63.
[269] P.R. Sharps, N.Y. Li, J.S. Hills, H.Q. Hou, P.C. Chang, A. Baca, I. Ieee, in, Conference Record of the Twenty-Eighth Ieee Photovoltaic Specialists Conference - 2000, 2000, pp. 1185-1188.
[270] J.G. Cederberg, S.R. Lee, Applied Physics Letters 91 (2007),F.D. Newman, M.A. Stan, S.L. Murray, C.S. Murray, J. Cryst. Growth 272 (2004) 650-657.
[271] F. Pascal, F. Delannoy, J. Bougnot, L. Gouskov, G. Bougnot, P. Grosse, J. Kaoukab, J. Electron. Mater. 19 (1990) 187-195.
[272] C.A. Wang, D.A. Shiau, R.K. Huang, C.T. Harris, M.K. Connors, J. Cryst. Growth 261 (2004) 379-384,J.G. Cederberg, R.M. Biefeld, Semiconductor Science and Technology 19 (2004) 953-958.
[273] C.A. Wang, H.K. Choi, J. Electron. Mater. 26 (1997) 1231-1236.
[274] J.G. Cederberg, M.J. Hafich, R.M. Biefeld, M. Palmisiano, J. Cryst. Growth 248 (2003) 289-295.
[275] S. Nakamura, Y. Harada, M. Seno, Applied Physics Letters 58 (1991) 2021-2023.
[276] A.C. Jones, J. Cryst. Growth 129 (1993) 728-773.
[277] Y. Jong-Ho, R. Shi-Woo, Journal of Materials Science: Materials in Electronics 9 (1998) 1-4.
[278] R.J. Betsch, J. Cryst. Growth 77 (1986) 210-218.
[279] R.S. Sillmon, N. Bottka, J.E. Butler, D.K. Gaskill, J. Cryst. Growth 77 (1986) 73-78.

[280] J.R. Creighton, D.D. Koleske, C.C. Mitchell, J. Cryst. Growth 287 (2006) 572-576.
[281] J.R. Creighton, W.G. Breiland, D.D. Koleske, G. Thaler, M.H. Crawford, J. Cryst. Growth 310 (2008) 1062-1068.
[282] D. Schmitz, E. Woelk, G. Strauch, M. Deschler, H. Jurgensen, Mater. Sci. Eng. B-Solid State Mater. Adv. Technol. 43 (1997) 228-236.
[283] G.A. Hebner, K.P. Killeen, R.M. Biefeld, J. Cryst. Growth 98 (1989) 293-301,S. Salim, K.F. Jensen, R.D. Driver, J. Cryst. Growth 145 (1994) 28-35.
[284] K.C. Baucom, K.P. Killeen, H.K. Moffat, J. Electron. Mater. 24 (1995) 1703-1706.
[285] J.P. Stagg, J. Christer, E.J. Thrush, J. Crawley, J. Cryst. Growth 120 (1992) 98-102.
[286] W.J. DeSisto, B.J. Rappoli, J. Cryst. Growth 191 (1998) 290-293.
[287] M. Fulem, K. Růžička, V. Růžička, E. Hulicius, T. Šimeček, J. Pangrác, S.A. Rushworth, L.M. Smith, J. Cryst. Growth 272 (2004) 42-46.
[288] D.V. Shenai-Khatkhate, R.L. DiCarlo Jr, C.J. Marsman, R.F. Polcari, R.A. Ware, E. Woelk, J. Cryst. Growth 298 (2007) 176-180,C.L. Andre, N. El-Zein, N. Tran, J. Cryst. Growth 298 (2007) 168-171.
[289] A. Love, S. Middleman, A.K. Hochberg, J. Cryst. Growth 129 (1993) 119-133.
[290] E. Woelk, R. DiCarlo, J. Cryst. Growth 393 (2014) 32-34.
[291] G.J. Grashoff, C.E. Pilkington, C.W. Corti, Platinum Metals Rev. 27 (1983) 157.
[292] J.L. Briesacher, M. Nakamura, T. Ohmi, J. Electrochem. Soc. 138 (1991) 3717-3723.
[293] D.R. Olander, Industrial & Engineering Chemistry Fundamentals 6 (1967) 178-&.
[294] G. Costrini, J.J. Coleman, J. Appl. Phys. 57 (1985) 2249-2252.
[295] L. Stock, W. Richter, J. Cryst. Growth 77 (1986) 144-150.
[296] D.I. Fotiadis, A.M. Kremer, D.R. McKenna, K.F. Jensen, J. Cryst. Growth 85 (1987) 154-164,E.P. Visser, C.R. Kleijn, C.A.M. Govers, C.J. Hoogendoorn, L.J. Giling, J. Cryst. Growth 94 (1989) 929-946.
[297] P.N. Gadgil, J. Cryst. Growth 134 (1993) 302-312.
[298] M.E. Coltrin, R.J. Kee, G.H. Evans, J. Electrochem. Soc. 136 (1989) 819-829.
[299] W.L. Holstein, Progress in Crystal Growth and Characterization of Materials 24 (1992) 111-211.
[300] W.G. Breiland, M.E. Coltrin, J.R. Creighton, H.Q. Hou, H.K. Moffat, J.Y. Tsao, Mater. Sci. Eng. R-Rep. 24 (1999) 241-274.
[301] A.G. Thompson, R.A. Stall, P. Zawadzki, G.H. Evans, J. Electron. Mater. 25 (1996) 1487-1494.
[302] T.G. Mihopoulos, S.G. Hummel, K.F. Jensen, J. Cryst. Growth 195 (1998) 725-732.
[303] L. Kadinski, V. Merai, A. Parekh, J. Ramer, E.A. Armour, R. Stall, A. Gurary, A. Galyukov, Y. Makarov, J. Cryst. Growth 261 (2004) 175-181,B. Mitrovic, A. Parekh, J. Ramer, V. Merai, E.A. Armour, L. Kadinski, A. Gurary, J. Cryst. Growth 289 (2006) 708-714.
[304] B. Mitrovic, A. Gurary, L. Kadinski, J. Cryst. Growth 287 (2006) 656-663,B. Mitrovic, A. Gurary, W. Quinn, J. Cryst. Growth 303 (2007) 323-329.
[305] A.G. Salinger, J.N. Shadid, S.A. Hutchinson, G.L. Hennigan, K.D. Devine, H.K. Moffat, J. Cryst. Growth 203 (1999) 516-533,E.V. Yakovlev, R.A. Talalaev, Y.N. Makarov, B.S. Yavich, W.N. Wang, J. Cryst. Growth 261 (2004) 182-189.
[306] R.P. Parikh, R.A. Adomaitis, J. Cryst. Growth 286 (2006) 259-278.
[307] W.G. Breiland, K.P. Killeen, in: O.J. Glembocki, S.W. Pang, F.H. Pollak, G.M. Crean, G. Larrabee (Eds.), Diagnostic Techniques for Semiconductor Materials Processing, 1994, pp. 99-104.
[308] W.G. Breiland, K.P. Killeen, J. Appl. Phys. 78 (1995) 6726-6736.
[309] H. Protzmann, M. Luenenbuerger, M. Bremser, M. Heuken, H. Juergensen, J. Cryst. Growth 221 (2000) 629-634.
[310] S. Nakamura, Jpn. J. Appl. Phys. Part 1 - Regul. Pap. Short Notes Rev. Pap. 30 (1991) 1348-1353.
[311] R.S. Balmer, C. Pickering, A.J. Pidduck, T. Martin, J. Cryst. Growth 245 (2002) 198-206.
[312] D.D. Koleske, M.E. Coltrin, A.A. Allerman, K.C. Cross, C.C. Mitchell, J.J. Figiel, Applied Physics Letters 82 (2003) 1170-1172.
[313] D.D. Koleske, M.E. Coltrin, K.C. Cross, C.C. Mitchell, A.A. Allerman, J. Cryst. Growth 273 (2004) 86-99.
[314] D.D. Koleske, M.E. Coltrin, M.J. Russell, J. Cryst. Growth 279 (2005) 37-54.
[315] R.M. Lum, M.L. McDonald, J.C. Bean, J. Vandenberg, T.L. Pernell, S.N.G. Chu, A. Robertson, A. Karp, Applied Physics Letters 69 (1996) 928-930.
[316] K.P. Killeen, W.G. Breiland, J. Electron. Mater. 23 (1994) 179-183.
[317] N. Kobayashi, Y. Kobayashi, J. Cryst. Growth 124 (1992) 525-530.
[318] N. Kobayashi, J. Cryst. Growth 145 (1994) 1-11.
[319] Y. Kobayashi, N. Kobayashi, J. Electron. Mater. 25 (1996) 691-694.

[320] N. Kobayashi, Y. Kobayashi, K. Uwai, J. Cryst. Growth 174 (1997) 544-549.
[321] Y. Kobayashi, N. Kobayashi, J. Cryst. Growth 189 (1998) 301-304.
[322] Y.D. Kim, F. Nakamura, E. Yoon, D.V. Forbes, J.J. Coleman, Applied Physics Letters 69 (1996) 4209-4211,F. Nakamura, Y.D. Kim, E. Yoon, D.V. Forbes, J.J. Coleman, J. Appl. Phys. 83 (1998) 775-778.
[323] H. Fujiwara, Spectroscopic Ellipsometry: Principles and Applications, Wiley, 2007.
[324] B. Johs, et al., in: P.A. Rosenthal, W.M. Duncan, J.A. Woollam (Eds.), In Situ Process Diagnostics and Intelligent Materials Processing, 1998, pp. 3-14.
[325] Y. Taniyasu, A. Yoshikawa, J. Electron. Mater. 30 (2001) 1402-1407.
[326] A. Bonanni, D. Stifter, A. Montaigne-Ramil, K. Schmidegg, K. Hingerl, H. Sitter, J. Cryst. Growth 248 (2003) 211-215.
[327] M. Leyer, J. Stellmach, C. Meissner, M. Pristovsek, M. Kneissl, J. Cryst. Growth 310 (2008) 4913-4915.
[328] D.E. Aspnes, J.P. Harbison, A.A. Studna, L.T. Florez, Applied Physics Letters 52 (1988) 957-959,E. Colas, D.E. Aspnes, R. Bhat, A.A. Studna, J.P. Harbison, L.T. Florez, M.A. Koza, V.G. Keramidas, J. Cryst. Growth 107 (1991) 47-55,D.E. Aspnes, et al., J. Cryst. Growth 120 (1992) 71-77.
[329] D.E. Aspnes, R. Bhat, E. Colas, V.G. Keramidas, M.A. Koza, A.A. Studna, Journal of Vacuum Science & Technology a-Vacuum Surfaces and Films 7 (1989) 711-716.
[330] E. Colas, D.E. Aspnes, R. Bhat, A.A. Studna, M.A. Koza, V.G. Keramidas, J. Cryst. Growth 94 (1989) 613-618.
[331] D.E. Aspnes, Mater. Sci. Eng. B-Solid State Mater. Adv. Technol. 30 (1995) 109-119.
[332] P. Weightman, D.S. Martin, R.J. Cole, T. Farrell, Reports on Progress in Physics 68 (2005) 1251-1341.
[333] M. Zorn, J.T. Zettler, Physica Status Solidi B-Basic Solid State Physics 242 (2005) 2587-2594.
[334] W.G. Breiland, Reflectance-Correcting Pyrometry in Thin Film Deposition Applications, Sandia National Laboratories, Sandia National Laboratories, Albuquerque, NM 87185, 2003, 85.
[335] J. Ramer, B. Patel, A. Patel, V. Boguslavskiy, A. Gurary, in: M.O. Manasreh, B.J.H. Stadler, I. Ferguson, Y.H. Zhang (Eds.), Infrared Applications of Semiconductors Iii, 2000, pp. 309-314.
[336] M.J. Fordham, R.F. Gansman, F.Y. Sorrell, Ieee, EMISSIVITY CORRECTING PYROMETER FOR TEMPERATURE-MEASUREMENT IN LOW-PRESSURE CHEMICAL-VAPOR-DEPOSITION, 1993.
[337] B.V. Shanabrook, J.R. Waterman, J.L. Davis, R.J. Wagner, D.S. Katzer, J. Vac. Sci. Technol. B 11 (1993) 994-997.
[338] S.R. Johnson, C. Lavoie, T. Tiedje, J.A. Mackenzie, J. Vac. Sci. Technol. B 11 (1993) 1007-1010.
[339] S.R. Johnson, T. Tiedje, J. Cryst. Growth 175 (1997) 273-280.
[340] R.N. Sacks, D. Barlett, C.A. Taylor, J. Williams, J. Vac. Sci. Technol. B 23 (2005) 1247-1251.
[341] I. Farrer, J.J. Harris, R. Thomson, D. Barlett, C.A. Taylor, D.A. Ritchie, J. Cryst. Growth 301 (2007) 88-92.
[342] J.J. Harris, R. Thomson, C. Taylor, D. Barlett, R.P. Campion, V.A. Grant, C.T. Foxon, M.J. Kappers, J. Cryst. Growth 300 (2007) 194-198.
[343] M. Belousov, B. Volf, J.C. Ramer, E.A. Armour, A. Gurary, J. Cryst. Growth 272 (2004) 94-99.
[344] V.T. Gillard, W.D. Nix, Zeitschrift Fur Metallkunde 84 (1993) 874-880.
[345] J.A. Floro, E. Chason, S.R. Lee, in: S.W. Pang, O.J. Glembocki, F.H. Pollak, F.G. Celii, C.M. SotomayorTorres (Eds.), Diagnostic Techniques for Semiconductor Materials Processing Ii, 1996, pp. 491-496.
[346] G.G. Stoney, Proceedings of the Royal Society of London Series a-Containing Papers of a Mathematical and Physical Character 82 (1909) 172-175.
[347] E.H. Chason, J.A. Floro, C.H. Seager, M.B. Sinclair, Measurement of the curvature of a surface using parallel light beams, Google Patents, 1999.
[348] H. Amano, M. Iwaya, T. Kashima, M. Katsuragawa, I. Akasaki, J. Han, S. Hearne, J.A. Floro, E. Chason, J. Figiel, Jpn. J. Appl. Phys. Part 2 - Lett. 37 (1998) L1540-L1542.
[349] S. Hearne, E. Chason, J. Han, J.A. Floro, J. Figiel, J. Hunter, H. Amano, I.S.T. Tsong, Applied Physics Letters 74 (1999) 356-358.
[350] S.R. Lee, D.D. Koleske, K.C. Cross, J.A. Floro, K.E. Waldrip, A.T. Wise, S. Mahajan, Applied Physics Letters 85 (2004) 6164-6166.
[351] W.G. Breiland, S.R. Lee, D.D. Koleske, J. Appl. Phys. 95 (2004) 3453-3465.
[352] B.P. Rodriguez, J.M. Millunchick, J. Cryst. Growth 264 (2004) 64-69,M. Zorn, F. Bugge, T. Schenk, U. Zeimer, M. Weyers, J.T. Zettler, Semiconductor Science and Technology 21 (2006) L45-L48.
[353] J.F. Geisz, A.X. Levander, A.G. Norman, K.M. Jones, M.J. Romero, J. Cryst. Growth 310 (2008) 2339-2344.

[354] A. Dadgar, M. Poschenrieder, A. Reiher, J. Blasing, J. Christen, A. Krtschil, T. Finger, T. Hempel, A. Diez, A. Krost, Applied Physics Letters 82 (2003) 28-30,A. Krost, F. Schulze, A. Dadgar, G. Strassburger, K. Haberland, T. Zettler, Physica Status Solidi B-Basic Solid State Physics 242 (2005) 2570-2574.
[355] A. Krost, A. Dadgar, F. Schulze, J. Blasing, G. Strassburger, R. Clos, A. Diez, P. Veit, T. Hempel, J. Christen, J. Cryst. Growth 275 (2005) 209-216.
[356] A. Dadgar, C. Hums, A. Diez, J. Blaesing, A. Krost, J. Cryst. Growth 297 (2006) 279-282.
[357] D. Zhu, D.J. Wallis, C.J. Humphreys, Reports on Progress in Physics 76 (2013).
[358] W.J. DeSisto, B.J. Rappoli, J. Cryst. Growth 170 (1997) 242-245.
[359] S. Cho, G.W. Rubloff, M.E. Aumer, D.B. Thomson, D.P. Partlow, R. Parikh, R.A. Adomaitis, J. Vac. Sci. Technol. B 23 (2005) 1386-1397.
[360] M.C. Johnson, K. Poochinda, N.L. Ricker, J.W. Rogers, T.P. Pearsall, J. Cryst. Growth 212 (2000) 11-20.
[361] B.S. Sywe, J.R. Schlup, J.H. Edgar, Chemistry of Materials 3 (1991) 737-742,B.S. Sywe, J.R. Schlup, J.H. Edgar, Chemistry of Materials 3 (1991) 1093-1097.
[362] K. Hanaoka, H. Ohnishi, K. Tachibana, Jpn. J. Appl. Phys. Part 1 - Regul. Pap. Short Notes Rev. Pap. 32 (1993) 4774-4778,M.L. Hitchman, S.H. Shamlian, G.G. Condorelli, F. ChabertRocabois, Journal of Alloys and Compounds 251 (1997) 297-302.
[363] S.H. Kim, H.S. Kim, J.S. Hwang, J.G. Choi, P.J. Chong, Chemistry of Materials 6 (1994) 278-281.
[364] W.M. Tolles, J.W. Nibler, J.R. McDonald, A.B. Harvey, Applied Spectroscopy 31 (1977) 253-271.
[365] R. Luckerath, P. Tommack, A. Hertling, H.J. Koss, P. Balk, K.F. Jensen, W. Richter, J. Cryst. Growth 93 (1988) 151-158,W. Richter, P. Kurpas, R. Luckerath, M. Motzkus, M. Waschbusch, J. Cryst. Growth 107 (1991) 13-25.
[366] J.I. Davies, M.J. Parrott, J.O. Williams, J. Cryst. Growth 79 (1986) 363-370.
[367] P.W. Lee, T.R. Omstead, D.R. McKenna, K.F. Jensen, J. Cryst. Growth 85 (1987) 165-174,P.W. Lee, T.R. Omstead, D.R. McKenna, K.F. Jensen, J. Cryst. Growth 93 (1988) 134-142.
[368] www.veeco.com.
[369] G.S. Tompa, M.A. McKee, C. Beckham, P.A. Zawadzki, J.M. Colabella, P.D. Reinert, K. Capuder, R.A. Stall, P.E. Norris, J. Cryst. Growth 93 (1988) 220-227.
[370] P.M. Frijlink, J. Cryst. Growth 93 (1988) 207-215.
[371] A.H. Dilawari, J. Szekely, J. Cryst. Growth 108 (1991) 491-498.
[372] K. Nishida, S. Haneda, K. Hara, H. Munekata, H. Kikimoto, J. Cryst. Growth 170 (1997) 312-315.
[373] H.X. Wang, T. Wang, S. Mahanty, F. Komatsu, T. Inaoka, K. Nishino, S. Sakai, J. Cryst. Growth 218 (2000) 148-154.
[374] www.aixtron.com.
[375] F. Lu, D. Lee, D. Byrnes, E. Armour, W. Quinn, Science China-Technological Sciences 54 (2011) 33-37.
[376] H. Aida, D.S. Lee, M. Belousov, K. Sunakawa, Japanese Journal of Applied Physics 51 (2012).
[377] A. Dadgar, J. Blasing, A. Diez, A. Alam, M. Heuken, A. Krost, Jpn. J. Appl. Phys. Part 2 - Lett. 39 (2000) L1183-L1185,A. Dadgar, J. Christen, T. Riemann, S. Richter, J. Blasing, A. Diez, A. Krost, A. Alam, M. Heuken, Applied Physics Letters 78 (2001) 2211-2213.
[378] R.R. Bradley, J. Cryst. Growth 55 (1981) 223-228.
[379] S.P. Tobin, S.M. Vernon, C. Bajgar, S.J. Wojtczuk, M.R. Melloch, A. Keshavarzi, T.B. Stellwag, S. Venkatensan, M.S. Lundstrom, K.A. Emery, Ieee Transactions on Electron Devices 37 (1990) 469-477.
[380] T. Kobayashi, K. Taira, F. Nakamura, H. Kawai, J. Appl. Phys. 65 (1989) 4898-4902.
[381] B.T. Cunningham, G.E. Stillman, G.S. Jackson, Applied Physics Letters 56 (1990) 361-363.
[382] R.D. Dupuis, J. Cryst. Growth 55 (1981) 213-222.
[383] S.P. Tobin, S.M. Vernon, C. Bajgar, V.E. Haven, Jr., S.E. Davis, Conference Record of the Eighteenth IEEE Photovoltaic Specialists Conference - 1985 (Cat. No.86CH2208-7) (1985) 134-9.
[384] T. Sakaguchi, F. Koyama, K. Iga, Electronics Letters 24 (1988) 928-929.
[385] R.W. Glew, B. Garrett, P.D. Greene, Electronics Letters 25 (1989) 1103-1104.
[386] H. Tanaka, H. Itoh, T. Ohori, M. Takikawa, K. Kasai, M. Takechi, M. Suzuki, J. Komeno, Jpn. J. Appl. Phys. Part 2 - Lett. 26 (1987) L1456-L1458.
[387] J.F. Geisz, D.J. Friedman, J.S. Ward, A. Duda, W.J. Olavarria, T.E. Moriarty, J.T. Kiehl, M.J. Romero, A.G. Norman, K.M. Jones, Applied Physics Letters 93 (2008).
[388] S.R. Kurtz, A.A. Allerman, E.D. Jones, J.M. Gee, J.J. Banas, B.E. Hammons, Applied Physics Letters 74 (1999) 729-731.
[389] P.C. Chang, A.G. Baca, N.Y. Li, P.R. Sharps, H.Q. Hou, J.R. Laroche, F. Ren, Applied Physics Letters 76 (2000) 2788-2790.

[390] A.W. Nelson, L.D. Westbrook, J.S. Evans, Electronics Letters 19 (1983) 34-36.
[391] T. Sasaki, M. Kitamura, I. Mito, J. Cryst. Growth 132 (1993) 435-443.
[392] A. Tauke-Pedretti, G.A. Vawter, E.J. Skogen, G. Peake, M. Overberg, C. Alford, W.W. Chow, Z.S. Yang, D. Torres, F. Cajas, Photonics Technology Letters, IEEE 23 (2011) 908-910.
[393] J.F. Geisz, S. Kurtz, M.W. Wanlass, J.S. Ward, A. Duda, D.J. Friedman, J.M. Olson, W.E. McMahon, T.E. Moriarty, J.T. Kiehl, Applied Physics Letters 91 (2007).
[394] T. Low, T. Shirley, C. Hutchinson, G. Essilfie, W. Whiteley, B. Yeats, D. D'Avanzo, Solid-State Electronics 43 (1999) 1437-1444.
[395] W. Guter, J. Schöne, S.P. Philipps, M. Steiner, G. Siefer, A. Wekkeli, E. Welser, E. Oliva, A.W. Bett, F. Dimroth, Applied Physics Letters 94 (2009) -.
[396] H.K. Choi, C.A. Wang, G.W. Turner, M.J. Manfra, D.L. Spears, G.W. Charache, L.R. Danielson, D.M. Depoy, Applied Physics Letters 71 (1997) 3758-3760.
[397] J.G. Cederberg, J.D. Blaich, G.R. Girard, S.R. Lee, D.P. Nelson, C.S. Murray, J. Cryst. Growth 310 (2008) 3453-3458.
[398] P. Madejczyk, W. Gawron, P. Martyniuk, A. Keblowski, A. Piotrowski, J. Pawluczyk, W. Pusz, A. Kowalewski, J. Piotrowski, A. Rogalski, Semiconductor Science and Technology 28 (2013).
[399] S.K. Chaudhuri, R.M. Krishna, K.J. Zavalla, L. Matei, V. Buliga, M. Groza, A. Burger, K.C. Mandal, Nuclear Science, IEEE Transactions on 60 (2013) 2853-2858.
[400] D. Kasahara, D. Morita, T. Kosugi, K. Nakagawa, J. Kawamata, Y. Higuchi, H. Matsumura, T. Mukai, Applied Physics Express 4 (2011).
[401] S. Nakamura, et al., Jpn. J. Appl. Phys. Part 2 - Lett. 37 (1998) L309-L312.
[402] E. Matioli, et al., Applied Physics Letters 98 (2011).
[403] D.A. Haeger, et al., Applied Physics Letters 100 (2012) -.
[404] U.K. Mishra, Y.F. Wu, B.P. Keller, S. Keller, S.P. Denbaars, Ieee Transactions on Microwave Theory and Techniques 46 (1998) 756-761.

Table I. MOVPE Materials and Associated Device Applications

Semiconductor Material	Device Application	References
GaAs	Solar Cells, transistors, lasers	[378],[379],[380], [381], [382]
AlGaAs	Solar Cells, Lasers, VCSEL, HBTs, HEMTs,	[383],[56],[384],[385],[381],[386]
InGaAs and InGaAsN	Solar Cells, HBT	[387],[388],[389]
InGaAsP	Lasers, PICs,	[390],[391],[392]
InGaP and InGaAs	IMM Solar Cells, Multi-junction Solar Cells, HBT	[393],[394], [395]
InAsSb	IR detectors, lasers	[26]
InGaAsSb, GaAsSb	Thermophotovoltaics	[396],[397]
HgCdTe	IR detectors	[398]
CdZnTe	Radiation detectors	[399]
InGaN	Visible LEDs and Lasers, solar cells	[400],[80],[401], [402],[107]
AlGaN	UV LEDs, HEMTs and Lasers	[403],[115],[404]

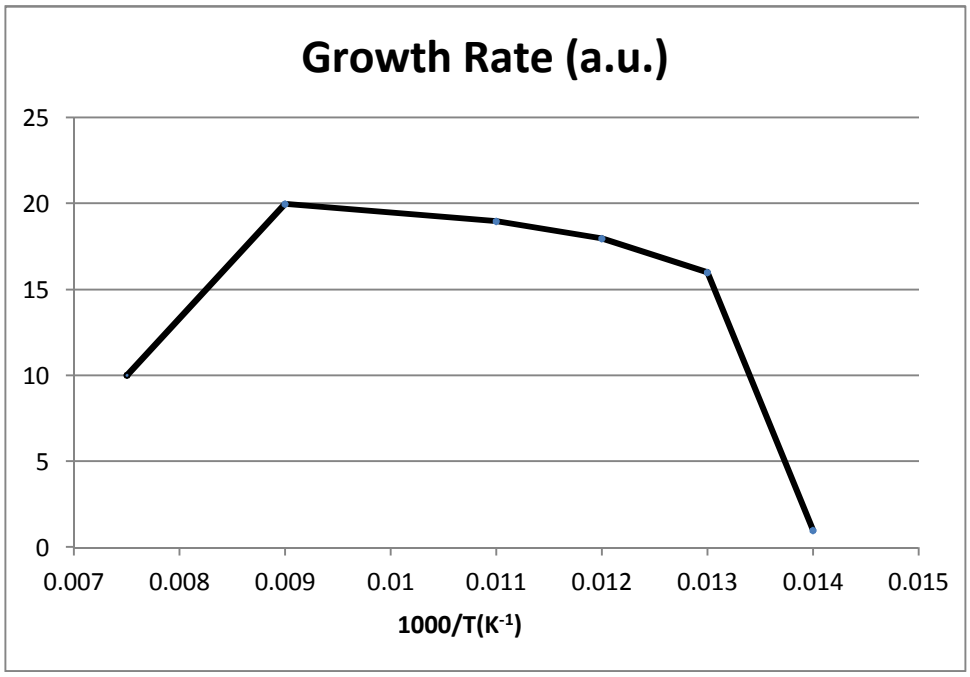

Figure 1. Growth rate in arbitrary units versus temperature for the growth of GaAs by MOVPE after Reep and Ghandhi [14].

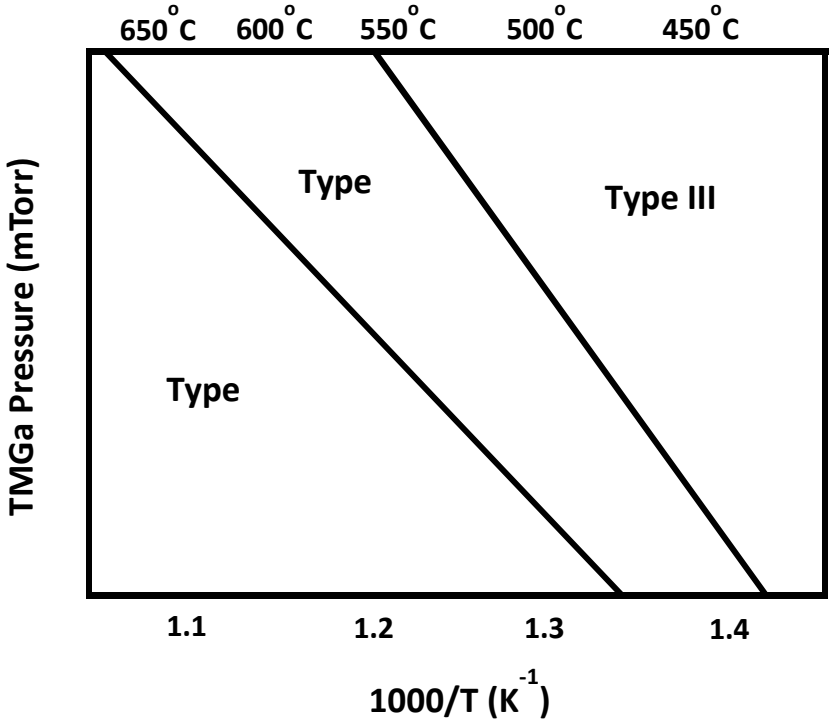

Figure 2. RDS lineshapes during MOVPE as a function of temperature and TMGa partial pressure. The arsine pressure was held constant at 460 mTorr. The lines designate approximate boundaries between RDS (surface reconstruction) types (after Creighton *et al.* [16; 38].

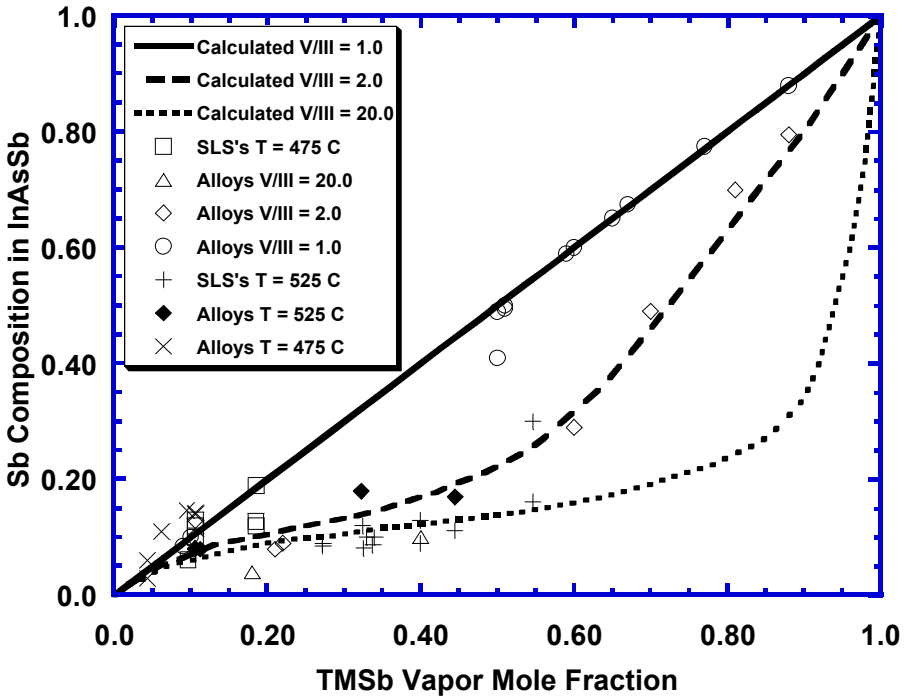

Figure 3. Mole fraction of InSb in solid $InAs_{1-x}Sb_x$ versus Group V mole fraction of organometallic antimony in the vapor. The curves are the calculated values for III/V = 1, solid line; 0.5, dashed line; and 0.05, dotted line. The open triangles, open diamonds, x's and open circles are values for $InAs_{1-x}Sb_x$ alloys grown at 475 ^{o}C with different III/V ratios. The solid diamonds are for alloys grown at 525 ^{o}C. The open squares and crosses represent the values for $InAs_{1-x}Sb_x$/InAs SLS's grown at 475 and 525 ^{o}C, respectively [57].

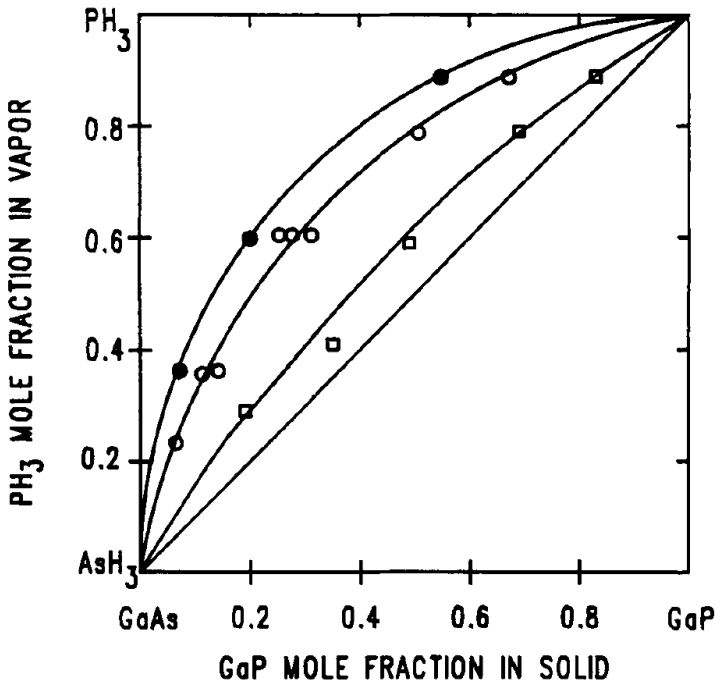

Figure 4. Variation of solid P composition with PH_3 vapor phase concentration. The PH_3 mole fraction in the vapor phase is equal to the number of moles of PH_3 divided by the number of moles of PH_3 plus the number of moles of AsH_3 in the input gas stream. The filled circles are for 700 ºC and 400 sccm total Group V flow; the open circles are for 700 ºC and 200 sccm; the squares are for 800 ºC and 200 sccm.

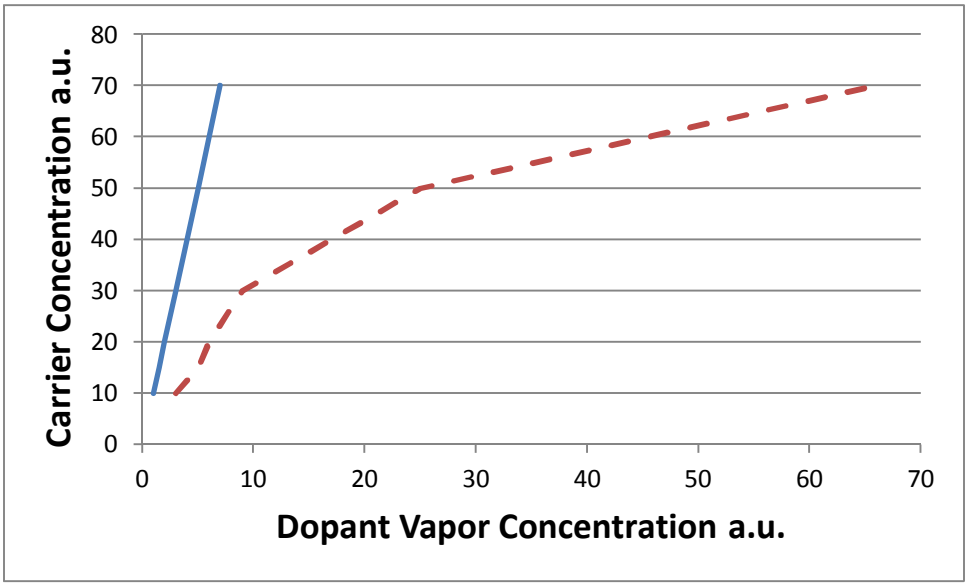

Figure 5. Resulting carrier concentration for different dopants where one is incorporated linearly, solid line, and the other sublinearly, dashed line. Different mechanisms can explain the sublinear behavior as discussed in the text.